Master's thesis

NTNU
Norwegian University of Science and Technology
Faculty of Natural Sciences
Department of Biotechnology and Food Science

Simen Jervell Lund

Exploring the Potential of *Bacillus methanolicus* for Expansion of C1 Substrate Range

Master's thesis in Biotechnology
Supervisor: Prof. Trygve Brautaset
Co-supervisor: May Laura Kilano Khider
June 2023

NTNU
Norwegian University of
Science and Technology

Simen Jervell Lund

Exploring the Potential of *Bacillus methanolicus* for Expansion of C1 Substrate Range

Master's thesis in Biotechnology
Supervisor: Prof. Trygve Brautaset
Co-supervisor: May Laura Kilano Khider
June 2023

Norwegian University of Science and Technology
Faculty of Natural Sciences
Department of Biotechnology and Food Science

NTNU
Norwegian University of
Science and Technology

Abstract

Using the methylotrophic and thermophilic bacterium *Bacillus methanolicus* as a host for synthetic methanotrophy provides a possibility to utilize cheap and abundant methane as a carbon source for biotechnological production. The conversion of methane to methanol could be coupled with pathway engineering to increase methanol assimilation through modulating the rate-limiting enzymes involved in the metabolic pathways. The result could be an efficient biotechnological production platform with *B. methanolicus* as a fast-growing producer of value-added compounds

Methane monooxygenases (MMOs) are responsible for the conversion of methane to methanol found in native methanotrophs. In this study, strains of *B. methanolicus* MGA3 that heterologously express the soluble form of MMO (soluble methane monooxygenase (sMMO)) were tested. The genes encoding the enzyme were carried in the pBV2xp plasmid under the xylose inducible promoter. Gro-EL/ES chaperonins from several sources were cloned in the pTH1mp plasmid under the methanol dehydrogenase inducible promoter to ensure proper folding and function of sMMO. A fluorescence-based assay was then adapted to measure enzyme activity through oxidation of coumarin to its fluorescent product, 7-hydroxycoumarin, by sMMO. An additional assay using the formation of a colored compound from naphthalene oxidized by sMMO in combination with tetrazotized o-dianisidine was also tested. Neither the fluorescence-based enzyme assay nor the naphthalene assay yielded any results attributable to functionally produced sMMO. Comparably low levels of fluorescence were seen in all strains including the wild type and empty vector negative controls. The low observed fluorescence could be attributed to natively produced compounds or cell autofluorescence. The absence of functional sMMO underlines the need for further elucidation of the catalytic mechanisms of sMMO and the regulatory mechanisms involved. Additionally, the potential for methane as a biotechnological feedstock warrants further research into synthetic methanotrophy.

B. methanolicus MGA3 converts methanol to formaldehyde by methanol dehydrogenase (MDH) before the rate-limiting enzymes 3-hexulose-6-phosphatase synthase (HPS) and 6-phospho-3-hexuloisomerase (PHI) further assimilate formaldehyde into synthetic pathways. Homologous expression of HPS and PHI and their effect on methanol assimilation were tested by cloning the *hps-phi* gene fragment in two plasmid constructs. The plasmids used were the high copy number pUB110Smp and the low copy number pTH1mp. Both plasmid constructs were cloned with both native promoter for *hps-phi* from *B. methanolicus* MGA3 as well as the *mdh* promoter. The strains were cultivated in 200 mM and 400 mM methanol. The strains homologously expressing the enzymes HPS and PHI showed the highest growth rate in the strains using the *mdh* promoter in the pUB110Smp plasmid, as well as increased growth rate in the strain carrying the pTH1mp plasmid with the native promoter. This suggested that the high copy number plasmid yielded the largest increase in growth rate. In addition, the low copy number plasmid with the native promoter displayed more stable growth rates in the 400 mM methanol concentration, suggesting a higher methanol tolerance using the native promoter. The strain carrying the high copy number plasmid and the native promoter could not be successfully transformed, and based on the observed growth rates this strain could provide the most efficient methanol assimilation.

Sammendrag

Bruken av den metylotrofe og termofile bakterien *B. methanolicus* MGA3 som en vert for syntetisk metanotrofi representerer en tiltalende mulighet til å bruke billig metangass som karbonkilde i bioteknologisk produksjon. Konverteringen av metan til metanol kan deretter kombineres med genetisk modifisering av diverse syntesespor for å øke metanolassimilering gjennom modulering av de hastighetsbestemmende enzymene HPS og PHI. Resultatet kan være effektive *B. methanolicus* stammer med et bredt anvendelsesfelt for produksjon av verdifulle stoffer.

Metan monooksygenaser (MMO) er ansvarlige for konverteringen av metan til metanol i metanotrofe bakterier. I denne studien ble bakteriestammer av *B. methanolicus* MGA3 som heterologt utrykte den løselige formen av metan monooksygenase (sMMO) testet. Genene som koder for enzymet ble uttrykt i plasmidet pBV2xp som er kontrollert av en induserbar xylosepromotor. GroEL/ES chaperoniner fra flere kilder ble klonet i pTH1mp plasmidet kontrollert av metanol dehydrogenasepromotoren for å forsikre korrekt sammensetning og funksjon av sMMO. Et fluorescensbasert assay ble deretter tilpasset for å måle enzymaktivitet gjennom oksideringen av kumarin til det fluorescerende produktet 7-hydroksykumarin av sMMO. Et alternativt assay basert på formasjonen av et farget stoff fra naftalen oksidert av sMMO i kombinasjon med o-dianisidin ble også testet. Hverken det fluorescensbaserte enzymassayet eller naftalenassayet gav resultater som kunne tilegnes funksjonelt produsert sMMO. De relativt lave fluorescensverdiene som eksperimentet viste ble observert i alle bakteriestammene, inkludert wild type og de negative kontrollene med tomme plasmidvektorer. De lave fluorescensverdiene som ble observert kan ha stammet fra stoffer naturlig produsert av *B. methanolicus,* eller autofluorescens fra bakteriecellene. Fraværet av funksjonell sMMO understreker behovet for å belyse de katalytiske og regulatoriske mekanismene til sMMO. Potensialet til metan som karbonkilde i bioteknologisk produksjon er i seg selv grunn for videre forskning innenfor syntetisk metanotrofi.

B. methanolicus MGA3 konverterer metanol til formaldehyd ved metanol dehydrogenase (MDH) før enzymene 3-heksulose-6-fosfatase syntase (HPS) og 6-fosfo-3-heksuloisomerase (PHI) videre assimilerer formaldehyd i metabolske syntesespor. Homologt uttrykt HPS og PHI og deres effekt på metanolassimilering ble testet gjennom kloning av *hps-phi* genene i to plasmidkonstruksjoner. Plasmidene bestod av pUB110Smp med et høyt kopinummer, og pTH1mp med et lavt kopinummer. Begge plasmidkonstruksjonene ble klonet med både den naturlige promotoren til *hps-phi* fra *B. methanolicus* MGA3 og *mdh* promotoren. Bakteriestammene ble kultivert i 200 mM og 400 mM metanol. Bakteriestammene som homologt uttrykte HPS og PHI demonstrerte den høyeste vekstraten i den stammen som benyttet *mdh* promotoren i pUB110Smp plasmidet, i tillegg til økt vekstrate i stammen som benyttet pTH1mp med den naturlige promotoren. Dette tydet på at det høye kopinummeret til plasmidet gav den største økningen i vekstrate. I tillegg demonstrerte pTH1mp plasmidet med den naturlige promotoren en mer stabil vekstrate ved høyere metanolkonsentrasjoner, som kan tyde på at høyere metanoltoleranse oppnås ved bruk av naturlig promotor. Bakteriestammen med pUB110Smp plasmidet og naturlig promotor kunne ikke transformeres, og basert på de observerte vekstratene så kan det type på at denne stammen kan fasilitere den mest effektive metanolassimileringen.

Acknowledgements

This study would not have been possible without the help of several individuals who, through their support, ensured the completion of this work. First and foremost, I would like to thank my immediate supervisors May Khider and Asst.Prof. Marta Irla for their continued support, encouragement, and advice in times of adversity, success, and less intelligent questions from my part. I would also like to thank my supervisor Prof. Trygve Brautaset for facilitating and allowing me to pursue a master thesis in a field I find highly interesting, and for being available in times of need.

I would also like to thank the lab coordinator of the Molecular Genetics and Microbiology lab, Dr. Hanne Jørgensen, for always being available for questions and assistance, and for ensuring that the laboratory work for this thesis was made possible. In addition, I would like to thank the members, both staff and students, of the Cell Factories research group for their encouragement, support, and for making it an enjoyable experience.

Finally, I would like to thank my friends and family for their support throughout this demanding and tough, yet inspirational and fun experience.

Table of content:

List of figures:

List of tables:

Abbreviations:

FT	Fischer-Tropsch
GHG	Greenhouse Gas
GABA	γ-aminobutyric acid
PE	Polyethylene
PET	Polyethylene Terephthalate
PHA	Polyhydroxyalkanoate
GABA	γ-Aminobutyric Acid
RuMP	Ribulose Monophosphate
MDH	Methanol Dehydrogenase
rpe	Ribulose-5-Phosphate-3-Epimerase
tkt/TK	Transketolase
pfk	Phosphofructokinase
glpX	Class II Sedoheptulose bisphosphatase
fba	Class II Fructose-1,6-Bisphosphate Aldolase
DHAP	Dihydroxyacetone Phosphate
GAP	Glyceraldehyde-3-phosphate
NAD	Nicotinamide Adenine Dinucleotide
FAD	Flavin Adenine Dinucleotide
PQQ	Pyrroloquinoline Quinone
Ru5P	Ribulose-5-Phosphate
H6P	D-*arabino*-Hexulose-6-Phosphate
HPS	3-Hexulose-6-Phosphatase Synthase
F6P	Fructose-6-Phosphate
PHI	6-Phospho-3-Hexuloisomerase
SBPase/SBP	Sedoheptulose-1,7-Bisphosphatase
TA	Transaldolase
FBP	Fructose-1,6-Bisphosphate
FBPA	Fructose-1,6-Bisphosphate Aldolase
KDPGA	2-Keto-3-Deoxy-6-Phosphogluconate
WT	Wild Type
TCA	Tricarboxylic Acid
RPI	Ribose-5-Phosphate Isomerase
RPE	Ribulose-5-Phosphate-3-Epimerase
E4P	Erythrose-4-Phosphate
S7P	Septuheptulose-7-Phosphate
X5P	Xylulose-5-Phosphate
SBP	Sedoheptulose-1,7-bisphosphate
MMO	Methane Monooxygenase
pMMO	Particulate Methane Monooxygenase
sMMO	Soluble Methane Monooxygenase
Rubisco	Ribulose Bisphosphate Carboxylase
GC	Gas Chromatography
HPLC	High-Performance Liquid Chromatography
SCP	Single Cell Protein
PCR	Polymerase Chain Reaction
dNTPs	Deoxynucleotide Trisphosphate
dsDNA	Double-Stranded DNA
MCS	Multiple Cloning Site

1 Introduction

1.1 One-carbon compounds as a carbon source for biotechnological production

Biotechnological production involves the usage of a variety of organisms to either perform a certain function or produce a specific compound, often achieved using genetic engineering. Traditionally, most biotechnological production has been done with the well-established industrial workhorses *Escherichia coli*, *Saccharomyces cerevisiae*, and their derivative strains, using common feedstocks like sugar cane or molasses (Theisen and Liao 2017; Parapouli et al. 2020). The main driving force in the search for alternative carbon sources is to find optional feedstocks that do not compete with other sectors. This increasing demand, in addition to the relatively high cost of common microbial feedstocks like glucose and molasses, is putting continued pressure on the industry to find alternative and cheaper carbon sources (Comer et al. 2017). The mentioned glucose and molasses both require cultivable land to produce which competes with the production of food for human consumption, as well as being used for other industrial sectors like the animal- or human feed industries, where they function as additives (Müller et al. 2015). Finding sustainable and cheap carbon sources is therefore a key factor for the future development and growth of the biotechnological industry.

One-carbon (C_1) compounds, like methanol (CH_3OH) and methane (CH_4), have gained increasing interest as microbial feedstock due to their availability from cheap natural gas and the possibility to be produced from renewable sources (Comer et al. 2017; Heux et al. 2018). Methanol is mainly derived from synthesis gas (syngas), a mixture of carbon monoxide (CO) and hydrogen (H_2), which is produced from fossil fuels like natural- and shale gas, coal, and oil. Renewable sources of methanol include using H_2 produced in electrolysis powered by renewable energy and carbon dioxide (CO_2) captured from the atmosphere, or other regenerative sources of hydrocarbons like waste wood or biodegradable biomass (Wernicke, Plass, and Schmidt 2014). Liquid methanol is less cumbersome to transport compared to its C1 gaseous counterparts which requires pressurized sealed containers and more complicated transfer methods to prevent leakage. This in turn provides a solid argument for the increased use of methanol. In addition, methanol's high miscibility compared to the low water solubility of C1 gases like methane and CO_2, means that its use in fermentation prevents low mass transfer rates seen in these gases. This also potentially allows for higher yields with comparatively small amounts of feedstock (Cotton et al. 2020; Yasin et al. 2015).

The potential application of methane as carbon source for microbial industrial production has also garnered much interest in recent years. Among natural- and shale gas, methane is the primary component making up as much as 90% of total gas reserves, of which there is estimated to be in excess of 6.614 trillion cubic feet of natural gas and 7.299 trillion cubic feet of shale gas (In Yeub et al. 2014). Methane is also produced in a variety of anthropogenic and natural processes. Anthropogenic sources include burning of biomass, anaerobic microbial processes in landfills, livestock farming, and usage of fossil fuels. Natural sources are made up by rivers, lakes, permafrost, wildfires, and wetlands to name a few (In Yeub et al. 2014; Strong, Xie, and Clarke 2015). Due to the large amounts of methane available, cost is kept low, and methane consistently outcompetes methanol,

mannitol, and glucose on price (Comer et al. 2017; Khider, Brautaset, and Irla 2021). In addition to favorable raw material cost, microbial conversion of methane to high-value compounds has other advantages over conventional methods. The chemical conversion of methane is inefficient in terms of cost, energy, yield, and time, in addition to a multi-step process being required. These include the production of syngas, followed by Fischer-Tropsch (FT) conversion where the syngas is converted to liquid long-chain hydrocarbons, in a process yielding less than 25% conversion rate with significant cost. Production of syngas also requires high temperatures (>900°C) (In Yeub et al. 2014; Hwang et al. 2018). Microbial conversion of methane into methanol can be achieved at ambient temperatures using methanotrophic bacteria in a single step process and gives higher conversion rates and selectivity, with lower cost and energy consumption (In Yeub et al. 2014). Seeing as methanotrophic bacteria share much of its carbon metabolism with other methylotrophs, many of the high-value compounds produced by methylotrophs can therefore potentially be produced from cheaper methane as opposed to the more expensive current feedstocks like glucose.

Although the cheaper cost and abundant supply of methane makes it a prospective feedstock for methanotrophic bacteria in biotechnological production, its negative impact on the environment highlights the need for more efficient methane capture. Both natural and anthropogenic methane acts as a greenhouse gas (GHG). Methane is a significantly more potent GHG than, for example CO_2 with a warming potential 28 times higher over a period of 100 years. This contributes ca. 20% of the total global warming potential per year (Haynes and Gonzalez 2014). Natural sources of atmospheric and terrestrial methane have in the past been offset by methane sinks capable of breaking down excess methane. The main methane sink is made up of tropospheric hydroxyl radicals which oxidizes methane and is responsible for about 90% of the global removal of the gas. Other atmospheric sinks include atomic oxygen radicals alongside chlorine radicals higher up in the stratosphere, and chlorine radicals generated in the marine boundary layer from sea salt (Kirschke et al. 2013). Smaller terrestrial sinks include breakdown by methanotrophic or aerobic bacteria in soil (Curry 2007). Anthropogenic sources of methane have been steadily on the rise since the time of the industrial revolution where large-scale land cultivation and agriculture started to supersede the capacity of natural methane sinks. The increased usage of fossil fuels further exacerbated the problem (Khider, Brautaset, and Irla 2021; Rigby et al. 2017). With methane being produced as a by-product from anthropogenic and natural processes as well as in natural gas production, a coupling of these processes with efficient methane capture technology could provide an alternative carbon source for biotechnological production. This also has the potential to simultaneously limit the release of the potent GHG to the atmosphere and promote industrial expansion from its current relatively limited usage.

The usage of methane today is mostly limited to being a combustion fuel for heating and energy and in the production of certain chemicals. The application of methane in biotechnology as a carbon source therefore has the potential to provide a vast carbon supply with little competition from other industrial sectors due to the limited usage of methane in other industries (Strong, Xie, and Clarke 2015; Haynes and Gonzalez 2014). Despite the potential of methane, certain hurdles still prevent its widespread application for microbial production.

1.1.1 Use of methylotrophic microorganisms for production of value-added compounds

Methylotrophy refers to the ability to utilize reduced carbon compounds as the only source of energy and carbon. These contains no carbon-carbon bonds and include compounds like methane and methanol (Chistoserdova, Kalyuzhnaya, and Lidstrom 2009). The ability of some methylotrophic bacteria to produce high-value compounds and the potential for these to be used in an industrial setting have been explored for decades (Sirirote, Tsuneo, and Shoichi 1988; Izumi et al. 1993; Kim et al. 1996). Several methylotrophic bacterial species produce a range of substances using methanol as the primary carbon source. Among these species are *Methylobacterium extorquens, Pseudomonas sp., Methylobacillus glycogenes, Bacillus methanolicus, and Methylophilus methylotrophus.* High-value compounds include the amino acids L-lysine, L-threonine, L-glutamate, and L-serine, the biodegradable polyester group polyhydroxyalkanoates (PHAs), the neurotransmitter γ-aminobutyric acid (GABA), and 1,5-diaminopentane (cadaverin). Amino acid production is perhaps the most desired product from methylotrophic bacteria (Schrader et al. 2009; Li, Yang, and Loh 2016; Irla et al. 2017; Müller et al. 2015).

Production and sales of amino acids constitute a major global market with an industry estimated at US$25.6 billion by 2022. The industry owes its significant growth to rapidly increasing demands in certain areas, like amino acid supplements in animal feeds, various medical treatments, cosmetics, and the fitness and wellness industry (Wendisch 2020; Sanchez et al. 2018). Using microbial production allows for more customizable products like cyclic-, proteogenic-, and omega-amino acids. Chemical modifications through for example halogenation and hydroxylation have also been achieved (Wendisch 2020).

PHAs make up several polyesters produced from microorganisms as part of a natural polymer for energy and carbon storage (Li, Yang, and Loh 2016). These are biodegradable and have been proposed as a potential replacement for several petroleum-based plastics, such as polyethylene (PE) and polyethylene terephthalate (PET) (Li, Yang, and Loh 2016; Tan et al. 2021). A methylotrophic production host therefore has many potential products.

1.1.2 *Bacillus methanolicus* MGA3

The gram-positive bacterium *Bacillus methanolicus* MGA3 has promising features for biotechnological applications. It has an optimum growth temperature of 50°C and being a facultative methylotroph allows for growth on the C1 compound methanol. *B. methanolicus* is able to grow in seawater with comparable growth yields and -rates to more common growth medium prepared using deionized water. This both demonstrates the versatility of the species in relation to growth medium and the potential to use seawater as a cheap and abundant growth medium (Komives et al. 2005). The facultative methylotrophic nature of this species allows for growth on a relatively broad range of carbon sources, including the more common feedstocks glucose, mannitol, and arabitol, in addition to the aforementioned C1 compound methanol (Irla et al. 2020; Delépine et al. 2020). The ribulose monophosphate (RuMP) pathway with methanol dehydrogenase (MDH) as its central enzyme provides a stable production platform for several high-value substances (Brautaset et al. 2007; Müller et al. 2015). Its metabolic flexibility, in addition to well-understood metabolic pathways and a fully sequenced genome makes *B. methanolicus* MGA3 a good candidate as production hosts for a range of different compounds.

1.1.3 *Bacillus methanolicus* MGA3 as host for biotechnological production

Using more reduced compounds like methanol as carbon source leads to increased heat production, and as a result requires extensive cooling when using non-thermophilic bacteria. Being thermophilic, *B. methanolicus* negates the need for this with its optimal growth temperature of 50°C (Müller et al. 2015). In addition, higher growth temperatures reduce the risk of contaminations by common mesophilic microorganisms (Delépine et al. 2020). Another desirable characteristic of using thermophilic Bacillaceae bacteria is that most of the various strains are nonpathogenic and potentially expensive and cumbersome safety precautions can therefore be avoided. *B. methanolicus* also demonstrates a relatively high growth rate, reaching 0.46 h^{-1}, which underlines their promising protein producing capabilities (Christendat et al. 2000; Irla et al. 2020). High levels of L-glutamate over-production have been shown in the wild type strain of *B. methanolicus* MGA3 with intracellular levels of about 90 mM. Secreted amounts of L-glutamate are even more substantial in fed-batch cultures with secretions as high as 58 g/L. In addition to L-glutamate production, L-lysine has also been produced in *B. methanolicus* MGA3 mutants (strain NOA2#13A52-8A66) yielding 37 g/L, underlying the industrial production potential of the strain (Brautaset et al. 2007).

The ever-evolving genetic engineering toolkit for *B. methanolicus* MGA3 has made it a more desirable host for production of a variety of compounds. Several plasmids with varying expression systems have been developed, including expression vectors controlled by the mannitol- and xylose inducible promoters. MDH promoters have also been applied to expression vectors inducible by methanol, mimicking a natively present plasmid (Drejer et al. 2020; Irla et al. 2016; Brautaset et al. 2007). The continuously evolving possibilities for genetically modifying *B. methanolicus* open up the opportunity for utilizing alternative carbon sources and feedstocks.

1.1.4 Methanol assimilation pathway in *Bacillus methanolicus* MGA3

The initial step of methanol assimilation in *B. methanolicus* MGA3 occurs through the oxidation of methanol to formaldehyde by the action of MDH. This step is shared among several methylotrophic and methanotrophic bacteria that utilizes various assimilation pathways, including the RuMP pathway or the serine pathway (Heggeset et al. 2012; Khider, Brautaset, and Irla 2021; Antoniewicz 2019). *B. methanolicus* is also an example of plasmid-dependent methylotrophy where MDH and other enzymes that belong to the RuMP cycle are encoded by genes present on the naturally occurring plasmid pBM19. This is evident by an inability of *B. methanolicus* to grow on methanol when pBM19 is cured. pBM19 contains five genes associated with the RuMP pathway; *rpe* (ribulose-5-phosphate-3-epimerase), *tkt* (transketolase), *pfk* (phosphofructokinase), *glpX* (class II sedoheptulose bisphosphatase), and *fba* (class II fructose-1,6-bisphosphate aldolase) (Müller et al. 2014; Brautaset et al. 2007). *B. methanolicus* also possess chromosomal homologs of the plasmid encoded RuMP pathway genes, but in contrast to those found in the plasmid, the chromosomal homologs have no increased transcription when methanol is provided as sole carbon source. This further emphasizes the plasmid-dependent methylotrophic nature of this bacterium. (Müller et al. 2014). They are, however, somewhat different in their biochemical functions, with enzymes like the chromosomal homolog of FBA having lower affinity for dihydroxyacetone phosphate (DHAP) and glyceraldehyde-3-phosphate (GAP) which suggests that the plasmid encoded homologs are more likely to promote gluconeogenesis (Stolzenberger, Lindner, and Wendisch 2013). MDH in *B. methanolicus* MGA3 is a nicotinamide adenine dinucleotide (NAD^+)-dependent, cytoplasmic, and single subunit enzyme (Krog et al. 2013; Price et al. 2016).

Once methanol is oxidized by MDH to formaldehyde, the latter enters the RuMP cycle to enable carbon assimilation. First, formaldehyde undergoes a condensation reaction with ribulose-5-phosphate (Ru5P), yielding D-*arabino*-hexulose-6-phosphate (H6P). The reaction is catalyzed by 3-hexulose-6-phosphatase synthase (HPS). H6P then undergoes an isomerization reaction to fructose-6-phosphate (F6P), catalyzed by 6-phospho-3-hexuloisomerase (PHI). F6P can then branch off into two different synthesis pathways. It can enter glycolysis to generate pyruvate and GAP or enter the Ru5P regenerative pathway where two molecules of F6P together with GAP reforms three molecules of Ru5P. This can occur through two versions of the pathway: the sedoheptulose-1,7-bisphosphatase (SBPase) or the transaldolase (TA). *B. methanolicus* MGA3 possess genes for both of these pathways, and although the TA version yields an additional ATP and might appear favorable, experimental evidence suggest that SBPase might be preferred when grown on methanol due to associated pBM19 encoded genes being upregulated under these conditions (figure 1.1). In addition, a gene specific for the SBPase variant ($glpX^P$) is present on the pBM19 plasmid, whereas the TA-specific gene (ta^C) is only found in genomic DNA (Brautaset et al. 2007; Price et al. 2016; Müller et al. 2014; Delépine et al. 2020). The path of F6P through glycolysis starts with its conversion by phosphofructokinase (PFK) to fructose-1,6-bisphosphate (FBP) using one molecule of ATP. FBP is subsequently broken down into DHAP and GAP by fructose-1,6-bisphoshpate aldolase (FBPA), which then continues through the lower glycolytic pathway to generate pyruvate. The GAP generated by this cleavage enters the mentioned Ru5P regenerative pathway. *B. methanolicus* can also use 2-keto-3-deoxy-6-phosphogluconate aldolase (KDPGA) through the Entner-Doudoroff pathway to generate pyruvate from GAP and F6P. The formation of pyruvate from F6P also generates two molecules of ATP and one of NAD(P)H (Brautaset et al. 2007).

The catalysis by HPS and PHI represents the non-reversible enzymatic steps of methanol assimilation, as the conversion of methanol to formaldehyde by MDH is reversible and significantly more favored as the equilibrium is naturally shifted towards methanol. In addition, the cytotoxicity of formaldehyde promotes the need for rapid conversion either back to methanol or further assimilation through HPS and PHI. Therefore, HPS and PHI are rate-limiting steps of formaldehyde assimilation as an increased enzymatic turn-over rate would shift the equilibrium towards the RuMP pathway (Price et al. 2016). *Hps* and *phi* are genomic genes as opposed to the plasmid-based RuMP pathway genes. When *B. methanolicus* is provided methanol as sole carbon source, *hps* and *phi* are approximately 2,5-fold upregulated, and pBM19-based RuMP genes have an increase in transcription 6 – 40 times higher compared to growth on mannitol (Brautaset et al. 2007; Müller et al. 2014). In mutants without pBM19 and its associated genes, the strains have a significant increase in growth rate on mannitol compared to wild type (WT) and no growth is possible on methanol. The superior growth rate on mannitol of the pBM19-deficient strain suggests that the plasmid constitutes metabolic burden for growth when plasmid-encoded genes are not necessary to support growth (Brautaset et al. 2007).

Changes in the fluxome and proteome when *B. methanolicus* is grown on mannitol and methanol show clear differences in which metabolic pathways are affected. *B. methanolicus* also expresses the enzymes required for a complete tricarboxylic acid (TCA) cycle when grown on both substrates. Four of the five energy-producing enzymes in the TCA cycle were upregulated when grown on mannitol, these being 2-oxoglutarate dehydrogenase, isocitrate dehydrogenase, succinate dehydrogenase, and succinyl-CoA ligase. During growth on mannitol, energy is primarily derived from the TCA cycle, and the increased expression of these enzymes could permit a higher influx of substrates (Müller et al. 2014).

The tolerance to methanol and, by extension, formaldehyde changes depending on carbon source. Strain MGA3AC-A6 was generated by successive growth of *B.methanolicus* on mannitol, leading to the subsequent loss of the pBM19 plasmid. Mutant cells displayed an increased tolerance to methanol by as much as a tenfold increase in concentration, when compared to wild type. Simultaneously, the same strain suffered cytotoxic effects at half the concentration of formaldehyde compared to wild type. The increased tolerance to methanol is a result of loss of activity of plasmid encoded MDH converting methanol to toxic formaldehyde, yielding a higher tolerance. The reduced tolerance to formaldehyde is linked to loss of plasmid-encoded RuMP pathway enzymes leading to decreased formaldehyde assimilation and the cytotoxic effects are observed earlier (Brautaset et al. 2007).

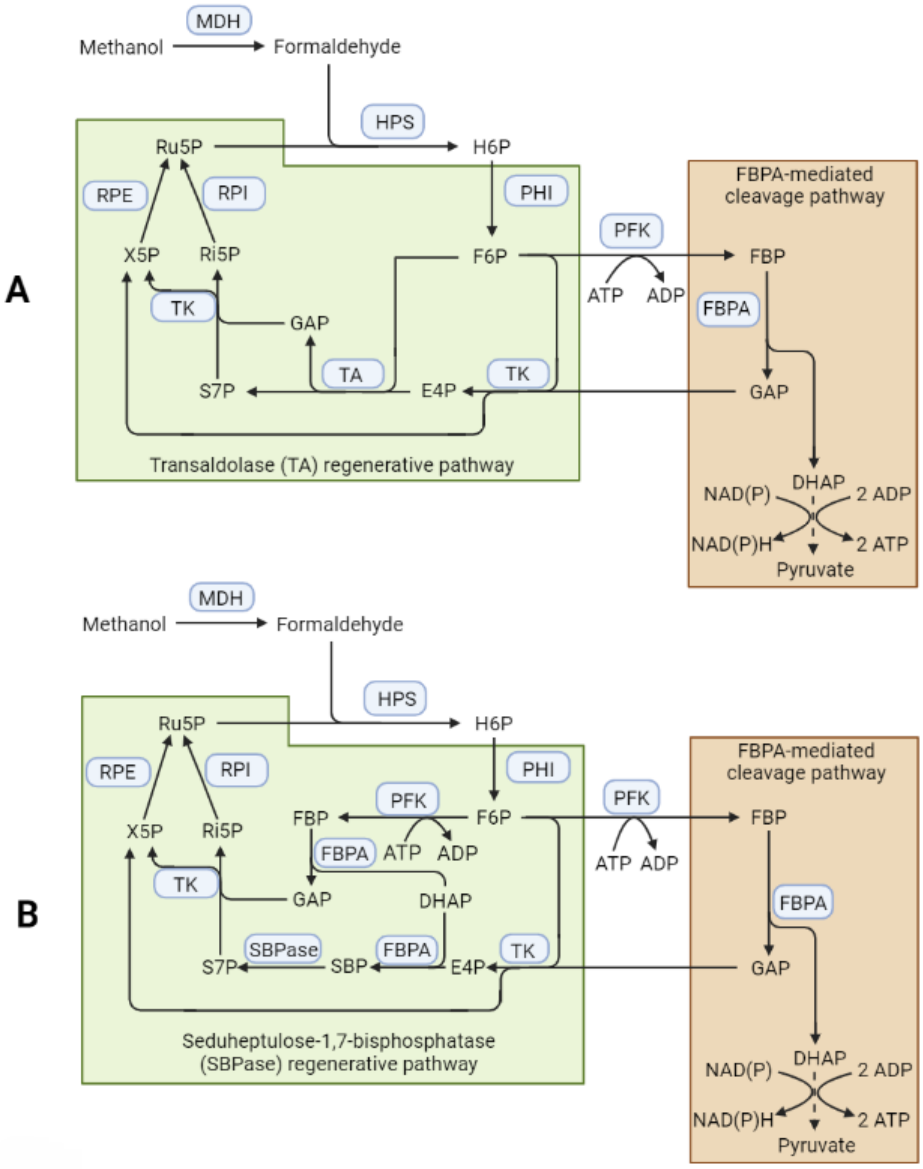

Figure 1.1 TA (A) and SBPase (B) regenerative pathways and their connection through F6P to the FBPA-mediated cleavage pathway of FBP. Formaldehyde undergoes a condensation reaction with Ru5P catalyzed by HPS to form H6P. H6P is then converted to F6P by PHI. F6P can either enter the regenerative pathways to form Ru5P and subsequently reform H6P, or it can be phosphorylated by PFK and enter the FBPA-mediated cleavage pathway. Here it will provide GAP for the RuMP pathways and DHAP for the lower glycolysis pathway. Enzymes are marked in blue: Transketolase (TK), ribose-5-phosphate isomerase (RPI), ribulose-5-phosphate-3-epimerase (RPE). Abbreviations of intermediates: erythrose-4-phosphate (E4P), septuheptulose-7-phosphate (S7P), xylulose-5-phosphate (X5P), sedoheptulose-1,7-bisphosphate (SBP). For other abbreviations see text (Brautaset et al. 2007; Müller et al. 2014).

1.1.5 Synthetic methanotrophy

The construction of heterologously expressed pathways for methane utilization in production hosts is a highly researched field having garnered substantial interest in the last decade. Using methylotrophs as a basis for synthetic methanotrophy is an appealing option, given the shared methanol assimilation pathways. With a bacterium such as *B. methanolicus* MGA3, synthetic methanotrophy can be achieved by the introduction of the single enzymatic step catalyzed by methane monooxygenase (MMO). Due to MDH being a central enzyme in methylotrophs, replenishment of reducing factors, crucial for efficient methane assimilation, is already present (Wang et al. 2019). Overexpression of HPS and PHI could also increase metabolic flux through, for example, the RuMP pathway and improve methane oxidation rates. Coupling oxidation by soluble methane monooxygenase (sMMO) with a high-flux assimilation pathway through homologous expression of the rate-limiting enzymes HPS and PHI has the potential to provide a platform for more efficient utilization of methane or methanol with increased product titers (Price et al. 2016).

Attempts to express sMMO and assimilation pathways in more common production hosts, like *E. coli*, have had limited success. Although two of the three subunits of sMMO have been successfully expressed in active forms, the multi-component nature of the third subunit involves the need for proper folding and assembly (Murrell, McDonald, and Gilbert 2000; West et al. 1992). Co-producing the appropriate chaperone proteins appears to be crucial to achieve production of a functional protein. Experimental evidence showed that native chaperones from the donor organism *Methylococcus capsulatus* (Bath) increased the conversion rate of MMO in the *E. coli* host (Clark 2019). In addition, host organism chaperones also increased conversion rate, suggesting some overlapping and protein interchangeability between the two species (Clark 2019). Optimizing chaperon composition is therefore a necessity for proper heterologous expression. The so far unsuccessful expression of sMMO in common production hosts could also be attributed to the complex nature of the MMO operon. The multi-subunit nature of sMMO complicates proper folding and maturation into a functional enzyme due to the multiple genes having to be correctly expressed and processed. Some of the MMO genes also serve secondary and auxiliary functions which could easily be overlooked or create unknown protein interactions limiting production of a functional enzyme or subunit (Khider, Brautaset, and Irla 2021). The effect of copper on functional MMO expression and production must also be considered in heterologous hosts, as copper is a common trace metal in growth media, including the mentioned methylotroph *B. methanolicus* MGA3. Although *B. methanolicus* MGA3 shares the majority of methanol assimilation pathways as native methanotrophs, expressing these in for example *E. coli* requires extensive metabolic engineering. However, important mechanisms associated with MDH, and the RuMP pathway must be taken into consideration. One of these being the need for an efficient system for regenerating electrons. The obvious solution would be to introduce systems already present in native methanotrophs like NAD or pyrroloquinoline quinone (PQQ), which adds to the list of requirements for functional expression of MMO (Wang et al. 2019).

Particulate MMO (pMMO) is the most prevalent catalyst for methane oxidation in nature and shows more favorable enzyme kinetics in relation to K_M than sMMO (Xin et al. 2019). However much of the electron transport in pMMO is unknown and the electron donor for natively expressed pMMO has yet to be elucidated. The difficulty in solubilizing and characterizing functional pMMO is also a major hurdle for heterologous expression in other production hosts. Another aspect in need of verification is the ability of methanotrophs to adapt to fluctuating environmental conditions, especially related to nitrogen and sulfur sources. These various knowledge gaps prevent the construction of accurate models for

metabolic engineering and make it difficult to predict useful pathway elements to target (Kalyuzhnaya, Puri, and Lidstrom 2015).

1.1.6 Native methanotrophs

Methanotrophs are aerobic or anaerobic proteobacteria capable of utilizing methane as their sole energy and carbon source and are a sub-group of methylotrophs. The aerobic methanotrophs share several features with other methylotrophs, and much of the carbon assimilation pathways are identical (figure 1.2), with the distinguishing feature being MMO, either as a soluble (sMMO) or particulate (pMMO) type. Methanotrophs are primarily categorized in *Gammaproteobacteria* (type I/X) and *Alphaproteobacteria* (type II), where the methane assimilation pathways and certain intracytoplasmic membrane structures determine the type. Type I uses the RuMP pathway to assimilate formaldehyde obtained via methane oxidation and have intracytoplasmic membranes arranged in a stacked formation. An example of type I methanotrophs is the genus *Methylobacter.* Type II methanotrophs assimilate methane through the serine cycle and have cytoplasmic membranes positioned peripherally. Examples of type II methanotrophs are *Methylocystis* and *Methylosinus*. Type X methanotrophs primarily utilize the RuMP pathway and are similar to type I methanotrophs which places them in the same *Gammaproteobacteria* class. However, type X methanotrophs also express enzymes related to the serine pathway, mainly ribulose bisphosphate carboxylase (Rubisco) which is found in the Calvin-Benson cycle (Hanson and Hanson 1996; Khider, Brautaset, and Irla 2021). In addition, some type X methanotrophs are classified based on nitrogen fixation or higher optimal growth temperature (Knief 2015). Aerobic methanotrophs universally utilizes MMO to oxidize methane to methanol, regardless of their type.

Certain characteristics of methanotrophs are less desirable in an applied biotechnology setting. Among these are more complicated growth conditions, as seen in *Methylococcus capsulatus* (Bath) requiring nitrate mineral salts medium (NMS), with associated relatively slow growth rates (0.25 h^{-1} and 0.37 h^{-1} in low- and high copper medium respectively), despite NMS being the optimal growth medium for the species (Joergensen and Degn 1987). Comparing the growth rate to *E. coli* in minimal media (0.4-0.7 h^{-1}) highlights the slower growing methanotroph (Pieja, Morse, and Cal 2017). In addition, much of the details surrounding the metabolic pathways of methanotrophic bacteria are still unknown. Native methanotrophs today are mainly used for single cell protein (SCP) production of animal feed biomass, like proteins for monogastric animals (Øverland et al. 2010). SCP production faces several issues on an industrial scale. Methane-to-oxygen mixtures in the ratios required for methanotrophic fermentation are highly flammable and pose a certain risk. In addition, significant risk of contamination, toxicity from heavy metals and *n*-alkane contaminants in natural gas, and having to treat and remove high levels of nucleic acid co-products seen in SCP, are some of the issues facing efficient SCP using methanotrophs (Kalyuzhnaya, Puri, and Lidstrom 2015). Although genetic engineering tools and methods for methanotrophs are evolving, they are still limited compared to production hosts like *E. coli* and this has been one of the key factors for the limited use of native methanotrophs in biotechnological production (Gregory, Bennett, and Papoutsakis 2022).

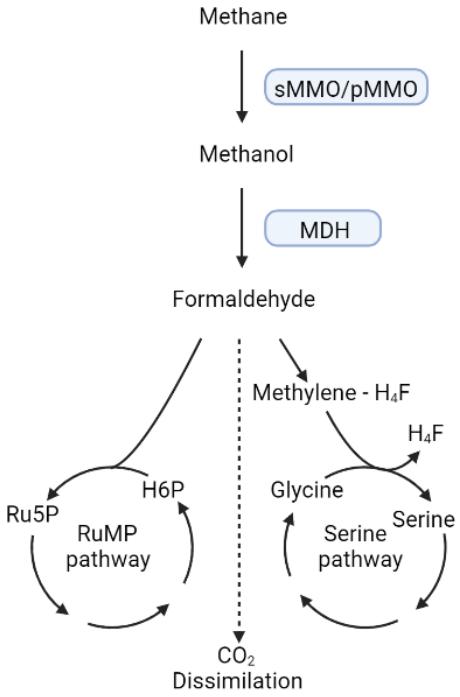

Figure 1.2: General metabolic pathway of carbon in methylotrophs with the oxidation of methane by sMMO/pMMO separating methanotrophs from other methylotrophs. Further methanol assimilation pathways used by methylotrophic bacteria where type I methanotrophs utilize the RuMP pathway, and type II utilize the serine cycle. Type X methanotrophs primarily use the RuMP pathway but produces enzymes (mainly Rubisco) of the serine pathway, through its connection with the Calvin-Benson cycle (Khider, Brautaset, and Irla 2021; Hanson and Hanson 1996).

1.1.7 Methane monooxygenase

Methane monooxygenases (MMOs) are multimeric oxidizing metalloenzymes catalyzing the conversion of methane to methanol. This is done through first splitting molecular oxygen, followed by breaking the C-H bond in methane (Khider, Brautaset, and Irla 2021; Wang et al. 2017). Atomic oxygen is subsequently incorporated with hydrogen to form methanol. MMO exists as two distinct types; the membrane-bound particulate MMO (pMMO), and the cytoplasmic soluble MMO (sMMO), both displaying differing characteristics in activity, stability, substrate range, and inhibitor susceptibility (In Yeub et al. 2014; Murrell and Smith 2010). Despite both catalyzing the same reaction, they share little in their genetic makeup. pMMO is expressed in most aerobic methanootrophs, whereas sMMO is only found in a subset of methanotrophic bacteria, most notably *Methylococcus capsulatus* (Bath) and *Methylosinus trichosporium* OB3b (Murrell, McDonald, and Gilbert 2000). pMMO incorporates copper in its active site and is expressed under conditions where copper is available in the environment. sMMO utilizes iron in the active site and its activity is suppressed with increasing copper concentration, and the enzyme is usually present in concentrations up to 5.64 µmole Cu^{2+} per gram protein (*Methylosinus trichosporium* OB3b) (Khider, Brautaset, and Irla 2021). This transition from soluble to particulate types of the enzyme is often referred to as the "copper switch", where the transition between the two can be seen within 48 hours after transferring cultures of *M. capsulatus* (Bath) from a low copper medium to a high copper medium (Stanley et al. 1983). The mechanism of the copper switch has not been fully discovered but proposed models suggest that a protein,

MMOD, encoded by the gene *mmoD* functions as a transcription regulator which represses the expression of pMMO at low copper concentrations while promoting the expression of sMMO. A peptide called methanobactin increases the expression of sMMO. In high copper conditions, both MMOD and methanobactin binds copper which inhibits the activity of both, leading to MMOD not being able to repress pMMO, as well as reduced expression of sMMO due to inactive methanobactin (Semrau et al. 2013). Structural differences of the two types of MMO have been difficult to establish, mostly due to the problematic purification of pMMO.

sMMO has been extensively studied and characterized, primarily from *Methylococcus capsulatus* (Bath) and *Methylosinus trichosporium* OB3b. sMMO is characterized as a bacterial multicomponent monooxygenase (BMMs), which as a group consists of at least three central enzymatic components; a hydroxylase, an oxidoreductase, and a regulatory protein. BMMs are further characterized by containing at least one non-heme carboxylate-bridged diiron protein. These enzymatic components are represented in sMMO by MMOH (hydroxylase), MMOR (reductase), and MMOB (regulatory protein). The three protein components total about 305 kDa. MMOH is a trimeric protein consisting of an $\alpha_2\beta_2\gamma_2$ homodimer. The α subunit of MMOH contains the catalytic diiron active site which facilitates the hydroxylation of methane and is the largest sMMO subunit of 251 kDa (Wang et al. 2017). Genetically, the α, β, and γ subunits are arranged as *mmoXYZ,* where *mmoX*, *mmoY,* and *mmoZ* corresponds to the α, β, and γ subunits respectively (figure 1.3) (Wang et al. 2017; Sirajuddin and Rosenzweig 2015).

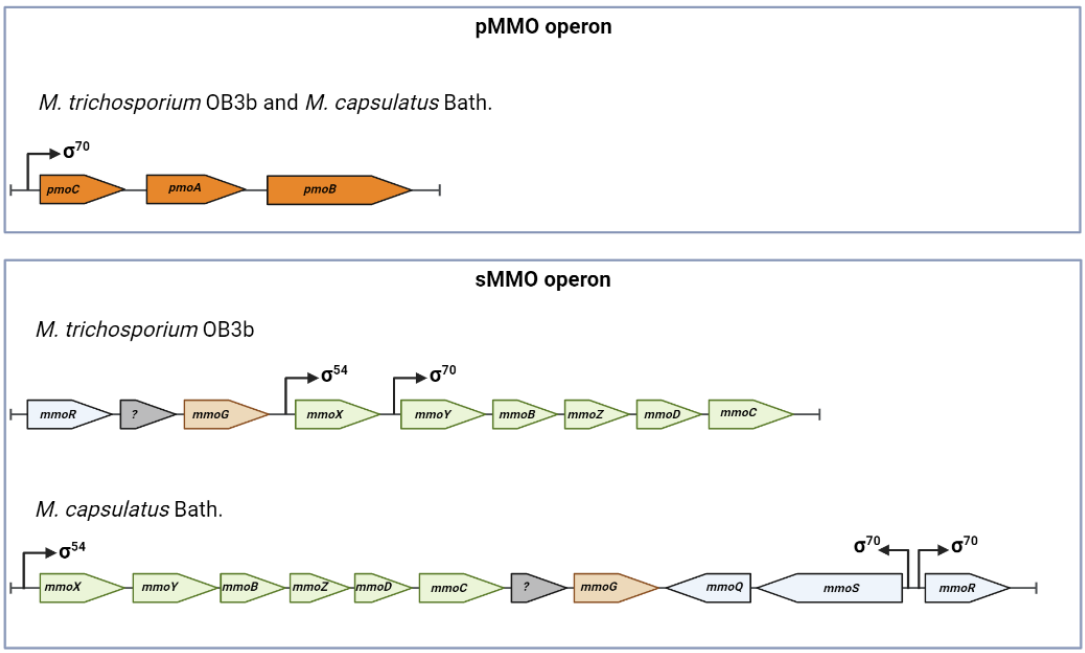

Figure 1.3: Gene arrangement of the MMO operons of *M. trichosporium* OB3b and *M. capsulatus* Bath. pMMO contains the three genes *pmoC, pmoA,* and *pmoB* where *pmoC* have three copies and *pmoA* and *pmoB* have two each and are identical in both *Methylosinus trichosporium* OB3b and *Methylococcus capsulatus* (Bath). The genes for sMMO (green) are arranged in six consecutive fragments, with MMOH having its α, β, and γ subunits encoded by *mmoX, mmoY, and mmoZ* respectively. The regulatory protein MMOB is encoded by *mmoB*, and the reductase MMOR is encoded by *mmoC.* The GroEL-like chaperonin is encoded by *mmoG* (light brown). A protein believed to have regulatory function is encoded by *mmoD*. *mmoQ* and *mmoS* (light blue) encode what is believed to be related to the "copper switch" through a dual-component protein system. *mmoR* (light blue) encodes the reductase MMOR component of sMMO, and the dark grey gene encodes an unidentified open reading frame, also referred to as a hypothetical protein (MCA1201). Promoter sites and their associated sigma factor families are shown by arrows (Khider, Brautaset, and Irla 2021; Sirajuddin and Rosenzweig 2015).

The reductase component MMOR of sMMO is responsible for the transfer of two electrons to the diiron active site in the α subunits of MMOH. This electron transfer occurs through ferrodoxin and flavin adenine dinucleotide (FAD) and is dependent on NADH. MMOR is encoded by *mmoC* and the subunit is 38.5 kDa (Sirajuddin and Rosenzweig 2015). In addition to MMOD and methanobactin, MMOH and MMOR also appear to play a major role in the "copper switch". Evidence suggests copper ions disrupt the structure of MMOH causing it to lose its diiron-sulfur center in the α-subunit which in turn stops the electrons from being delivered by MMOR. The copper ions additionally cause FAD to dissociate from MMOR, resulting in the protein not being able to receive electrons from NADH (Green, Prior, and Dalton 1985). The regulatory MMOB subunit interacts with MMOH to increase the reaction rate by 1000-fold. This is achieved through affecting the structure of the diiron center and lowering its redox potential, altering the structure through conformational changes, and changing the regioselectivity of the oxidation reaction (Sirajuddin and Rosenzweig 2015; Wang et al. 2017).

The enzymatic activity of sMMO starts with priming the active site by the reduction of the diiron center from Fe(III) to Fe(II), catalyzed by MMOR. The Fe(II) active site reacts with O_2 to generate a diiron(III)-peroxo intermediate, often referred to as intermediate P. The

transport of O_2, as well as methane, to the active site is facilitated by the mentioned allosteric changes induced by MMOB. Intermediate P then undergoes a conversion to intermediate Q by breaking the O-O bond. Intermediate Q facilitates the breaking of the C-H bond in methane and its subsequent conversion to methanol. Intermediate Q also alters the oxidation state of the diiron sites from Fe(III) to Fe(IV) (figure 1.4) (Wang et al. 2017; Khider, Brautaset, and Irla 2021; Sirajuddin and Rosenzweig 2015).

Compared to the narrow substrate range of pMMO, sMMO oxidizes a range of compounds and displays significant catalytic versatility. This is somewhat exemplified by the ability sMMO possesses to oxidize compounds whose product is incompatible as a nutrient source for the bacteria. Among the substrates for sMMO are alkanes, like methane and propane, alkenes, including alkene oxidation to epoxides, alicyclic hydrocarbons, like cyclohexane and methylene, halogenated aliphatics, like trichloroethene, mono- and diaromatics, like benzene and naphthalene respectively, and substituted methane derivatives, like chloromethane and chloroform (Smith and Dalton 2004). The known substrates of sMMO's extend beyond a 100 compounds, and this significantly broad substrate range makes it a prime candidate for synthetic biotechnological applications (Smith and Nichol 2018).

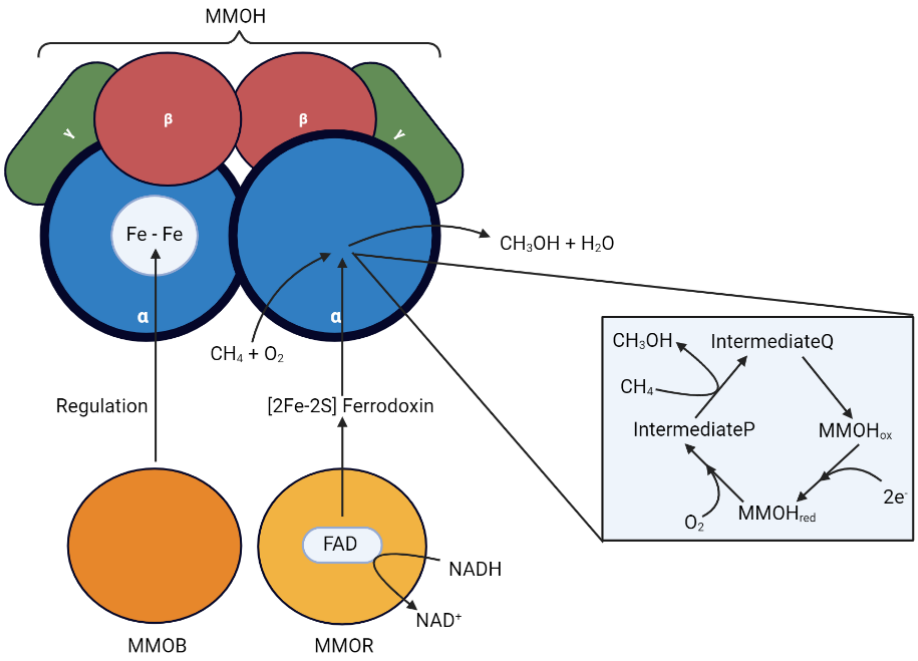

Figure 1.4: Simplified schematic overview of sMMO with MMOH (hydroxylase), MMOB (regulatory), and MMOR (reductase). The trimeric protein conformation of MMOH is responsible for the oxidation of methane in the presence of oxygen to methanol and water, which occurs in the α subunit of MMOH. Oxidation of methane accompanies the conversion of intermediate P into intermediate Q. MMOB regulates the catalytic activity through interactions with, among other things, the diiron center in the α subunit of MMOH. This regulation also facilitates a conformational change, opening up the α subunit to permit the transport of methane and oxygen to the active site. MMOR delivers electrons for the oxidation reaction through the reduction of FAD by NADH. The electrons are then transported using ferrodoxin to the active site of subunit α of MMOH (Wang et al. 2017; Hwang et al. 2018).

1.2 Enzymatic acitivity of MMO

With the broad substrate range and potent oxidative capabilities of sMMO, finding a suitable substrate for assaying its activity might appear unproblematic. Accurate measurements of enzyme activity are crucial in determining how efficient the enzyme catalyzes reactions when changing parameters like carbon source, growth medium, temperature, pH, trace elements, and incubation time. Measurements of sMMO activity have been conducted on native methanotrophs for some time, however the impact of cellular mechanisms like electron donation means that measuring heterologously expressed sMMO is more difficult. In native methanotrophs, existing electron donation systems are present, meaning that in heterologously expressed strains, reducing agents needs to be added. This has often been achieved by formate or sodium formate in enzyme activity measurements (Sirajuddin and Rosenzweig 2015). Using methylotrophs as hosts for synthetic methanotrophy means that certain electron replenishment systems, like PQQ or NAD, could provide the necessary reducing equivalents. However, these systems in methylotrophic bacteria are used to facilitate enzymatic reactions such as that of MDH and other assimilatory enzymes, and it is unknown how the addition of MMO could affect availability of reducing agents. In addition, being able to distinguish between the activity of sMMO and pMMO is important (Miller et al. 2002).

1.2.1 Current methods for measurements of MMO activity

Previous and current methods for measuring MMO activity have relied on detection and quantification of oxidated co-metabolic substrates by gas chromatography (GC) or high-performance liquid chromatography (HPLC). Substrates such as propylene are oxidized to propylene oxide, which can be measured through separation in GC. Propylene oxide cannot be further processed by assimilation pathways in methanotrophs or other methylotrophs and therefore accumulates, yielding a stable quantifiable product. In addition, propylene oxide is detectable in supernatant fractions when tested on *Methylococcus capsulatus* and *Methylosinus trichosporium*, showing that propylene oxide is transported out of the cell after formation. The substrate oxide therefore provides a fairly accurate measurement of MMO activity. This does not however provide a distinction between pMMO and sMMO as propylene is a substrate for both forms of the enzyme (Sirajuddin and Rosenzweig 2015; Hou et al. 1979). Measuring the epoxidation rate of propene and the conversion of cyclohexane to cyclohexanol and cyclohexanone with GC are also options to determine MMO activity (Park et al. 1992; Esmelindro et al. 2005). HPLC can be used to determine the concentration of 1-naphthol and 2-naphthol, both results from oxidizing naphthalene by MMO (Zhou et al. 2016). 1-naphthol can also be observed spectrophotometrically where 2-naphthylamine-5,7-disulfonic acid is added to the solution containing 1-naphthol. The resulting interactions create a reddish coloration which can be quantified by measuring the resulting absorbance (Parsons, Seaman, and Woods 1955). Being able to distinguish the soluble and particulate versions of MMO can be achieved through enzyme specific substrates. Chloroform is a substrate specific to sMMO and cannot be oxidized by pMMO. Chloroform degradation rates can therefore be used to determine specific sMMO catalytic activity by GC, often as a cometabolite with for example propylene (Jahng and Wood 1994).

Chromatographic methods display high accuracy and allow for the detection and measurement of specific enzyme products, like propylene oxide or cyclohexanol. Although chromatographic approaches to measuring MMO activity have been used for decades, they also have several downsides. GC and HPLC are expensive machines which often require accessory components. To achieve the highest accuracy possible with these methods it often needs associated equipment like mass spectrometers, making them time-consuming

and cumbersome. This can be further exacerbated by slow growth rates of cultures and substrate incubation time. Spectrophotometric measurements, as the mentioned interactions between 1-naphthol and 2-naphthylamine-5,7-disulfonic acid, are fast and relatively simple but does not possess the desired accuracy, especially when analyzing more complex culture media (Wackett and Gibson 1983). GC and HPLC additionally require training and expertise for proper operation of the machine. Fast, reliable, and accurate assay techniques using readily available substrates without the need for further processing is therefore highly sought after.

1.2.2 Formation of fluorescent products from oxidized substrates

Miller et al. described a fluorescence-based assay for observing the presence of sMMO, by measuring the fluorescence of several products after oxidation by the enzyme. Of the compounds tested, only coumarin had measurable fluorescence (Miller et al. 2002). Coumarin is an organic compound containing benzopyrone, characterized by fused benzene and pyrone rings, and is an o-hydroxycinnamic acid. The compound is found naturally in many plants, most notably the tonka bean. Coumarin has a pleasant vanilla-like odor and has been used extensively as sweetener and odor stabilizer (Egan et al. 1990). Coumarin has been shown to be a substate of sMMO and when oxidized forms, among other things, 7-hydroxycoumarin which is also referred to as umbelliferone (Mazimba 2017; Miller et al. 2002). The conversion of coumarin by sMMO have been demonstrated in several native methanotrophs, including *Methylosinus trichosporium* OB3b (Miller et al. 2002). 7-hydroxycoumarin exhibits fluorescence emission over a relatively broad wavelength (ca. 330-450 nm) when subjected to appropriate excitation wavelength (figure 1.5) (Ye et al. 2019). Much like propylene oxide, 7-hydroxycoumarin cannot be further assimilated by methanotrophs and therefore negates the need for rapid processing due to degrading oxidated product. Other colorimetric assays have also been developed to negate the need for instruments for fluorescence measurements.

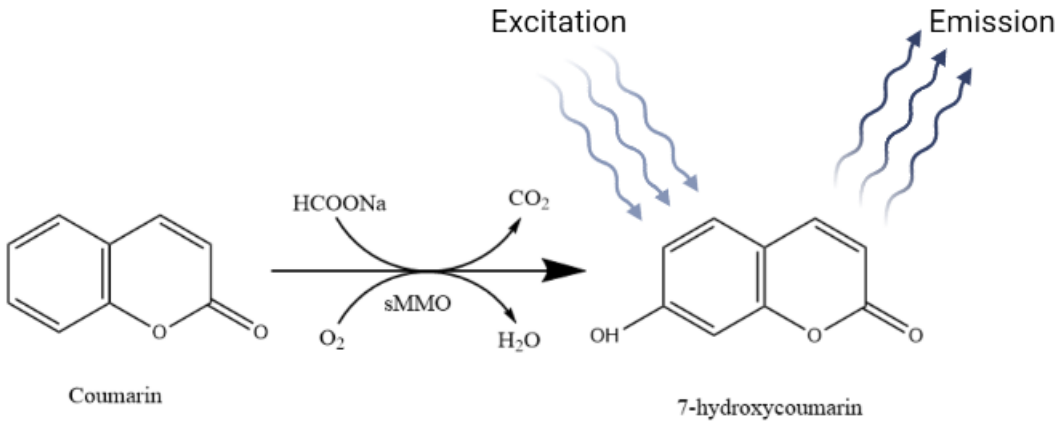

Figure 1.5: Conversion of coumarin to 7-hydroxycoumarin by sMMO. Sodium formate (HCOONa) acts as the reducing agent, providing electrons for the oxidation reaction with oxygen catalyzed by the MMOH subunit of sMMO. The resulting product, 7-hydroxycoumarin, displays fluorescence under the right excitation wavelength and can be measured. Amount of measured fluorescence is proportional to the amount of 7-hydroxycoumarin formed from coumarin, and therefore proportional to oxidation rate of sMMO (Sirajuddin and Rosenzweig 2015; Miller et al. 2002).

1.2.3 Formation of color complexes from oxidized substrates

The oxidation of naphthalene to 1- and 2-naphthol can be quantitatively and qualitatively assessed through an alternative assay to the ones already mentioned, as reported by Wackett and Gibson (Wackett and Gibson 1983). Interactions between naphthol and tetrazotized o-dianisidine create a purple-colored diazo compound which can be measured by spectrophotometry, or visually inspected, as the compound formed displays a bright and strong color (figure 1.6). It has been repeatedly demonstrated to detect naphthols in several organisms. These include the bacteria *Pseudomonas putida, Pseudomonas sp., Methylosinus trichosporium* OB3b, *Methylococcus capsulatus* (Bath)*, E. coli* and the fungus *Cunninghamella elegans* (Wackett and Gibson 1983; Graham et al. 1992; Brusseau et al. 1990). Thus far, the colorimetric naphthalene assay has only been applied to native methanotrophs and its usage for qualitative determination of heterologously expressed sMMO is therefore unknown. Despite this, it can theoretically be used to determine the presence of functional sMMO in heterologous organisms.

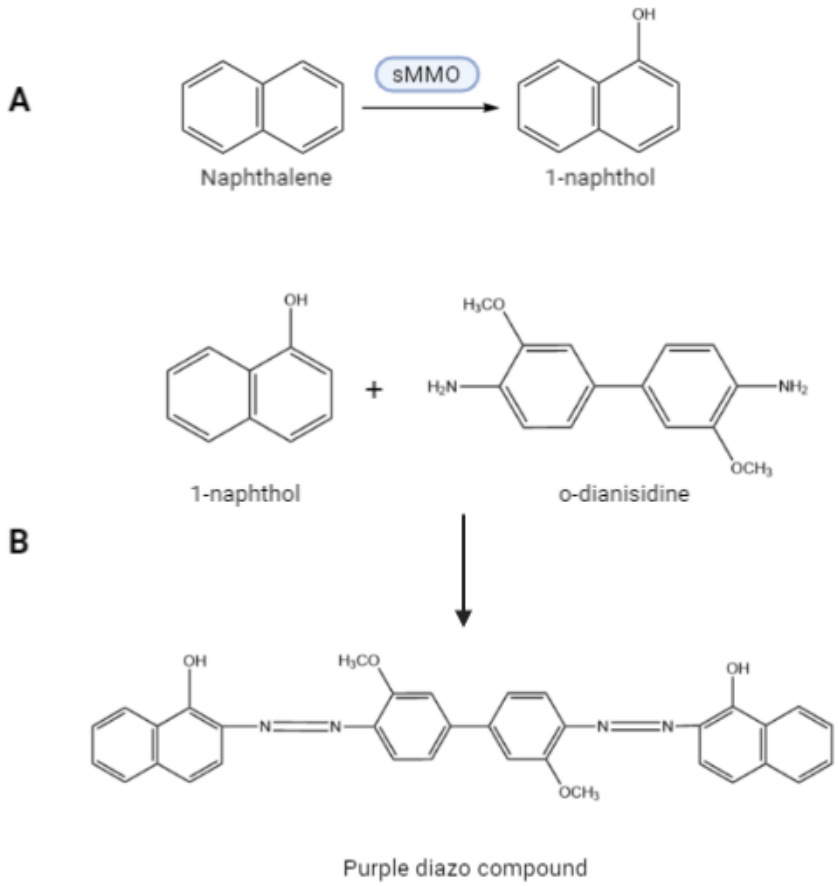

Figure 1.6: Formation of the diazo colored compound from 1-naphthol and tetrazotized o-dianisidine. A: 1-naphthol is formed from the oxidation of naphthalene by sMMO. B: 1-naphthol reacts with tetrazotized o-dianisidine to form the purple diazo complex (Wackett and Gibson 1983; Cieśla et al. 2015).

1.3 Aims of the project

To assess functional proteins of sMMO in *B. methanolicus* MGA3, expression- and co-expression strains will be created carrying both sMMO and various chaperonins. In addition, expression- and co-expression strains carrying the hypothetical protein (MCA1201) would permit the assessment of the proteins effect on sMMO activity. These strains will allow for the study of the interactions between sMMO and various chaperonins from both the donor species *Methylococcus capsulatus* (Bath) and the host organism itself.

The heterologous expression of sMMO in *Bacillus methanolicus* MGA3 lacks easy and convenient assay methods. This study aims to adapt and test a fluorescence-based assay of sMMO expression in *B. methanolicus* MGA3 which could be applied without the need for chromatography-based analysis of oxidized products. The assay was originally based on detection of sMMO in native methanotrophs, and its application in *B. methanolicus* MGA3 can allow for a proof-of-concept determination of heterologously produced sMMO without the need for growth on methane. The assay will be applied to whole cell cultures and supernatant after cell lysis to determine the potential efficacy of the assay on different cell conditions. The impact of copper will also be investigated with both high- and low copper concentration growth medium.

In addition, this study aims to assess the effects on methanol assimilation through over-expression of the two rate-limiting enzymes for methanol metabolism: 3-hexulose-6-phosphate synthase (HPS, EC:4.1.2.43) encoded by the gene *hps* (BMMGA3_06845) and 3-hexulose-6-phosphate isomerase (PHI, EC:5.3.1.27) encoded by the gene *phi* (BMMGA3_06840) to determine the effects on growth rate and methanol tolerance under varying concentrations of methanol. The effects of promoter will also be examined where both genes will be cloned to be controlled by both their native promoter and the *mdh*-inducible promoter.

2 Materials and methods

2.1 Growth media and solutions

The content and components of all growth media, buffers, and solutions used in this study are presented in appendix A.

2.2 Bacterial strains, fragments, and plasmids

E. coli strain used consisted of DH5α (Stratagene) as general cloning host for plasmid constructs. For heterologous expression in synthetic methanotrophy and methanol assimilation, *B. methanolicus* MGA3 (ATCC 51375) was used as expression host. List of all strains of *B. methanolicus* MGA3 are presented in table 2.1. Plasmids and their relevant gene fragments are listed in table 2.2. *Methylococcus capsulatus* (Bath) (ATCC 33009) was used as positive control in the naphthalene oxidation assay.

Table 2.1: Strains of *B. methanolicus* MGA3 used in this study

Strain:	Abbreviation:	Description:	Reference:
Wild type	WT	Wild type strain	ATCC 51375
pBV2xp	BVEV	Empty vector strain	Previous work
pTH1mp	THEV	Empty vector strain	Previous work
pUB110Smp	UBEV	Empty vector strain	This study
pBV2xp-mmo	mmo	Strain carrying sMMO without the hypothetical protein (MCA1201)	Previous work
pBV2xp-mmoH	mmoH	Strain carrying sMMO with hypothetical protein (MCA1201)	Previous work
pUB110Smp-hps-phi	UBMet.P	Strain for homologous expression of *hps* and *phi* under P_{xyl}	This study
pUB110-hps-phi	UBNat.P	Strain for homologous expression of *hps* and *phi* controlled by native promoter	This study
pTH1mp-hps-phi	THMet.P	Strain for homologous expression of *hps* and *phi* controlled by mdh promoter (P_{mdh})	
pTH-hps-phi	THNat.P	Strain for homologous expression of *hps* and *phi* controlled by native promoter	
pBV2xp-mmoH + pTH1mp-groESL1	groESL1	Co-expression strain carrying sMMO with hypothetical protein and chaperonins groES1 and groEL2 from *M. capsulatus* (Bath)	This study
pBV2xp-mmoH + pTH1mp-groESL2	groESL2	Co-expression strain carrying sMMO with hypothetical protein and chaperonins groES2 and groEL2 from *M. capsulatus* (Bath)	This study
pBV2xp-mmoH + pTH1mp-groESL_BM	groESL_BM	Co-expression strain carrying sMMO with hypothetical protein and chaperonin groS-groL from *B. methanolicus* MGA3	This study

Table 2.2: Plasmid backbones and constructs with relevant fragments used in this study.

Plasmid	Description	Fragment(s)	Reference
pBV2xp	Kan^R; pHCMC04 derivative under control of the inducible xylose promoter (P_{xyl}), theta replicating	-	Drejer et al. (2020)
pBV2xp-mmo	Kan^R; pHCMC04 derivative, contains the genes for the sMMO enzyme from *M. capsulatus* (Bath), P_{xyl}	*smmoX-Y-B smmoZ-D-C*	Previous work
pBV2xp-mmoH	Kan^R; pHCMC04 derivative, contains the genes for sMMO enzyme from *M. capsulatus* (Bath) including the unidentified ORF/hypothetical protein (MCA1201), P_{xyl}	*smmoX-Y-B smmoZ-D-C-H*	Previous work
pTH1mp	Cm^R; pTH1mp-*lysC* derivative with *lysC* being substituted with a multiple cloning site, controlled by P_{mdh}	-	Irla et al. 2016
pTH1mp-groESL1	Cm^R; pTH1mp-*lysC* derivative, contains the genes for chaperonins groES1 and groEL2 from *M. capsulatus* (Bath), P_{mdh}	*groEL2 groES1*	Previous work
pTH1mp-groESL2	Cm^R; pTH1mp-*lysC* derivative, contains the genes for chaperonins groES2 and groEL2 from *M. capsulatus* (Bath), P_{mdh}	*groEL2 groES2*	Previous work
pTH1mp-groESL_BM	Cm^R; pTH1mp-*lysC* derivative, contains the gene for chaperonin groS-groL from *B. methanolicus* MGA3, P_{mdh}	*groS-groL*	Previous work
pTH1mp-hps-phi	Cm^R; pHCMC04 derivative, contains the genes for HPS and PHI from *B. methanolicus,* P_{mdh}	*hps phi*	This study
pTH-hps-phi	Cm^R; pHCMC04 derivative, contains the genes for HPS and PHI from *B. methanolicus* under control of the native promoter	*hps phi* Native promoter	This study
pUB110Smp	Kan^R; pUB110 derivative, Shuttle vector for *E. coli*/*Bacillus* spp., controlled by *mdh* promoter (P_{mdh})	-	Irla et al. 2016
pUB110Smp-hps-phi	Kan^R; pUB110 derivative, contains the genes for HPS and PHI from *B. methanolicus* MGA3, P_{mdh}	*hps phi*	This study
PUB110-hps-phi	Kan^R; pUB110 derivative, contains the genes for HPS and PHI from *B. methanolicus* MGA3, controlled by native promoter from *B. methanolicus* MGA3	*hps phi* Native promoter	This study

2.3 Growth conditions and storage of strains

E. coli DH5α was cultivated using liquid LB-medium at 225 rpm and 37°C using an Infors™ Multitron Standard shaker incubator. For colony incubation of DH5α on solid medium, LB with added agar was used (37°C). All strains of *B. methanolicus* MGA3 were cultivated at 50°C, with 200 rpm shaking in liquid media using a New Brunswick™ Innova 42 Incubator Shaker (Eppendorf). Media used for *B. methanolicus* MGA3 was SOB or MVcM/MVcMY minimal medium supplemented with 200 mM methanol (MVcM/MVcMY$_{200\ mM\ (MeOH)}$) and the additional components listed in appendix A. For colony cultivation of *B. methanolicus* MGA3 on solid media, SOB, MVcM or MVcMY supplemented with agar was used. Liquid SOB and MVcMY were used in preparing electrocompetent *B. methanolicus* MGA3 cells. Selective cultivation of transformants with reporter gene and cultivation of plasmid-containing strains were done using the antibiotics chloramphenicol (Cm) or kanamycin (Kan). A concentration of 25 µg/mL Cm and 50 µg/mL Kan was used for *E. coli* DH5α and 5 µg/mL Cm or 25 µg/mL Kan for *B. methanolicus* MGA3. Co-expression strains of *B. methanolicus* MGA3 had growth media supplemented with both Cm and Kan in the stated concentrations. Antibiotic resistance for each plasmid is listed in table 2.2. Induction of strains containing the pBV2xp plasmid and constructs using this backbone was done using a final concentration of 0.5% xylose in liquid media, and 1% in solid media. Remaining constructs using the pTH1mp and pUB110Smp plasmid backbones under the control of P_{mdh} were induced with 200 mM MeOH. *M. capsulatus* (Bath) was cultivated on nitrate mineral salts (NMS) (ATCC medium 1306) supplemented with agar and 0.8% methanol (V/V) at 40°C. Growth rate and cell density of liquid cultures were determined by measuring the optical density at 600 nm (OD_{600}) with a Ultrospec™ 10 Cell Density Meter (Amersham Biosciences).

Long term storage of all strains used in this study was done with glycerol stocks stored at -80°C. For *E. coli,* overnight cultures in LB media were mixed with a 50% glycerol stock to a final concentration of 25% glycerol (V/V). Overnight cultures of *B. methanolicus* MGA3 in MVcMY media were mixed with an 87% glycerol stock to a final concentration of 21-22% (V/V). Colonies on solid LB agar of *E. coli* DH5α were stored at 4°C for up to two weeks before being replaced by re-streaking on fresh agar plates. Colonies on solid SOB agar of *B. methanolicus* were stored at room-temperature (25°C) for up to four days before being re-streaked and replaced. Colonies of *M. capsulatus* on solid NMS agar were stored at incubation temperature (40°C) for up to one month due to their slow growth rate.

2.4 Molecular cloning

Molecular cloning involves the insertion of one or more genetic fragments from a template, into an expression vector, like a plasmid. The template DNA can originate from several sources like a genome, DNA fragment, or other plasmids. The initial step involves amplifying the DNA fragment of interest using a polymerase chain reaction (PCR). Depending on the cloning method, primers need to be designed accordingly (see section 2.5).

2.4.1 Polymerase chain reaction

Amplification of DNA is a crucial step of molecular cloning, and PCR allows for the production of thousands of copies of the target DNA fragment. This is achieved using specific primers in conjunction with a DNA polymerase in a solution containing deoxynucleotide triphosphates (dNTPs) of all four nitrogenous bases and a reaction buffer. The denaturation, primer binding, and extension steps all use optimal temperatures specific for their individual function. The PCR reaction consists of denaturing the double-

stranded DNA (dsDNA). Following denaturation, the primers are annealed where the temperature is primarily based on the primer's GC content. The next step involves extending the DNA strands using DNA polymerases. When the strands have been extended, the process repeats for a set number of cycles to generate thousands of copies of the DNA fragment. A list of all primers used are presented in appendix B.

All PCR reactions were carried out using an Eppendorf Mastercycler® Nexus GX2 thermal cycler. For DNA fragment amplification, Takara Bio's CloneAmp™ HiFi DNA polymerase and associated reaction mix was used. The CloneAmp™ reaction mix is listed in table 2.3 and was mixed to a total volume of 25 µL. The CloneAmp™ protocol was used for general amplification of DNA fragments using *B. methanolicus* genomic DNA or plasmid backbone. PCR reaction conditions are listed in table 2.4. None of the CloneAmp™ PCR reaction used more than 100 ng of DNA template, and the 3-step PCR program for these conditions were used.

Table 2.3: Components of reaction mixture for CloneAmp™ HiFi PCR protocol.

Component	**Volume**
CloneAmp™ HiFi PCR Premix.	12.5 µL
Primer 1	0.63 µL (0.25 µM final conc.)
Primer 2	0.63 µL (0.25 µM final conc.)
Template	<100 ng
Sterilized deionized water	Up to 25 µL
Total volume per PCR reaction:	25 µL

Table 2.4: 3-step PCR reaction program temperature, time, and number of cycles for reactions with less than 100 ng template.

Temperature (°C)	**Time (sec.)**	**Nr. of cycles**
98	10	30-35 cycles
55	5 or 15	
72	5 sec/kb	

Colony PCR was done to determine correct insertion in the plasmid construct after the cloning reaction. Colony growth of successful transformants on selective plates after the Gibson assembly cloning reaction was followed by individual colonies being picked and re-streaked before being added to the reaction mixture. Specific colony PCR primers were used (appendix B). Colony PCR was conducted with Promega GoTaq® DNA polymerase and associated reaction mixture. Optimally, a minimum of 16 colonies were picked, however in situations with limited colony growth, all colonies were picked. The reaction mix was set up to a total volume of 10 µL per reaction/colony and is presented in table 2.5, with the PCR reaction conditions presented in table 2.6. The green GoTaq® reaction buffer was preferred due to its ability to be directly loaded onto agarose gel without the addition of loading dye. When green buffer was not available, clear buffer was used with added loading dye before gel electrophoresis.

Elements of this study required plasmids containing the native promoter for the *hps* and *phi* genes from *B. methanolicus* MGA3 genomic DNA. The plasmid backbone was amplified with the CloneAmp™ protocol using primers with binding sites upstream and downstream of the promoter, yielding a plasmid backbone without promoter.

Table 2.5: Colony PCR reaction mixture using GoTaq® DNA polymerase. The listed volumes are for one reaction/colony.

Component	Volume
5X green/clear GoTaq® buffer	2 µL
dNTPs (10 mM each)	0.2 µL
Primer 1	0.1 µL
Primer 2	0.1 µL
GoTaq® DNA polymerase	0.05 µL
Sterilized deionized water	7.55 µL
Total reaction volume	10 µL

Table 2.6: Colony PCR reaction temperature, time, and number of cycles.

Step	Temperature (°C)	Time (min)	Nr. of cycles
Initial denaturation	95	10	1
Denaturation	95	1	25-35
Annealing	52	1	25-35
Extension	72	1 min/kb	25-35
Final extension	72	5	1
Storage	4	Indefinite	1

2.4.2 Plasmid linearization by restriction enzymes

Before a DNA fragment can be cloned into a plasmid, the backbone needs to be cut and linearized. This is achieved using restriction enzymes with specific cut-sites based on nucleotide sequence. To make this process easier and more accessible, stretches of DNA called multiple cloning sites (MCSs) are added to the plasmids to provide a cut-site for several different restriction enzymes. The addition of an MCS also permits the usage of several restriction enzymes simultaneously and with the broad range of enzymes available, several of them have shared reaction conditions like temperature and reaction buffer. The linearization process is also referred to as a digest, and the nucleotide cuts can lead to blunt or sticky ends. Sticky ends have an overhang of a few unpaired nucleotides, which facilitates the ligation of the inserted DNA fragments, whereas blunt ends have no unpaired nucleotides.

In this study, the restriction enzymes used, PciI and BamHI-HF, both resulted in sticky ends, and were provided by New England Biolabs (NEB). The plasmids requiring linearization were pTH1mp and pUB110Smp. The reaction mixture was set up according to the NEBcloner online restriction digest tool (New England Biolabs 2023, retrieved 20. April 2023 from https://nebcloner.neb.com/#!/redigest). Table 2.7 shows the reaction mixture

using 10X NEBuffer r1.1, with the amount of PciI being doubled to that of BamHI-HF due to PciI having 50% activity in the buffer compared to 100% activity of BamHI-HF. The reaction mixture was made to a total volume of 100 µL. Total amount of plasmid in each digest was 1 µg where the volume added varied based on plasmid stock concentration. Figure 2.1 shows the restriction enzymes with their specific cut-sites and subsequent overhangs.

Table 2.7: Reaction mixture for double restriction digest of plasmids in this study.

Component	Volume
DNA (plasmid)	1 µg
10X NEBuffer r1.1	10 µL
BamHI-HF	1.5 µL
PciI	2.5 µL
Sterilized deionized water	Up to 100 µL
Total volume	100 µL

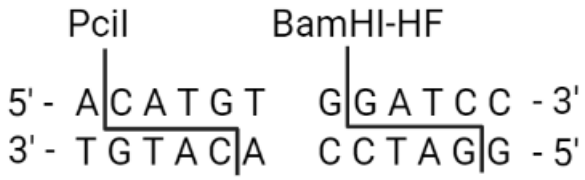

Figure 2.1: Restriction enzyme cut-site sequences for PciI and BamHI-HF.

2.4.3 Gel electrophoresis

Visualization of DNA fragments and size estimation is an important verification step in the cloning of constructs and general molecular biology. This is achieved through separating DNA fragments based on their size in agarose gel electrophoresis. The phosphate-containing DNA backbone has a universally distributed negative charge. Therefore, when subjected to an electric field, the negatively charged DNA will migrate towards the positive anode. By introducing a porous gel, the DNA fragments will migrate based on their size as larger fragments will move slower through the pores and smaller fragments will move faster. Introducing a DNA ladder with known and specific fragment sizes allows for DNA size comparison. In this study, a Thermo Fischer Scientific GeneRuler™ 1 kb Plus DNA Ladder with fragments ranging from 75–20 000 kb was used. The ladder is presented in appendix C. 3 µL of the ladder was used per well.

All gel electrophoresis conducted in this study used an 8% (W/V) agarose gel solution. 3.2 g agarose was mixed with 400 mL 1X Tris-Acetate-EDTA (TAE) buffer and 20 µL of a nucleotide-specific fluorescent dye. For pure fragment visualization, GelRed® (Biotium) was added, and for gel extraction, GelGreen® (Biotium) was used. Both fragment size and relative concentration can be estimated through UV light. The intensity of the resulting image under UV light is proportional to the concentration of DNA. For visualization of

Gibson assembly products with the 5X Green GoTaq® buffer the samples were loaded directly onto the gel. In the few cases where the 5X Clear GoTaq® buffer was used, Purple (6X) Gel Loading Dye (New England BioLabs) was added before samples were loaded on the gel. 4 µL Gibson assembly product was loaded per well. The Purple (6X) Gel Loading Dye (New England BioLabs) was also used for gel electrophoresis of linearized plasmids with table 2.8 displaying the components and amounts of sample per well.

Table 2.8: Components and volume per sample loaded onto agarose gel.

Component	Volume
DNA	1 µL
Distilled deionized water	4 µL
Purple (6X) Gel Loading Dye	1 µL
Total amount per well	6 µL

The gel electrophoresis was done on a BioRad PowerPac™ Basic power supply and ran for 40 minutes at 90 V. One exception to this was when using gels with two parallel lines of wells for 20+ samples during colony PCR. In this case the gel electrophoresis ran for 30 minutes to prevent samples from the top lanes from overlapping the bottom lanes. Imaging of gels was done using a BioRad Molecular Imager ChemiDoc™ XRS+ with the associated BioRad ImageLab™ software.

2.5 Gibson assembly for constructs

Gibson assembly (Gibson et al. 2009) is a molecular cloning method enabling the production of plasmid constructs using a single isothermal reaction cycle with all components present in the same reaction mixture. This allows for rapid cloning of constructs without the need for multi-step processes and multiple reaction mixtures. The Gibson assembly Master Mix (table 2.9) consists of an exonuclease, a DNA polymerase, a DNA ligase, and distilled deionized water, all dissolved in a 5X isothermal reaction buffer (IRB). The exonuclease excises nucleotides at the 5'-end resulting in a single-stranded overlapping sequence between the fragments to be joined. The fragments then anneal to each other in the overlapping sequence, and the DNA polymerase closes the gaps. DNA ligase then seals the nicks in the DNA left by the polymerase. Two primers are required for Gibson assembly: a forward primer containing complementary base pairs to the 5' end of the DNA fragment to be inserted, and a reverse primer containing complementary base pairs to the 5' end of the plasmid backbone.

Table 2.9: Gibson assembly Master Mix components.

Component	Volume
5X IRB	320 µL
T5 Exonuclease	0.64 µL
Phusion® High-Fidelity DNA Polymerase	20 µL
Taq DNA ligase	160 µL
Distilled deionized water	700 µL
Total volume	1200.64 µL

The Gibson assembly Master Mix was distributed into 10 µL aliquots. The total reaction volume for the Gibson assembly was 15 µL, where 10 µL were made up by the Gibson assembly Master Mix and 5 µL was made up of a mix of vector and DNA fragment to be inserted. Vector and fragment were initially added in equimolar amounts, using distilled deionized water to fill up to 5 µL total volume. In the events where equimolar amounts of vector and insert did not yield a successful product, 50-100 ng of vector with 2-3-fold excess of insert was used. The reaction was conducted at 50°C for 60 minutes using an Eppendorf Mastercycler® Nexus GX2 thermal cycler. Plasmid maps of all constructed plasmids and their backbones used in this study are added in appendix D.

2.6 Competent cells preparation and transformation

Competent cells of *E. coli* DH5α, *B. methanolicus* MGA3 WT and *B. methanolicus* MGA3 pBV2xp-mmoH were prepared for this study. *E. coli* DH5α were made chemically competent for heat-shock transformation, whereas both strains of *B. methanolicus* MGA3 were made electrocompetent for transformation through electroporation. All incubation of *E. coli* DH5α and *B. methanolicus* MGA3 was done in accordance with section 2.3 unless stated otherwise. All centrifugation steps were done using an Eppendorf 5430 R High-Speed tabletop centrifuge. The calculations for inoculation volume are presented in appendix E.

2.6.1 Preparation of competent *E. coli* DH5α and *B. methanolicus* MGA3 cells

All centrifugation of *E. coli* DH5α was done at 4000 rpm, for 10 minutes at 4°C. *E. coli* DH5α from frozen glycerol stock was plated out on a plate containing LB agar for overnight incubation. A single colony from the same plate was used to inoculate 20 mL of liquid LB medium in 13 mL tube with ventilation cap and grown overnight. 3 mL of the overnight culture was used to inoculate 300 mL of pre-warmed (37°C) yB medium in a 1 L shake flask and set to incubate until the OD_{600} measurements had reached 0.3-0.4. The OD_{600} was measured using 1 mL culture with 2 x 1 mL yB medium as blanks. The culture was subsequently chilled on ice for 5 minutes before being transferred into six pre-chilled 50 mL centrifugation tubes (Falcon™) and centrifuged. The supernatant was discarded, and each cell pellet was resuspended in 15 mL pre-chilled transformation buffer I (TfBI), before being centrifuged. The supernatant was discarded, and each cell pellet was gently resuspended in 1 mL of pre-chilled transformation buffer II (TfBII), before being distributed in 100 µL aliquots in 1.5 mL microcentrifuge tubes (Eppendorf) and snap-frozen using liquid nitrogen. The cells were stored at -80°C.

The protocol for preparing electrocompetent *B. methanolicus* MGA3 cells was identical for wild type and pBV2xp-mmoH strains. The competent cells of the mmoH strain were used to make co-expression strains with the various chaperonins listed in table 2.1. *B. methanolicus* MGA3 from frozen stock was used to inoculate 25 mL room-temperature SOB medium in 250 mL baffled flask and incubated overnight. The overnight culture was used to inoculate a 25 mL SOB pre-culture in a 250 mL baffled flask to a final OD_{600} of 0.2 and left to grow for 3-4 hours. The pre-culture was then used to inoculate 4 x 100 mL pre-warmed SOB medium in 500 mL baffled flasks to an initial OD_{600} of 0.05 and left to incubate to an OD_{600} of 0.25 (0.18-0.30 was acceptable). The cultures were transferred to 50 mL centrifugation tubes (Falcon™), using 2 tubes per flask, and centrifuged at 7830 rpm for 10 minutes at 25°C. The supernatant was discarded, and each cell pellet was resuspended in 4.5 mL electroporation buffer (EPB) before combining cell suspensions from two tubes, yielding 4 tubes total. These tubes were then centrifuged at 7830 rpm for 10 minutes at 25°C and resuspended in 9 mL EPB, followed by an additional centrifugation. The supernatant was discarded, and the cell pellets were resuspended in the remaining supernatant left in the tubes. The cell suspensions were transferred in 100 µL aliquots to 1.5 mL microcentrifuge tubes (Eppendorf) and stored at -80°C.

2.6.2 Heat-shock transformation of *E. coli* DH5α

100 µL aliquots of chemically competent *E. coli* DH5α cells were thawed on ice for 10 minutes before adding 10 µL of plasmid or Gibson assembly mix. The cells were incubated on ice for 10 minutes before being heat-shocked using a 42°C water bath for 45 seconds. The cells were then incubated on ice for 2 minutes before the addition of 900 mL room-temperature LB medium. The cells were incubated for 60 minutes with shaking and subsequently centrifuged at 8000 rpm for 3 minutes at 24°C. The supernatant was discarded, and the cells were resuspended in the remaining LB medium in the tube (ca. 100 µL), before being plated out on LA plates supplemented with the appropriate antibiotic as stated in section 2.3. The plates were incubated overnight. Successful transformants were verified with colony PCR before glycerol stocks were made and stored at -80°C.

2.6.3 Electroporation of electrocompetent *B. methanolicus* MGA3

100 µL aliquots of electrocompetent *B. methanolicus* MGA3 cells were thawed on ice for 10 minutes before 1 µg of the plasmid was added (amount depending on plasmid stock concentration). The cells were then incubated on ice for 30 minutes before being transferred to pre-chilled 2 mm BTX Cuvettes Plus™ electroporation cuvettes. 12.5 mL SOB in a 150 mL flask was pre-warmed for 30 minutes at 50°C. The cells were electroporated using a Bio-Rad Gene Pulser Xcell modular electroporation system running an exponential waveform program with 200 Ω, 25 µF, 12.5 kV/cm (2.5 kV), and a 4.5-5.5 time constant. 1 mL of the pre-warmed SOB was immediately added to the electroporation cuvette and pipetted up and down a few times before being returned to the flask and incubated for 6 hours. The cell culture was transferred to a 15 mL centrifuge tube (Falcon™) and centrifuged at 7830 rpm for 5 minutes at 25°C. The cell pellet was resuspended in 100 µL SOB and plated out on SOB agar plate with appropriate antibiotic as stated in section 2.3. The plates were incubated overnight and colonies with successful transformants were inoculated in 25 mL pre-warmed MVcMY medium in a 250 mL baffled flask and incubated overnight. The cultures were grown until OD_{600} was 1-2 before being stocked in glycerol at -80°C.

2.7 Purification and extraction of plasmids, restriction digest products, and agarose gel fragments

All DNA fragments and constructs used required purification and/or extraction before being used with cell cultures. This is to prevent contamination from unwanted chemicals and compounds originating from the various protocols used, and to maximize the success rate of these DNA products when applied to living cells. After verification of product using gel electrophoresis, PCR purification and/or gel fragment extraction was done using the QIAGEN QIAquick® PCR Purification Kit and Gel Extraction Kit (Cat.no. 28106 and 28706). Plasmid extraction from *E. coli* DH5α was done using the Zymo Research Plasmid Miniprep Classic kit (Cat. no. D4016). Columns and collection tubes used were supplied in their respective kits unless stated otherwise. All centrifugation of microcentrifuge tubes was done using a Thermo Scientific Heraeus Pico™ 17 Microcentrifuge or an Eppendorf 5424 Microcentrifuge. For overnight cultures of *E. coli* DH5α for plasmid extraction, the Eppendorf 5430 R High-Speed tabletop centrifuge was used.

2.7.1 PCR product purification

In this study, purification of PCR product was required after running Takara Bio's CloneAmp™ HiFi protocol. All centrifugation steps were done at 13 000 rpm. 5 volumes of Buffer PB were added to 1 volume of the PCR product mixture which was then transferred to a QIAquick® column placed in a 2 mL collection tube and centrifuged for 1 minute. 750 µL of Buffer PE was then added to the column and centrifuged for 1 minute. An additional 1-minute centrifugation was done to remove any residual Buffer PE. The column was placed in a sterile 1.5 mL microcentrifuge (Eppendorf) tube and 30 µL distilled deionized water was added and left to incubate at room-temperature for 1 minute, before being centrifuged for 1 minute. Concentration of PCR product was measured using NanoDrop™ (section 2.8).

2.7.2 Plasmid extraction and purification

After Gibson assembly cloning, the plasmid constructs were stored in *E. coli* DH5α glycerol stocks at -80°C. To extract the plasmids for further use, 5 mL of antibiotic supplemented LB medium in 13 mL tubes with ventilated cap was inoculated with the desired strain and incubated overnight. The culture was centrifuged at 7830 rpm for 5 minutes at 25°C and the supernatant was discarded. Remaining centrifugation steps were done at 11 000 g. 200 µL P1 Buffer was added and the cell pellet resuspended by vortexing. The resuspension was transferred to a sterile 1.5 mL microcentrifuge tube (Eppendorf). 200 µL P2 Buffer was then added and the content was mixed by inverting the tube 4 times, before it was incubated at room-temperature for 2 minutes. The sample was then centrifuged for 4 minutes. The supernatant was transferred to a Zymo-Spin™ IIN column placed in a 2 mL collection tube and centrifuged for 30 seconds. The flow-through was discarded and 200 µL Endo-Wash Buffer was added before centrifugation for 30 seconds. 400 µL Plasmid Wash Buffer was added to the column and centrifuged for 1 minute. The Zymo-Spin™ IIN column was placed in a sterile 1.5 mL microcentrifuge tube (Eppendorf) and 50 µL distilled deionized water was added and set to incubate for 1 minute at room-temperature. A final 30 second centrifugation eluted the plasmid DNA. Concentration of plasmid extract was measured using NanoDrop™ (section 2.8).

2.7.3 Agarose gel fragment extraction

Extraction of DNA fragment from agarose gel was done by running a gel electrophoresis at 90 V for 40 minutes in a thick 0.8% agarose gel substituted with GelGreen®. The fragment was excised from the gel using Promega x-tracta™ Gel Extractor tool and placed in a 1.5 mL microcentrifuge tube (Eppendorf), before being weighed. 3 volumes of Buffer QG to 1 volume of gel (100 mg gel ~ 100 µL) were added and the tube was incubated at 50°C for 10 minutes with vortexing every 2 minutes until the gel had completely dissolved. 1 volume isopropanol was added and mixed by vortexing. All centrifugation steps were done at 13 000 rpm. The sample was transferred to a QIAquick® spin column placed in a 2 mL collection tube and centrifuged for 1 minute. 500 µL Buffer QG was added and the column was centrifuged for 1 minute. The flow-through was discarded and 750 µL Buffer PE was added to the column and centrifuged for 1 minute. The column was placed in a sterile 1.5 mL microcentrifuge tube (Eppendorf) and 30 µL distilled deionized water was added and set to incubate at room-temperature for 1 minute. The DNA was eluted by centrifugation for 1 minute. DNA concentration was determined using NanoDrop™ (section 2.8).

2.8 Determining DNA concentrations

In laboratory settings, DNA concentrations are usually measured in micro- or nanograms, and precise measuring techniques are therefore important. In addition, being able to determine the quality of the DNA in relation to potential contamination can alleviate possible problems from using low quality samples. Measurements of DNA amounts was done through a Thermo Fischer Scientific NanoDrop™ One/One^C Microvolume UV-Vis Spectrophotometer. First, a blank was established by applying 2 µL distilled deionized water to the measuring pedestal. All DNA samples were eluted in distilled deionized water. After establishing the blank, 2 µL of the DNA sample was applied to the measuring pedestal and measured. The NanoDrop™ measures absorbance (A) of the sample with UV light at 230-, 260, and 280 nm wavelength. DNA concentration is measured at A260 nm, whereas the ratio between A260/A280 nm determined contamination of primarily protein or phenol. The A260/A230 ratio primarily measured carbohydrate carryover, residual guanidine, phenol, or other reagents originating from the chosen DNA extraction protocol. Optimum ratios at A260/A280 are ~1.8 for "pure" DNA and ~2.0 for "pure" RNA. For ratios of A260/230, 2.0–2.2 is considered "pure" nucleic acid (Wilfinger, Mackey, and Chomczynski 1997).

2.9 Sequencing of constructs and DNA alignment analysis

The plasmid constructs after Gibson assembly were verified with DNA sequencing and subsequent sequence alignment analysis. The sequencing was done by Eurofin Genomics and samples were prepared in accordance with the "LightRun" Sanger sequencing sample requirements from GATC Biotech (table 2.10). This technique is based on the chain termination method (Sanger sequencing) with sequences visualized by a chromatogram from the measured fluorescence created by the fluorescently labelled dideoxynucleoside triphosphate (ddNTPs) chain terminators.

Table 2.10: Sequencing sample requirements (LightRun).

Component	Concentration	Volume
Purified template DNA	50-100 ng/µL	5 µL
Primer	5 pmol/µL (5 µM)	5 µL
Total volume		10 µL

Plasmid constructs and the sequence alignment were done by *in silico* cloning and subsequent analysis using the Benchling online cloud-based bioinformatics platform (Benchling, 2023, retrieved 17 April 2023 from www.benchling.com). The analysis was done to rule out any mutations in the plasmid constructs after Gibson assembly cloning and to determine proper insertion of correct fragments. Sequence alignment raw data is presented in appendix J. The sequencing primers used were the forward primer for each specific insert and the same primers used for colony PCR as they bind slightly upstream of the insert (appendix B), yielding three sequences per plasmid construct.

2.10 Coumarin fluorescence-based enzyme assay of sMMO

Measuring the activity of heterologously expressed sMMO in *B. methanolicus* MGA3 was done through a fluorescence-based enzyme activity assay using the substrate coumarin. Coumarin is a substrate for sMMO and is converted into 7-hydroxycoumarin (umbelliferon) in the presence of an electron donor. The fluorescence intensity is proportional to the amount of 7-hydroxycoumarin produced and therefore an indication of enzyme activity. The strains of *B. methanolicus* MGA3 used in the five experiments are listed in table 2.11. Strain descriptions are listed in table 2.1. The standard concentrations of 7-hydroxycoumarin were made from a 100 mM stock solution, final concentrations of coumarin and sodium formate were made from 100 mM and 200 mM stock solutions respectively, and final xylose concentrations were achieved using a 50% stock solution (appendix A). All centrifugation steps were done using an Eppendorf 5430 R High-Speed tabletop centrifuge.

Table 2.11: Strains used the coumarin fluorescence-based enzyme assay of sMMO in the individual experiments.

Strains	Whole cell culture	Crude extract (50°C)	Crude extract (50°C)	Crude extract (50°C)	Crude extract (37°C)
WT				✓	✓
BVEV		✓	✓	✓	✓
mmo	✓	✓	✓	✓	✓
mmoH		✓	✓		
groESL1	✓	✓	✓	✓	✓
groESL2		✓	✓	✓	✓
groESL_BM		✓	✓	✓	✓

2.10.1 Excitation and emission scans

To determine the optimal wavelengths for emission and excitation of 7-hydroxycoumarin, scans of 7-hydroxycoumarin with a known concentration was done. The excitation- and emission scans, as well as the fluorescence measurements were conducted using a Tecan Infinite® M200 Pro microplate reader and the Tecan i-control™ 2.0 software. All experiments used a Thermo Fischer Scientific Nunc™ MicroWell™ 96-Well, flat-bottom black microplate. A single well with a concentration of 100 µM 7-hydroxycoumarin was chosen for the excitation- and emission scans. For the excitation scan, the starting excitation wavelength was set to 300 nm and increased in 2 nm increments up to 600 nm, with the emission wavelength set to 450 nm based on Miller et. al (2001). The gain was set to 50 for all measurements. For the emissions scans, the starting emission wavelength was set to 300 nm and increased in 2 nm increments up to 600 nm, with the excitation wavelength set to 338 nm based on Miller et. al (2001). The resulting scans showed optimal excitation- and emission wavelengths at 330 nm and 378 nm respectively, and this was used in subsequent fluorescence measurements (appendix F).

2.10.2 Whole cell culture

Determining whether whole cells could utilize coumarin, and if the potential product (7-hydroxycoumarin) was transported out of the cell was initially investigated. All centrifugation steps were done at 7830 rpm for 10 minutes at 25°C. Pre-cultures for overnight incubation of the tested strains were inoculated from frozen stock using 25 mL SOB in 250 mL baffled flasks. These were subsequently used to inoculate 6 x 40 mL SOB main cultures per strain in 250 mL baffled flasks to a starting OD_{600} of 0.2 and left to grow for at least one doubling in OD_{600}. Xylose was added to a final concentration of 0.5%, methanol to a final concentration of 200 mM, and sodium formate to a final concentration of 20 mM from a 200 mM stock solution. Coumarin was added from a 100 mM stock solution to five of the six flasks per strain to the final concentrations of 0 µM, 10 µM, 25 µM, 50 µM, 100 µM, 250 µM, and a control without added coumarin. Samples were taken after 2, 4, and 24 hours where both OD_{600} and fluorescence measurements were taken. For the fluorescence measurements, 1 mL of the pure cell culture from each substrate concentration was sampled. 200 µL was directly added to separate wells. The remaining 800 µL was centrifuged and 200 µL of the supernatant was added to separate wells in the same plate. The remaining supernatant was discarded, and the cell pellet was resuspended in 1 mL TRIS-HCl buffer (50 mM, pH 7.5) and 200 µL was added to separate wells in the same plate. MVcMY minimal medium was used as blank.

2.10.3 Crude extract

Determining the activity of sMMO in whole cells versus lysed cells was done through sonication. This process consisted of an induction and storage step, followed by sonication and enzyme assay. The MVcMY medium used was supplemented with the components stated in appendix A. The exception was the third and fourth experiment where a copper-deficient trace element solution was used. The strains were inoculated from frozen stock on SOB agar plates containing suitable antibiotics and colonies were subsequently used to inoculate overnight pre-cultures of 80 mL MVcMY medium in 250 mL baffled flasks. Once the pre-cultures had reached an OD_{600} between 1-2, 5 x V_{inoc} was transferred to 50 mL centrifugation tubes (Falcon™) and centrifuged at 7830 rpm for 5 minutes at 40°C. They were then resuspended in 5 mL pre-warmed MVcMY medium, before 1 mL of the resuspension was used to inoculate 50 mL MVcMY main cultures in 250 mL baffled flasks to an OD_{600} of 0.2. Inoculation OD_{600} was measured, and the cells were incubated until a doubling of OD_{600} had occurred. Xylose was then added to a final concentration of 0.5%

and the cultures were incubated until at least two more OD_{600} doublings had occurred. The cells were then transferred to 50 mL centrifugation tubes (Falcon™), followed by centrifugation at 7830 rpm for 10 minutes at 4°C, and washed twice in MOPS buffer (20 mM, pH 7.0) before being stored at -80°C.

For the sonication, the cells were thawed on ice for 10 minutes before being resuspended in 1 mL MOPS buffer (20 mM, pH 7.0). The cells were then sonicated using a Thermo Fisher Scientific Fisherbrand™ Model 505 Sonic Dismembrator with 25% amplitude, 2 second pulses, and 1 second pauses for 5 minutes. The sonicated cell solutions were transferred to 1.5 mL microcentrifuge tubes (Eppendorf) and cell debris were removed by centrifugation at 9870 rpm for 1 hour at 4°C. Crude extract and coumarin were added to the final concentrations stated in table 2.12. The 0 µM samples had no added coumarin. Sodium formate was added to a final concentration of 20 mM from a 200 mM stock solution, and MOPS buffer was added to a total sample volume of 1 mL. The strains were incubated in an eppendorf Thermomixer® Comfort benchtop incubator. Fluorescence scans were done using the parameters stated in section 2.10.1. Table 2.12 also summarizes the other conditions of all three experiments.

Table 2.12: Parameters for the four experiments of the fluorescence-based coumarin assay using sonicated crude extract.

Parameter	**1st**	**2nd**	**3rd**	**4th**
Pre-culture incubation temp.	50°C	50°C	50°C	45°C
Pre-culture copper	Yes	Yes	No	No
Experiment temp.	50°C	50°C	50°C	37°C
Shaking	900 rpm	0 rpm	0 rpm	0 rpm
Crude extract	200 µL	800 µL	800 µL	800 µL
Coumarin concentration	0 µM 25 µM 50 µM 100 µM	0 µM 1 mM 2 mM 4 mM	0 µM 250 µM 500 µM 1000 µM	0 µM 250 µM 500 µM 1000 µM
Timepoints for sample collection	4 hours 8 hours 24 hours	2 hours 4 hours 8 hours 24 hours	4 hours 8 hours 24 hours	2 hours 4 hours 8 hours 24 hours

2.11 Naphthalene oxidation assay

Qualitatively measuring the heterologous expression of sMMO in *B. methanolicus* MGA3 was also attempted using a naphthalene oxidation assay where the reaction between the oxidated naphthalene product, 1-naphthol, and o-dianisidine dissolved in methanol to a concentration of 5 mg/mL creates a purple-colored diazo compound which can be visually observed. Table 2.13 shows the strains used. The strains were plated out on SOB agar plates with suitable antibiotics before fresh colonies were used to inoculate SOB induction agar plates supplemented with xylose and methanol as stated in section 2.3. The SOB induction plates then had ca. 10-20 naphthalene crystals sprinkled in the lid of the plate and incubated upside down for 15 minutes to allow the naphthalene to saturate the air in

the plate. The colonies were then lightly sprayed with a solution of o-dianisidine and left to incubate for 15 minutes (Graham et al. 1992). Colonies were then visually examined for any purple color change. *M. capsulatus* (Bath) was used as control and followed the same protocol with incubation temperature as stated in section 2.3.

Table 2.13: Strains of *B. methanolicus* MGA3 and *M. capsulatus* (Bath) used in the naphthalene oxidation assay.

Strain
WT
BVEV
mmo
mmoH
groESL1
groESL2
groESL_BM
M. capsulatus (Bath) (control)

2.12 Growth experiment of *B. methanolicus* MGA3

Additional aspects of carbon metabolism in *B. methanolicus* MGA3 were investigated by assessing the assimilation of methanol through overexpression of *hps* and *phi*. This was done by expressing *hps* and *phi* in two plasmids, pTH1mp and pUB110Smp, where pUB110Smp has a higher copy number (Irla et al. 2016). In addition, the effects on growth rate of native promoter versus the standard *mdh* promoter used in the plasmids, were investigated. Table 2.14 shows the *B. methanolicus* MGA3 strains used in this experiment. Table 2.1 and 2.2 provide strain- and plasmid construct descriptions respectively.

Table 2.14: *B. methanolicus* MGA3 strains used in the growth experiment.

Strain
THEV
THMet.P
THNat.P
UBEV
UBMet.P
UBNat.P

2.12.1 Growth rate at 200 mM and 400 mM methanol concentrations

All centrifugation was done using an Eppendorf 5430 R High-Speed tabletop centrifuge. The strains listed in table 2.14 were plated out on SOB agar plates with suitable antibiotics using frozen stock and incubated overnight. The following day, fresh colonies from the plate were used to inoculate two 80 mL pre-cultures per strain with pre-warmed MVcMY with 200 mM methanol and the additives listed in appendix A. Pre-cultures were incubated until the OD_{600} was above 1. Six main cultures per strain were prepared with three

replicates per condition. These had 40 mL MVcM medium with the additives listed in appendix A, where three main cultures had 324 µL methanol added to a final concentration of 200 mM. The remaining three had 648 µL methanol added to a final concentration of 400 mM. Inoculation volume was calculated to an OD_{600} of 0.2 and 5 x calculated volume from pre-cultures was spun down and resuspended in 5 mL pre-warmed MVcM. 1 mL of the resuspension was used to inoculate main cultures. OD_{600} of main cultures were measured at the time of inoculation and subsequently every two hours until the same or declining OD_{600} value had been measured in two subsequent measurements. The cultures were transferred to 50 mL centrifuge tubes (Falcon™) and centrifuged at 24°C, 7830 rpm for 5 minutes. 1 mL supernatant from each sample was transferred to sterile 1.5 mL microcentrifuge tubes (Eppendorf) and stored at -20°C for future HPLC measurements. Calculations are shown in appendix E.

3 Results

This study intended to investigate synthetic methanotrophy and methanol assimilation in *B. methanolicus* MGA3 through three areas of focus. These included the creation of various strains of *B. methanolicus* MGA3 and assessment of their ability to heterologously produce sMMO, the conversion of methane to methanol through the action of active sMMO, and the subsequent assimilation of methanol through increased metabolism of formaldehyde by the enzymes HPS and PHI. The aims of the project therefore consisted of first the creation of expression and co-expression strains of *B. methanolicus* MGA3 carrying both sMMO and GroES-EL chaperonins. Second, adapting and establishing a protocol for assessment of sMMO activity in *B. methanolicus* based on an existing fluorescence-based coumarin assay previously developed for native methanotrophs. An additional colorimetric plate assay for detecting sMMO will also be tested using the oxidation of naphthalene to 1-naphthol by sMMO and the subsequent interaction with tetrazotized o-dianisidine to form a purple color complex. Third, creation and homologous expression of *hps* and *phi* operon together with either native promoter or the *mdh*, followed by an assessment of the effects on growth rate at 200 mM and 400 mM methanol.

3.1 Adaptation of a fluorescence-based coumarin sMMO assay for *B. methanolicus* MGA3

The original fluorescence-based assay was developed by examining which substrates of sMMO yielded a fluorescent product once oxidized by the enzyme, where coumarin demonstrated the highest levels of fluorescence observed in its oxidized product, 7-hydroxycoumarin. This assay was developed for native methanotrophic bacteria, and the adaptation of this methodology to heterologously produced sMMO in *B. methanolicus* MGA3 could provide an easy and fast way of determining the presence of functional sMMO. A total of five individual experiments were conducted in an attempt to achieve measurable fluorescence as a result of functional sMMO in *B. methanolicus* MGA3. The first experiment used whole cell culture of *B. methanolicus* MGA3 mmo and groESL1 strains to examine if functional sMMO could be observed in cultures without the need for further processing, and if the substrate could be utilized by whole cells of *B. methanolicus* MGA3. The absence of activity of sMMO in this experiment lead to the subsequent four experiments using crude extract from sonicated cells. The parameters: temperature, substrate concentration, shaking during incubation, amount of crude extract, and copper concentration were altered between each of the four experiments using crude extract to elucidate any potential negative effect these might have had on functional production of sMMO. The fluorescence intensity raw data for all tested strains, blank samples, and standard concentrations of 7-hydroxycoumarin are presented in appendix G. OD_{600} measurements for the first experiment using whole cell culture are presented in appendix H. The fluorescence intensity unit is designated "arbitrary unit" (a.u.). Each strain had one sample tested per condition, as opposed to in triplicates in order to test all strains and all fractions on the same 96 well microplate together with blank samples and standards of 7-hydroxycoumarin. Testing everything in triplicates would have required an unpractical number of 96 well microplates, in addition to the experiment being a proof-of-concept trial as opposed to a quantitative measurement. The standard concentrations of 7-hydroxycoumarin are shown up to 100

µM concentration, due to the 250 µM cusing detector saturation and were outside the linear range.

3.1.1 Whole cell culture

In the first experiment, the potential sMMO activity in whole cell culture, supernatant, and cell pellet resuspended in TRIS-HCl buffer was evaluated to determine if the cells could take up the substrate (coumarin) and if the reaction product was subsequently transported out of the cell following oxidation by sMMO. In addition, determining if sMMO was active in the different cell fractions. Overnight pre-cultures were inoculated with the strains stated in section 2.10, table 2.11, which was subsequently used to inoculate main cultures. The following compounds were added to the growth medium: xylose, coumarin, and sodium formate to induce the expression from P_{xyl} promoter, provide substrate, and electron donor for the enzyme, respectively. Samples were taken at 2-, 4-, and 24 hours, and any potential fluorescence was examined in each of the cell fractions. Potential changes in fluorescence were assessed for each coumarin concentration and were compared to the controls without added substrate, and the standard concentrations of fluorescent product (7-hydroxycoumarin) to determine sMMO activity. Standard concentrations of 7-hydroxycoumarin are shown in figure 3.1, ranging from 10 to 100 µM. Table 3.1 displays the fluorescence in different fractions for the mmo strain with measurements being made at 2-, 4-, and 24 hours after substrate was added. Table 3.2 displays the fluorescence intensity in the groESL1 strain with measurements being made at 2-, 4-, and 24 hours after substrate was added. Coumarin concentration 0 µM indicates that no coumarin was added. Fluorescence was observed in the whole cell culture and supernatant fractions with low fluorescence observed in the resuspended cell pellet. In the mmo strain, the fluorescence was somewhat higher in the whole cell culture fractions in comparison to the supernatant at the 2- and 4-hour samples, with the fluorescence values reaching similar levels in these two fractions after 24 hours. Compared to the groESL1 strain where the whole cell culture and supernatant fractions had comparable fluorescence intensity at all timepoints. The 0 µM samples with no coumarin added had similar fluorescence to those with substrate supplementation, suggesting that the observed fluorescence intensity was not caused by the conversion of coumarin to 7-hydroxycoumarin by functionally produced sMMO. Additionally, when the background fluorescence for test samples 24 hours after induction are compared with hydroxycoumarin standards, it is clear that very low fluorescence values were achieved.

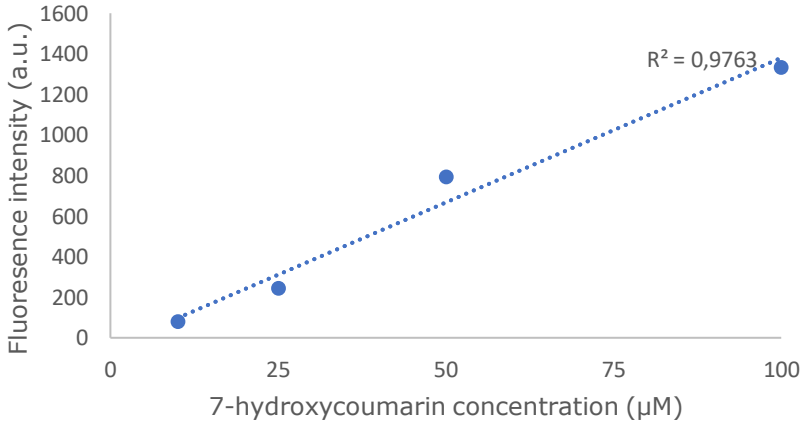

Figure 3.1: Fluorescence intensity (a.u.) of standard concentrations of 7-hydroxycoumarin (10 µM, 25 µM, 50 µM, 100 µM). All samples of the 7-hydroxycoumarin were made from the same 100 mM stock. Raw data for fluorescence of standards are added in appendix G.

Table 3.1: Measured fluorescence intensity in the *B. methanolicus* MGA3 mmo strain in pure cell culture, supernatant, and resuspended cell pellet. The pure cell fraction and supernatant had somewhat higher fluorescence in the 24-hour samples.

Coumarin concentration	Fraction	2 hours	4 hours	24 hours
0 µM	Pure cell culture	6	4	26
	Supernatant	5	5	28
	Resuspended pellet	-5	-5	10
10 µM	Pure cell culture	8	10	27
	Supernatant	4	5	28
	Resuspended pellet	-5	-2	8
25 µM	Pure cell culture	7	6	27
	Supernatant	3	4	22
	Resuspended pellet	-4	-5	9
50 µM	Pure cell culture	5	7	28
	Supernatant	1	5	27
	Resuspended pellet	-5	-5	9
100 µM	Pure cell culture	5	6	19
	Supernatant	3	3	18
	Resuspended pellet	-5	-5	9
250 µM	Pure cell culture	6	6	24
	Supernatant	5	6	23
	Resuspended pellet	-5	-4	9

Table 3.2: Measured fluorescence intensity in the *B. methanolicus* MGA3 groESL1 strain in pure cell culture, supernatant, and resuspended cell pellet. The pure cell fraction and supernatant had somewhat higher fluorescence in the 24-hour samples.

Coumarin concentration	Fraction	2 hours	4 hours	24 hours
0 µM	Pure cell culture	11	14	33
	Supernatant	10	12	30
	Resuspended pellet	-1	2	15
10 µM	Pure cell culture	11	14	33
	Supernatant	8	12	32
	Resuspended pellet	-1	2	11
25 µM	Pure cell culture	10	14	33
	Supernatant	9	13	30
	Resuspended pellet	0	1	13
50 µM	Pure cell culture	12	13	32
	Supernatant	10	12	30
	Resuspended pellet	0	3	13
100 µM	Pure cell culture	10	12	31
	Supernatant	11	11	29
	Resuspended pellet	-3	1	13
250 µM	Pure cell culture	9	9	30
	Supernatant	8	10	28
	Resuspended pellet	-4	-5	13

3.2 Crude extract

The experiment using whole cell cultures did not yield any fluorescence attributable to functional sMMO, and subsequent experiments were done using crude extract from sonicated cells. This was done to exclude the possibility that the limiting step in the enzyme assay was the transport of the substrate into the *B. methanolicus* cells. Prior to conducting the assay, the strains were cultivated in minimal medium supplemented with methanol and the expression of heterologous genes from the vectors was induced by addition of xylose. The cell pellets were collected via centrifugation 6.5 hours after induction, before being stored at -80°C until the day of the experiment. The cells were resuspended in MOPS buffer before being sonicated and centrifuged. The resulting crude extract was then used in the experiments. The full list of experimental parameters is shown in table 2.12 in section 2.10.3 for all four experiments using crude extract. Fluorescence intensity using crude extract as opposed to whole cell cultures averted the potential problem of coumarin transport into the cell, and the resulting supernatant should have contained expressed protein. However, experiments using crude extract showed much the same results as the initial trial using whole cell cultures, namely overall low fluorescence, no increasing fluorescence with increasing substrate concentrations, and similar fluorescence for 0 µM samples as compared to test conditions with substrate supplementation. Negative controls consisted of the BVEV empty vector strain as well as the 0 µM coumarin concentrations.

The first experiment with crude extract used 50°C incubation temperature, 25 µM, 50 µM, and 100 µM substrate concentrations, 900 rpm shaking during incubation, 200 µL crude extract, and copper at 0.00016 mM concentration which is typically used in the growth medium during strain cultivation. The experiment displayed no measurable fluorescence in the 0 µM samples without added coumarin. However, only two of the six tested strains had measurable fluorescence, those being the BVEV and mmoH strains, with the highest value being 2 a.u. in the BVEV strain, which is an empty vector strain. Table 3.3 shows the fluorescence measured at all coumarin concentrations in all strains at the different time points. The standard concentrations of the fluorescent product 7-hydroxycoumarin showed significantly higher levels of fluorescence, even at the lowest concentration of 10 µM, with a value above 60 a.u. (figure 3.2). With fluorescence intensity values being low and four of the six strains not exhibiting any fluorescence and one of the strains with any measurable fluorescence being the empty vector control, the observed values were not a result of functionally expressed sMMO.

Table 3.3: Fluorescence intensity (a.u.) of the tested *B. methanolicus* MGA3 strains in the first experiment using crude extract at the various coumarin concentrations at the specified time points after coumarin was added.

Sample	Strain	4 hours	8 hours	24 hours
0 µM	BVEV	1	-1	1
	mmo	-2	-3	-2
	mmoH	0	1	2
	groESL1	-1	-1	-3
	groESL2	-3	-3	-3
	groESL_BM	-2	-3	-5
25 µM	BVEV	-1	1	6
	mmo	-3	3	2
	mmoH	2	4	4
	groESL1	-1	2	3
	groESL2	-2	3	3
	groESL_BM	-3	3	2
50 µM	BVEV	2	4	6
	mmo	-2	2	3
	mmoH	1	4	4
	groESL1	-3	4	2
	groESL2	-3	5	2
	groESL_BM	-4	2	2
100 µM	BVEV	0	-1	6
	mmo	-2	4	3
	mmoH	1	5	4
	groESL1	0	3	2
	groESL2	0	3	2
	groESL_BM	-2	2	2

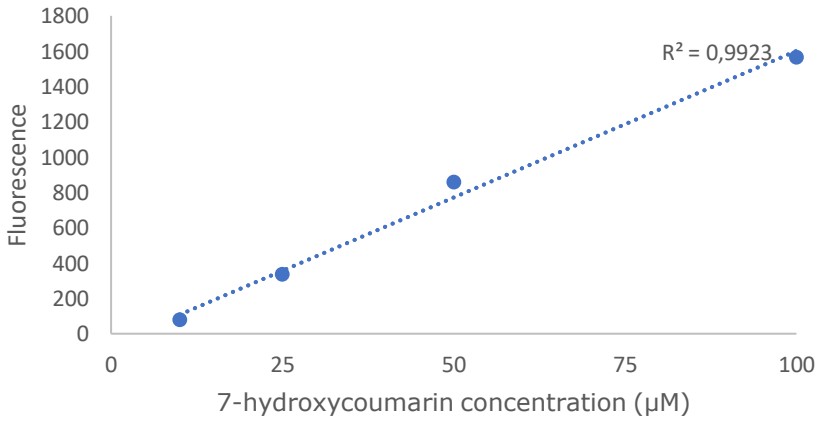

Figure 3.2: Fluorescence intensity (a.u.) of standard concentrations of 7-hydroxycoumarin (10 µM, 25 µM, 50 µM, 100 µM). All samples of the 7-hydroxycoumarin were made from the same 100 mM stock. Raw data for fluorescence of standards are added in appendix G.

Due to no fluorescence attributable to functional sMMO observed in the first experiment using crude extract, the second experiment was conducted with an increased coumarin concentration to 1 mM, 2 mM, and 4 mM. The experiment was also done without shaking during incubation due to concerns regarding the negative effect of shaking on enzyme stability. The crude extract concentration was also increased from 20% to 80% in a final volume of 1000 µL, to assess if the amount of enzyme led to detectable enzyme activity. The fluorescence in the tested strains was low and relatively stable across all strains with the highest fluorescence seen in the control BVEV strain at all time points with a maximum observed value of 8 a.u. (table 3.4). The negative controls without added substrate had no fluorescence in the majority of the strains with only minimal amounts (2 a.u.) seen in the BVEV strain in the 8- and 24-hour samples. The increased coumarin concentrations did not appear to lead to higher fluorescence, nor did the absence of shaking during incubation. Comparing the fluorescence intensity with those of the standard concentrations of 7-hydroxycoumarin (figure 3.3) further underlines the low observed fluorescence and absence of functional sMMO.

Table 3.4: Fluorescence intensity (a.u.) of the tested *B. methanolicus* MGA3 strains in the second experiment using crude extract at the various coumarin concentrations and negative control at the specified time points after coumarin was added.

Sample	Strain	2 hours	4 hours	8 hours	24 hours
0 mM	BVEV	0	0	2	1
	mmo	-3	-2	0	-1
	mmoH	-4	-4	-3	-3
	groESL1	-3	-5	-2	-1
	groESL2	-5	-4	-2	-2
	groESL_BM	-3	-3	-3	-4
1 mM	BVEV	5	4	5	5
	mmo	2	1	4	4
	mmoH	4	3	6	4
	groESL1	2	2	2	4
	groESL2	2	0	2	1
	groESL_BM	-1	-1	2	1
2 mM	BVEV	5	3	5	6
	mmo	3	1	4	4
	mmoH	5	2	4	4
	groESL1	3	2	3	3
	groESL2	2	0	3	3
	groESL_BM	2	-1	2	2
4 mM	BVEV	5	3	6	8
	mmo	4	1	4	2
	mmoH	4	3	2	4
	groESL1	1	3	4	5
	groESL2	4	0	4	4
	groESL_BM	4	2	4	2

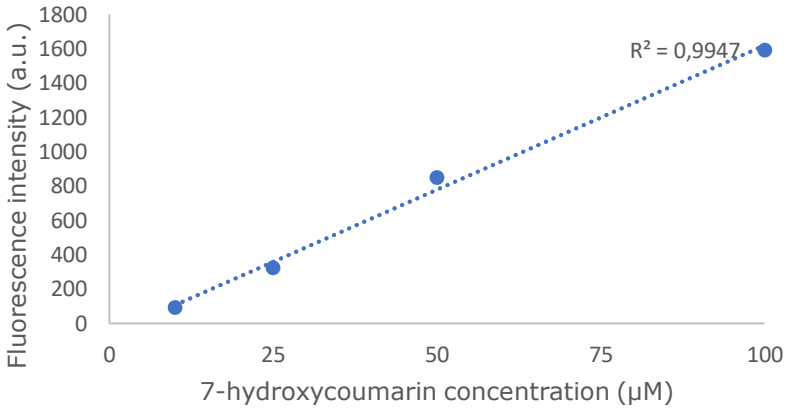

Figure 3.3: Fluorescence intensity (a.u.) of standard concentrations of 7-hydroxycoumarin (10 µM, 25 µM, 50 µM, 100 µM). All samples of the 7-hydroxycoumarin were made from the same 100 mM stock. Raw data for fluorescence of standards are added in appendix G.

Due to no product formation suggesting no functional sMMO production in the second experiment with higher coumarin concentrations, in the third experiment the coumarin were reduced to 250 µM, 500 µM, and 1000 µM. The reasoning for this was also based on the fact that 7-hydroxycoumarin even at low concentration in the range of 10 µM leads to higher fluorescence intensity (figure 3.3), with measured fluorescence above 90 a.u. The *B. methanolicus* strains with *mmo*-expression vectors were cultivated in minimal medium supplemented with methanol and a copper-deficient trace element solution to examine the potential inhibitory effects of copper on the enzyme. The remaining parameters were kept the same as in the previous experiment. The mmoH strain was also replaced by the wild type (WT) strain due to difficulty in cultivation of the mmoH strain. The overall fluorescence was higher than in the previous experiments with the highest values observed in the WT strain at all time points with a maximum observed value of 31 a.u. The remaining strains had similar fluorescence to each other (table 3.5), and the fluorescence measurements also showed stable values across all substrate concentrations. A slight decline in fluorescence was observed from the four-hour samples to the eight-hour samples which remained relatively stable in the 24-hour samples. Unlike the previous experiments using crude extract, the 0 µM samples without added substrate showed fluorescence comparable to the values seen in the samples with added substrate. Despite a higher overall fluorescence, the observed values were still significantly lower than those measured in the standard concentrations of 7-hydroxycoumarin (figure 3.4).

Table 3.5: Fluorescence intensity (a.u.) of the tested *B. methanolicus* MGA3 strains in the third experiment using crude extract at the various coumarin concentrations at the specified time points after coumarin was added.

Sample	Strain	4 hours	8 hours	24 hours
0 µM	BVEV	30	22	23
	mmo	16	12	12
	WT	15	9	11
	groESL1	16	8	13
	groESL2	17	8	11
	groESL_BM	18	9	11
250 µM	BVEV	31	26	27
	mmo	17	9	10
	WT	16	8	12
	groESL1	18	9	9
	groESL2	17	7	9
	groESL_BM	17	12	9
500 µM	BVEV	27	24	23
	mmo	19	9	10
	WT	15	8	10
	groESL1	16	9	7
	groESL2	15	7	8
	groESL_BM	20	12	10
1000 µM	BVEV	28	24	26
	mmo	14	9	8
	WT	13	8	8
	groESL1	15	8	9
	groESL2	13	8	7
	groESL_BM	17	8	8

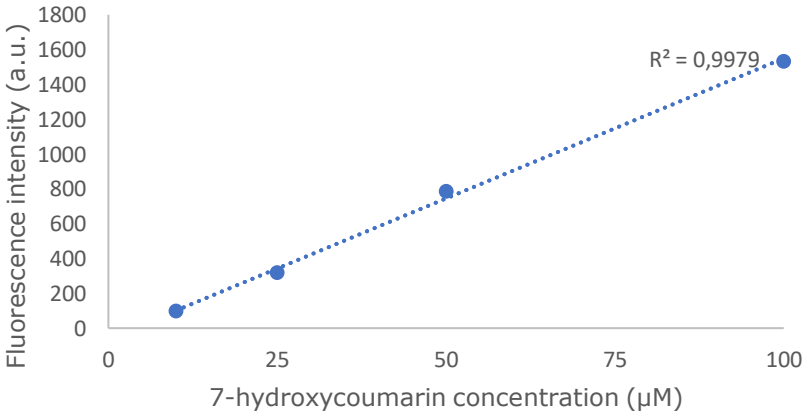

Figure 3.4: Fluorescence intensity (a.u.) of standard concentrations of 7-hydroxycoumarin (10 µM, 25 µM, 50 µM, 100 µM). All samples of the 7-hydroxycoumarin were made from the same 100 mM stock. Raw data for fluorescence of standards are added in appendix G.

As no functional sMMO had been observed in three experiments using crude extract, in the fourth experiment the incubation temperature of the liquid cultures of *B. methanolicus* strain with *mmo*-expression vectors was reduced to 45°C, and the incubation temperature of the assay to 37°C. The temperature was reduced from the 50°C used in the previous three experiments, to examine the potential negative effects on enzyme stability in relation to denauration of protein structure. The remaining parameters were identical to the third experiment. The fluorescence showed similar and stable measurements in all tested strains with the highest overall values observed in the four-hour sample with a peak of 41 a.u. in the 0 µM sample of the groESL_BM strain (table 3.6). The overall fluorescence showed that all the strains except the WT strain had higher fluorescence compared to the previous experiment. The WT had similar fluorescence to the values that were measured in the previous experiment. The groESL_BM strain showed some deviation from the other strains with the highest observed fluorescence at the lowest 250 µM coumarin concentration, followed by a sharp decline and stabilization in the 500 µM and 1000 µM concentrations respectively. As observed previously, the 0 µM samples without added substrate had similar fluorescence to the samples with added substrate. Figure 3.5 shows the standard concentrations of 7-hydroxycoumarin with a fluorescence value above 70 a.u. in the 10 µM standard concentration. Comparing this to the highest observed value in the tested strains in addition to no increased fluorescence with increased substrate concentration demonstrated the absence of functional sMMO.

Table 3.6: Fluorescence intensity (a.u.) of the tested *B. methanolicus* MGA3 strains in the fourth experiment using crude extract at the various coumarin concentrations at the specified time points after coumarin was added.

Sample	Strain	2 hours	4 hours	8 hours	24 hours
0 µM	BVEV	33	34	22	15
	mmo	9	16	10	9
	WT	11	19	8	11
	groESL1	7	16	7	8
	groESL2	23	31	10	12
	groESL_BM	37	41	28	19
250 µM	BVEV	23	25	23	14
	mmo	21	26	16	8
	WT	27	24	20	13
	groESL1	17	21	8	8
	groESL2	22	26	22	10
	groESL_BM	37	13	19	11
500 µM	BVEV	20	25	17	11
	mmo	21	26	15	8
	WT	23	24	16	12
	groESL1	16	21	13	6
	groESL2	18	26	17	12
	groESL_BM	6	13	4	5
1000 µM	BVEV	14	19	12	10
	mmo	17	23	12	9
	WT	17	23	15	9
	groESL1	13	19	9	4
	groESL2	18	21	14	9
	groESL_BM	8	14	4	4

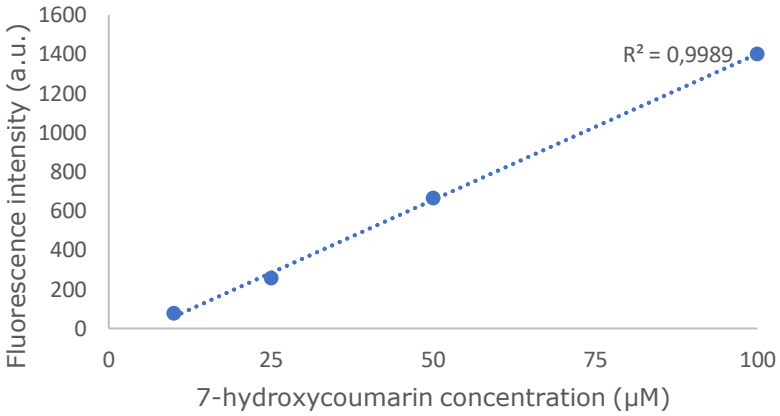

Figure 3.5: Fluorescence intensity (a.u.) of standard concentrations of 7-hydroxycoumarin (10 µM, 25 µM, 50 µM, 100 µM). All samples of the 7-hydroxycoumarin were made from the same 100 mM stock. Raw data for fluorescence of standards are added in appendix G.

3.3 Colorimetric plate assay with naphthalene

A colorimetric plate assay for detecting heterologous production of sMMO in *B. methanolicus* MGA3 was attempted through oxidation of naphthalene. The strains were grown on SOB plates supplemented with 200 mM methanol and 1% xylose to induce both plasmid constructs. About ten naphthalene crystals were sprinkled in the lid of the agar plate and incubated upside down for 15 minutes to saturate the air with naphthalene. The colonies were then lightly sprayed with tetrazotized o-dianisidine dissolved in methanol (5 mg/mL) before being incubated for an additional 15 minutes. The presence of functional sMMO would be determined by a purple coloration in colonies as a result of the interaction between o-dianisidine and the oxidized naphthalene product 1-naphthol, forming a purple diazo compound. The strains used in the experiment are listed in section 2.11, table 2.13. The positive control in the native methanotroph *M. capsulatus* (Bath) showed a single purple colony (figure 3.6). The remaining strains did not display any coloration indicative of formation of the purple diazo compound. None of the tested enzyme assays indicated that functional sMMO had been expressed in *B. methanolicus* MGA3. Images of agar plates with *B. methanolicus* MGA3 strains are added in appendix I.

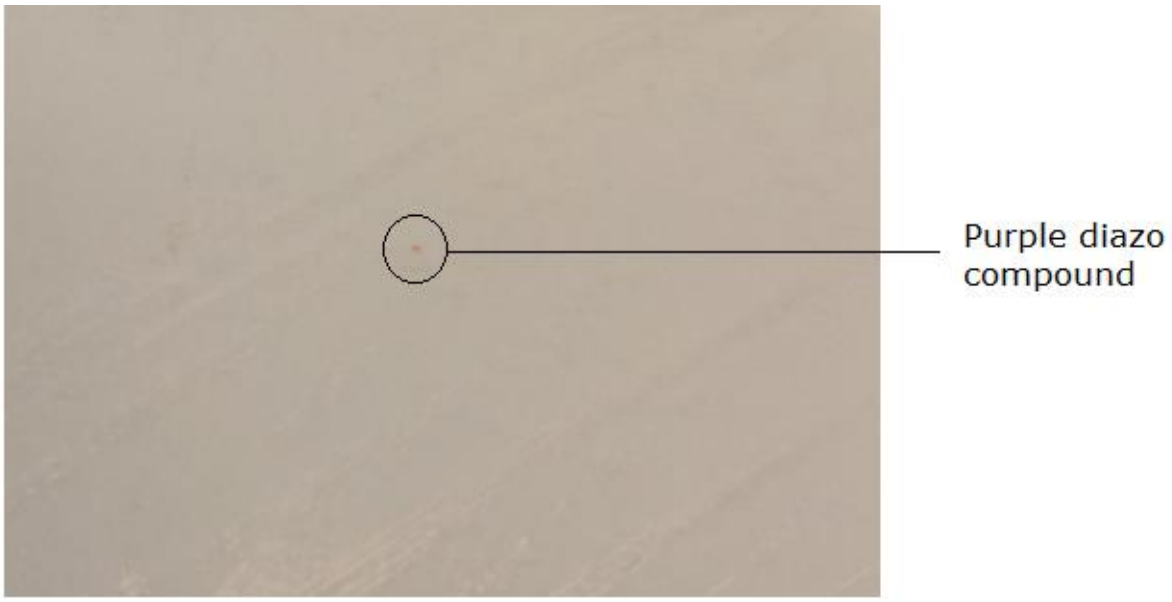

Figure 3.6: Single purple colony in *M. capsulatus* (Bath) showing the purple diazo compound formed from the interaction between 1-naphthol and tetrazotized o-dianisidine.

3.4 Homologous expression of *hps* and *phi* for methanol assimilation

Methanol is converted in *B. methanolicus* MGA3 to formaldehyde by the action of MDH, followed by further assimilation in metabolic pathways by the rate-limiting enzymes HPS and PHI. The availability of these enzymes is believed to influence the efficiency of formaldehyde metabolism, and as an extension, methanol assimilation. Overexpression of *hps* and *phi* and its impact on methanol assimilation in *B. methanolicus* MGA3 was investigated through a growth experiment with each strain grown at both 200 mM and 400 mM methanol. The plasmid constructs were first created *in silico* using the *hps-phi* insert with both native- and *mdh* promoter in the low copy number plasmid pTH1mp and the high copy number plasmid pUB110Smp. This was followed by isolation of the *hps-phi* fragment, with and without native promoter, and the subsequent linearization of plasmid backbones. The plasmid backbones were linearized through a double restriction digest and PCR amplification to yield backbones containing both the *mdh* promoter and no promoter to facilitate the cloning of the native promoter. Gibson assembly was used to clone the constructs followed by verification through colony PCR and sequencing. After transformation of strains, a growth experiment was conducted to assess the effects of homologously expressed *hps-phi* on growth rate. Table 2.14 displays the strains intended to be used in the experiment, however the UBNat.P strain could not be successfully transformed. As a result, native versus *mdh* promoter in the pUB110Smp plasmid backbone could not be attained.

3.4.1 Amplification of *hps-phi* fragment and plasmid backbones without *mdh* promoter

The constructs were first created *in silico* using the Benchling online cloud-based bioinformatics platform (appendix D). The following step in the cloning process was the creation of *hps-phi* fragments both with and without native promoter via PCR using *B. methanolicus* MGA3 genomic DNA as a template. This was done through PCR amplification using CloneAmp™ as stated in section 2.4.1 with table 2.3 showing the components used. In addition, the plasmid backbones pTH1mp and pUB110Smp had to be amplified without the *mdh* promoter present in the plasmids, in order for the *hps-phi* fragment with native promoter from *B. methanolicus* MGA3 to be cloned. Following the amplification, PCR product purification was done as stated in section 2.7.1. Table 3.7 shows the expected size (bp) of the fragments, and figure 3.7 shows the resulting gel electrophoresis of the *hps-phi* fragment without the native promoter which was of the expected size.

Table 3.7: Amplified fragments and their expected size (bp).

Fragment	Size (bp)
hps-phi	1196
hps-phi native promoter	1447
pTH1mp backbone without *mdh* promoter	4790
pUB110Smp backbone without *mdh* promoter	4575

Figure 3.8 shows the amplified *hps-phi* fragments with native promoter as well as the plasmid backbones without the *mdh* promoter. Primers used for the amplification were designed for the two plasmid backbones and the *hps-phi* fragment had to be amplified twice due to slight differences in primer sequences between the two plasmids. All PCR products were of the expected size. Appendix B displays the primer sequences used for all fragments and backbones.

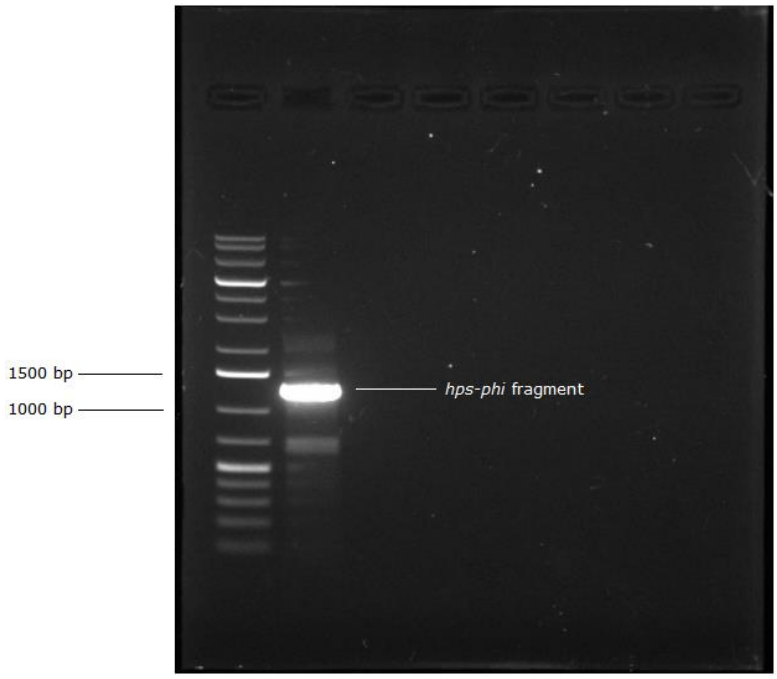

Figure 3.7: *hps-phi* fragment without native promoter obtained from PCR amplification. Lane one contained the Thermo Fischer Scientific GeneRuler 1 kb Plus. Lane two contained the amplified fragment. The expected size of fragment was 1196 bp.

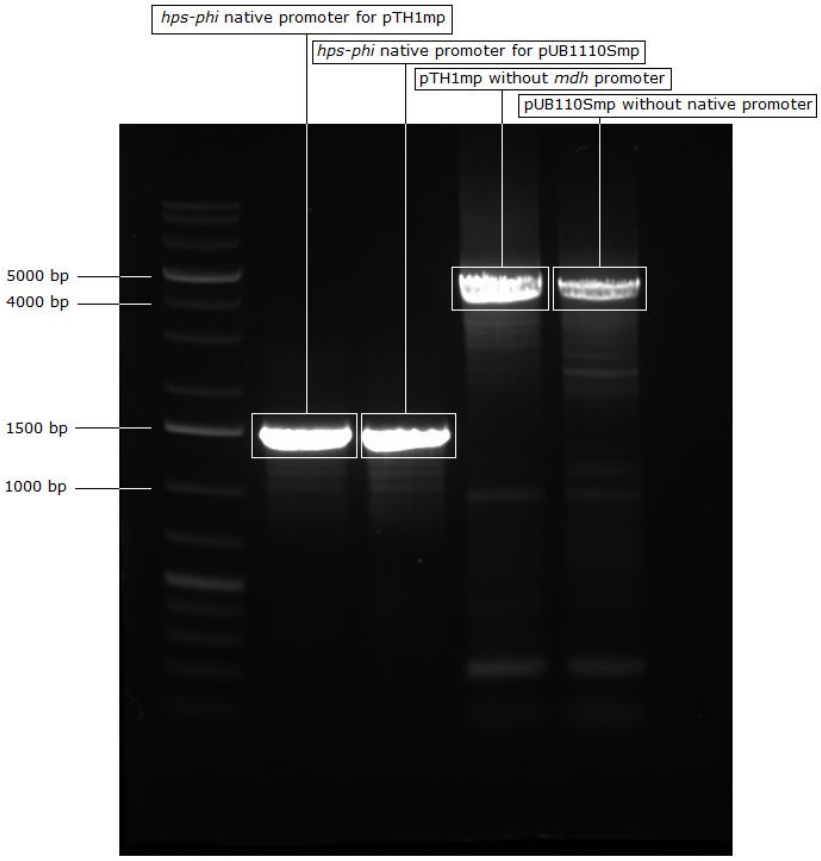

Figure 3.8: *hps-phi* fragments with native promoter for both pTH1mp and pUB110Smp with an expected fragment size of 1447 bp in lane two and three. Lane one contained the Thermo Fischer Scientific GeneRuler 1 kb Plus. Lane four contained the amplified pTH1mp backbone without the *mdh* promoter with an expected size of 4790 bp. Lane five contained the amplified pUB110Smp backbone without the *mdh* promoter with an expected size of 4575 bp.

3.4.2 Linearization of plasmid backbones

The plasmid backbones utilizing the *mdh* promoter had to be linearized in preparation for cloning with the *hps-phi* fragment. Linearization was done through a double restriction digest using the restriction enzymes PciI and BamHI-HF as described in section 2.4.2 with table 2.7 showing the components used. Figures 3.9 and 3.10 show the linearized pTH1mp and pUB110Smp plasmid backbones respectively. After linearization was confirmed, gel extraction of linearized plasmids pTH1mp and pUB110Smp was performed as stated in section 2.7. The sizes of the linearized plasmids were as expected.

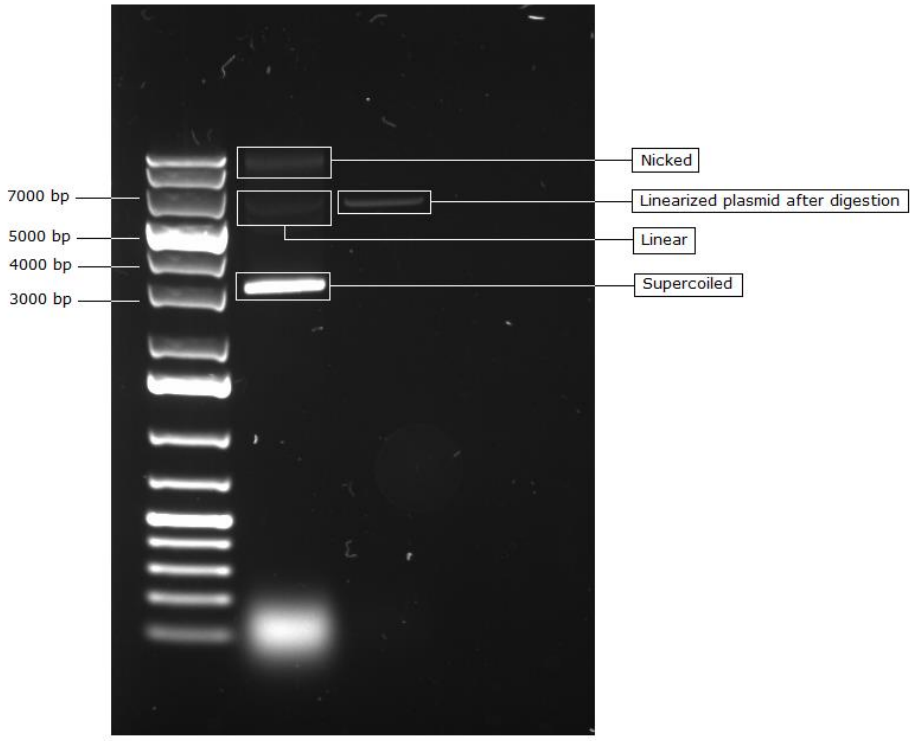

Figure 3.9: Linearized pTH1mp after double restriction digest. Lane one contained the Thermo Fischer Scientific GeneRuler 1 kb Plus. Lane two contained the uncut plasmid displaying the nicked, linear, and supercoiled conformations. Lane three contained the linearized plasmid after restriction digest.

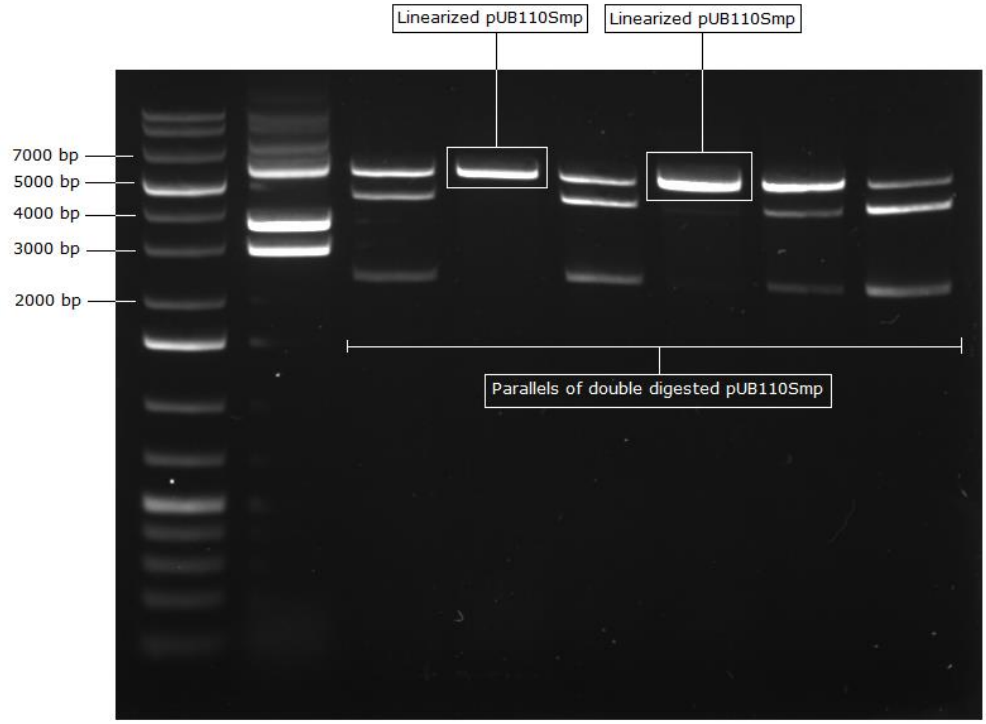

Figure 3.10: Linearized pUB110Smp after double restriction digest. Lane one contained the Thermo Fischer Scientific GeneRuler 1 kb Plus. Lane two contained the uncut plasmid displaying the nicked, linear, and supercoiled conformations as described in figure 3.13. Lanes three to eight contained parallels of pUB110Smp after double restriction digest, with lanes four and six showing successfully linearized plasmid.

3.4.3 Colony PCR of cloned constructs

Following amplification and linearization, the resulting elements used in the cloning process consisted of *hps-phi* fragment, *hps-phi* fragment with native promoter for both plasmids, and linearized plasmid backbones with and without *mdh* promoter. The cloning was done using the Gibson assembly protocol as stated in section 2.5 with table 2.9 stating the components for each cloning reaction. Colony PCR was then conducted to verify the newly cloned constructs, with visualization of constructs on agarose gel using gel electrophoresis. The chosen primers bound upstream and downstream of the insert, so the *hps-phi* and *hps-phi* with native promoter fragments were used as control for comparison in their respective constructs. A negative control was also added consisting of the Gibson assembly reaction mixture with empty vector and water. Section 2.4.1 describes the procedure using individual *B. methanolicus* MGA3 colonies and the Promega GoTaq® DNA polymerase and associated reaction mixture. Figures 3.11-3.14 present the resulting agarose gels after gel electrophoresis. The product sizes for positive clones were 1196 bp for the pTH1mp-hps-phi and pUB110Smp-hps-phi, and 1447 bp for the pTH-hps-phi and pUB110-hps-phi.

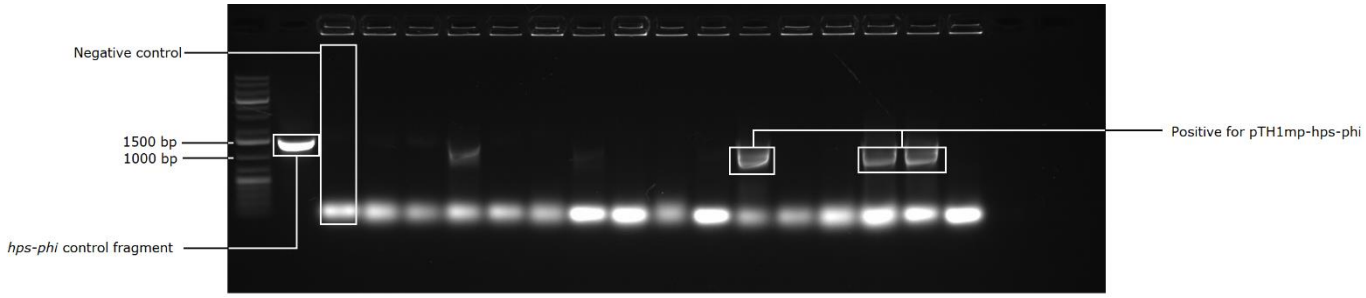

Figure 3.11: Colony PCR of the construct pTH1mp-hps-phi. Lane one from the left contained the Thermo Fischer Scientific GeneRuler 1 kb Plus. Lane two contained the *hps-phi* control fragment. Lane three contained the negative control. Lanes thirteen, sixteen, and seventeen contained fragments comparable to the control, and were chosen for further sequencing. Several other lanes also showed weakly positive samples, however only the three mentioned were chosen for further sequencing.

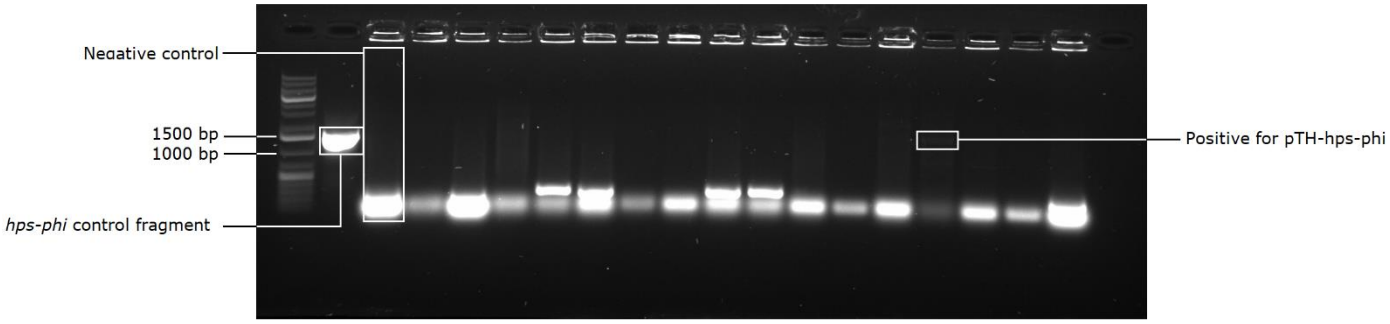

Figure 3.12: Colony PCR of the construct pTH-hps-phi. Lane one from the left contained the Thermo Fischer Scientific GeneRuler 1 kb Plus. Lane two contained the *hps-phi* control fragment. Lane three contained the negative control. Lane sixteen contained a weakly positive fragment comparable to the control and was chosen for further sequencing.

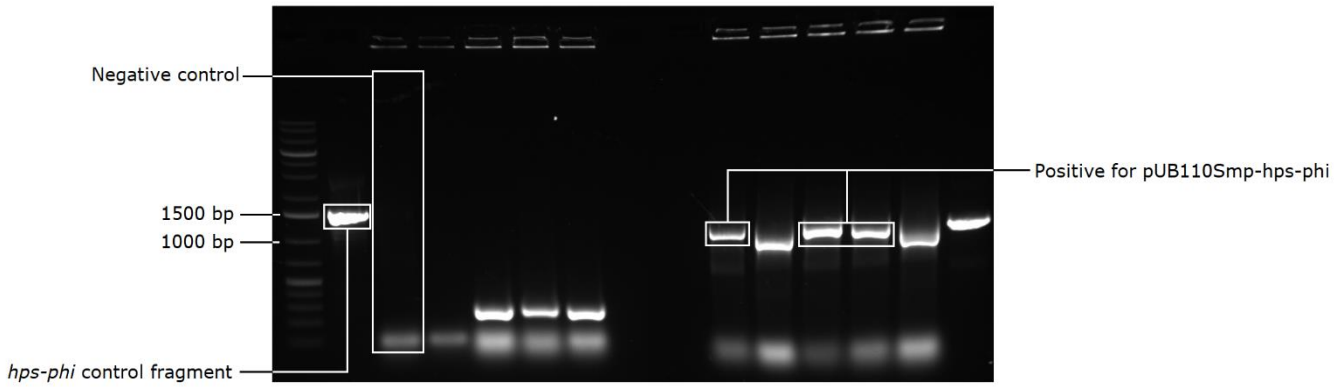

Figure 3.13: Colony PCR of the construct pUB110Smp-hps-phi. Lane one from the left contained the Thermo Fischer Scientific GeneRuler 1 kb Plus. Lane two contained the *hps-phi* control fragment. Lane three contained the negative control. The lanes marked positive for pUB110Smp-hps-phi were chosen for further sequencing. Lanes four, five, six, and seven from the left contained samples for pTH-hps-phi as these were tested simultaneously but did not yield positive results on this occasion.

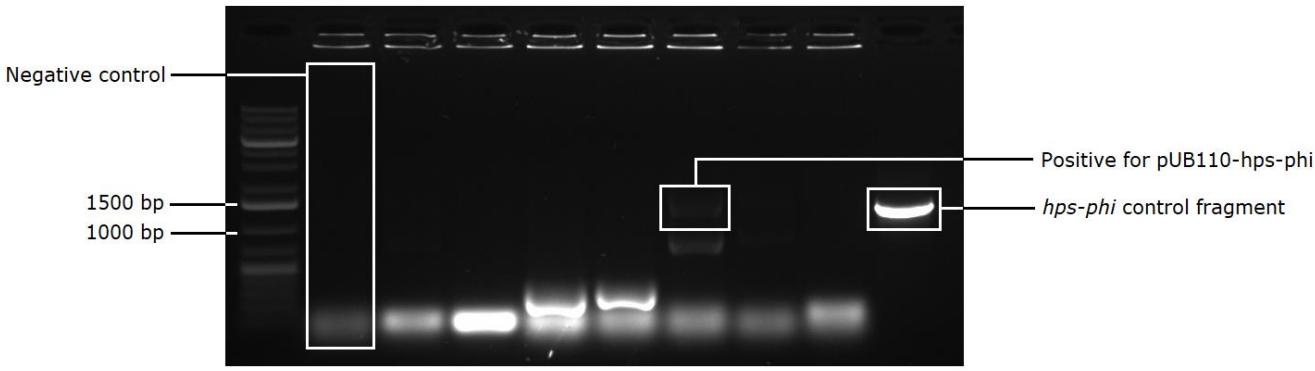

Figure 3.14: Colony PCR of the construct pUB110-hps-phi. Lane one from the left contained the Thermo Fischer Scientific GeneRuler 1 kb Plus. Lane two contained the negative control. Lane one from the right contained the *hps-phi* control fragment. Lane seven from the left contained a weakly positive fragment comparable to the *hps-phi* control and was chosen for further sequencing.

3.4.4 Sequence alignment analysis

Following confirmation of constructs in the colony PCR, sequence alignment analysis was conducted to examine potential mutations in the cloned constructs. For each positive colony in the colony PCR, three sequencing samples were created in accordance with the "LightRun" Sanger sequencing requirements as stated in section 2.9. The primers used were the forward and reverse colony PCR primers with complementary sequences upstream and downstream of the insert, and the forward primer of the insert itself. This yielded three sequences per construct with overlapping reads covering the *hps-phi* insert and the native promoter in the relevant constructs. Observed mutations in single sequences were compared with the two remaining sequences and the reads showing few or no mutations were assumed to be correct. In a few cases the resulting sequencing results did not yield three complete reads. However, the remaining two reads did not display mutations. The resulting alignment analysis therefore did not find mutations in constructs from the tested colonies. The full sequence alignments are added in appendix J.

3.4.5 Growth rate at 200 mM and 400 mM methanol

After confirmation of sequence alignment and the absence of mutations, a growth experiment was conducted following transformation of *B. methanolicus* MGA3 with the plasmid constructs. *B. methanolicus* strains were cultivated in minimal medium with supplementation of either 200 mM or 400 mM methanol. Samples were then taken every two hours and OD_{600} was measured until stagnant or dropping OD_{600} values were observed. Inoculating the strains in both 200 mM and 400 mM methanol was done to assess the effects of overexpressed *hps* and *phi* on growth rate and methanol tolerance at the two methanol concentrations. Figure 3.15 shows the growth curve of all tested strains and table 3.8 displays the average growth rate with standard deviations. Calculations of average growth rates with standard deviations and raw data for the growth experiment are added in appendices E and K respectively.

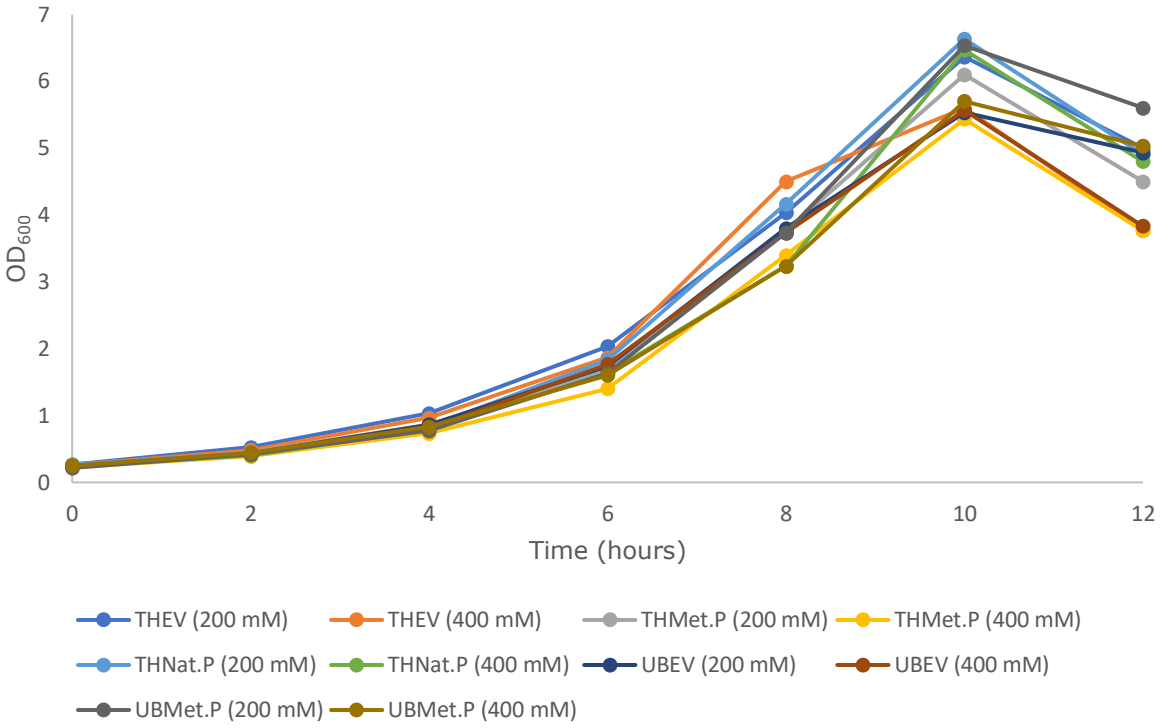

Figure 3.15: OD_{600} measurements of all tested strains of *B. methanolicus* MGA3 carrying fragments for *hps* and *phi* expressed in the plasmids pTH1mp and pUB110Smp, either with native- or *mdh* promoter. Each strain was grown in triplicates of 200 mM and 400 mM methanol.

Table 3.8: Average growth rate (h^{-1}) with standard deviation of each tested strain at 200 mM and 400 mM methanol concentration.

Methanol conc. (mM)	Strain	Average growth rate (h^{-1})
200	THEV	0.32±0.00
	THMet.P	0.33±0.00
	THNat.P	0.34±0.01
	UBEV	0.33±0.03
	UBMet.P	0.35±0.00
400	THEV	0.32±0.01
	THMet.P	0.33±0.00
	THNat.P	0.33±0.00
	UBEV	0.33±0.01
	UBMet.P	0.32±0.02

The highest growth rate at 200 mM methanol supplementation was observed for the UBMet.P strain, followed by the THNat.P strain with average growth rates of 0.35±0.00 h^{-1} and 0.34±0.01 h^{-1}, respectively. The UBMet.P strain carried the construct with the *mdh* promoter for the *hps* and *phi* genes in the high copy number pUB110Smp plasmid, while the THNat.P strain carried the native promoter for *B. methanolicus* MGA3 in the low copy number pTH1mp plasmid. The strain carrying the pTH1mp construct with the *mdh* promoter displayed a slightly lower average growth rate compared to the strain with native promoter, but higher than the growth rates observed in the THEV and UBEV empty vector strains with 0.32±0.00 h^{-1} and 0.33±0.03 h^{-1} respectively.

During growth in minimal medium with 400 mM methanol, the highest growth rate was observed in THNat.P strain with an average growth rate of 0.33±0.00 h^{-1}. The UBMet.P strain grew slower in the medium with 400 mM methanol in comparison to 200 mM methanol medium with the lowest average growth rate of all tested strains with a value of 0.32±0.01 h^{-1}. The behavior of both empty vector strains remained stable between the two methanol concentrations.

Comparing the growth in minimal medium supplemented with 200 mM and 400 mM, the strain with the high copy number plasmid UBMet.P displayed the highest average growth rate of all strains at 200 mM methanol and the lowest at 400 mM. Of the strains homologously expressing *hps* and *phi,* only the THNat.P had an increased growth rate compared to the empty vector strains in the 400 mM methanol sample. The empty vector strains maintained a steady growth rate between the two methanol concentrations but showed lower growth rates in both compared to the THNat.P strain. All strains heterologously expressing *hps* and *phi* showed increased growth rates compared to the empty vector control strains when supplemented with 200 mM methanol, with the high copy number plasmid strain pUB110Smp-hps-phi displaying the most potential in increased growth rate.

4 Discussion

The utilization of *B. methanolicus* MGA3 as a candidate for synthetic methanotrophy and as a platform for biotechnological production has several potential benefits. Achieving functional heterologous production of sMMO has been problematic in the past and the complexity of this issue is reflected in this study. However, despite unsuccessful attempts at functional sMMO production in *B. methanolicus*, the possibility of methane as biotechnological feedstock is still worth pursuing. A potential way to improve carbon assimilation by *B. methanolicus* is homologous expression of *hps* and *phi*. The increased growth rates of the strains homologously expressing *hps* and *phi* could lead to the creation of an efficient biotechnological production platform with *B. methanolicus* as a fast-growing producer of value-added compounds.

4.1 Adapting and establishing an enzyme assay for sMMO activity in *B. methanolicus*

One of the main aims of this study was to test sMMO activity in *B. methanolicus* MGA3 strains carrying sMMO and various chaperonins. An existing coumarin fluorescence-based assay was adapted for use in *B. methanolicus* MGA3. The fluorescence intensities seen in the *B. methanolicus* MGA3 strains expressing sMMO and associated chaperonins could not be attributed to functionally expressed sMMO as shown in section 3.1 and 3.2 (supplementary data in appendix G and H). The substrate, coumarin, when oxidized by sMMO forms the fluorescent product 7-hydroxycoumarin. Functional sMMO is reliant on correct translation of its genes followed by proper folding assisted by chaperonins. If functional sMMO had been produced, the resulting increased fluorescence would have most likely been observed in the co-expression strains, expressing both sMMO and one of the GroES/EL chaperonins. However, the fluorescence observed in both the wild type and empty vector control strain was higher or comparable to the levels seen in the test strains. This indicates that the minor levels of fluorescence observed (tables 3.1 and 3.2) in *B. methanolicus* MGA3 appears to originate from a natively produced fluorescent compound which could correspond to a product like riboflavin (Yang et al. 2016; Klein et al. 2023; Sim et al. 2021). The comparable fluorescence between the 250 µM sample and the 0 µM sample initially suggested that *B. methanolicus* MGA3 was potentially not able to transport the coumarin into the cell from the surrounding environment, and that the fluorescence observed came from the natively produced compound(s). Due to this reason the experiment was changed from using whole cell culture to crude extract from sonicated cells. In the first two experiments using crude extract, the fluorescence in the 0 µM/mM samples was not present. However, as seen in the whole cell and supernatant fractions of the first experiment using whole cell cultures, the overall fluorescence was very low. The standards using 10 µM, 25 µM, 50 µM, 100 µM, and 250 µM 7-hydroxycoumarin concentrations had fluorescence intensities ranging from ca. 77 a.u. at the lowest concentration to ca. 2000 a.u. at the highest. Comparing the overall fluorescence in the tested strains with the values seen in the standards, the absence of functional sMMO becomes more evident.

The third and fourth experiments examined the potential negative effects of copper and temperature on sMMO. The "copper-switch" between the particulate and soluble versions of MMO is regulated through expression modulation by methanobactin and direct copper-protein interactions (Semrau et al. 2013). Regulation by copper-protein interactions is the only applicable regulatory mechanism in this study, as the expression-regulated part of the "copper-switch" is reliant on the methanobactin operon. This operon was not present in the plasmid constructs used in this study. Copper ions directly interact with the hydroxylase (MMOH) component of sMMO causing it to lose its diiron-sulfur center. This prevents electrons from being delivered by the reductase (MMOR) component. In addition, it causes FAD to dissociate from MMOR, preventing the transfer of electrons from NADH. As a result, expression of plasmid encoded sMMO genes during cultivation in copper-rich medium without the methanobactin operon could still lead to inhibition through these direct copper-protein interactions (Green, Prior, and Dalton 1985; Semrau et al. 2013). The influence of high cultivation temperature of *B. methanolicus* at 50°C on protein stability leading to denaturation could have contributed to the low enzyme activity. The consequence of this could be that no product was formed, and low fluorescence intensities were measured in the tested strains. The donor for sMMO in this study was *M. capsulatus* (Bath) which is a thermotolerant methanotroph with an optimum growth temperature of 37°C (Foster and Davis 1966). *B. methanolicus* MGA3 is a thermophilic methylotroph with an optimum growth temperature of 50°C (Irla et al. 2016). The increased cultivation of *B. methanolicus* at 50°C could have led to inappropriate folding of sMMO, potentially through breakdown of its quaternary structure, preventing the individual subunits from forming a functional protein (Lee 1991). Although Foster and Davis reported growth of *M. capsulatus* (Bath) up to 50°C, the increased temperature could still affect enzyme stability, either of sMMO itself or chaperonins (Foster and Davis 1966). In the final iteration of the experimental setup, all *B. methanolicus* strains were cultivated at 45°C instead of the usual 50°C, and the enzyme assay was conducted at 37°C. All tested strains had similar fluorescence intensities, including the negative controls displaying equal fluorescence. The lower temperatures and absence of copper did not appear to influence enzyme expression or function.

These factors combined mean that the observed fluorescence was most likely a result of natively produced fluorescent compounds or cell autofluorescence. This could also explain why the wild type strain had the highest fluorescence in the third experiment as no substrates or nutrients had to be shunted towards producing plasmid encoded proteins, and could instead be channeled towards native synthesis pathways (Bienick et al. 2014). The reduced fluorescence for the wild type strain cultivated at lower temperature could be explained by diminished protein synthesis and therefore reduced production of fluorescent compounds due to the sub-optimal temperatures used during induction, in conjunction with reduced growth rate (Price and Sowers 2004). The absence of functionally produced sMMO also prevented the assessment of functions and interactions of the hypothetical protein.

4.1.1 Adapting an alternative assay for sMMO activity through oxidation of naphthalene

The additional assay using *B. methanolicus* MGA3 and *M. capsulatus* (Bath) colonies on solid media with the addition of naphthalene crystals and tetrazotized o-dianisidine supported the initial findings of the absence of functionally expressed sMMO. The *M. capsulatus* (Bath) positive control resulted in a single purple colony, confirming the presence of sMMO. The colonies of *M. capsulatus* (Bath) were grown on NMS medium supplemented with 0.8% methanol as carbon source instead of methane. This medium

supplemented with methanol was chosen due to not having the appropriate equipment and facilities for growth on methane. Experimental evidence has shown that methane oxidation rates decrease when grown on methanol over time, suggesting a downregulation of sMMO (Stanley and Warwick 1977). This could explain why only a single purple colony was observed in the positive control. The colonies were also on average smaller in diameter (figure 3.6) than those normally seen when grown using an optimum methane-to-air mixture which further underlines the sub-optimal conditions (Graham et al. 1992). The expression of sMMO in the naphthalene assay was done without the addition of sodium formate as an electron donor. *B. methanolicus* MGA3 natively possess some electron regeneration systems, especially in relation to MDH and RuMP pathway components, but the introduction of an additional component in need of electron regeneration could have negatively influenced the activity of the enzyme (Wang et al. 2019). It is however unlikely that this alone would result in no enzyme activity if functional sMMO was expressed due to some, although limited, electron availability from the already existing electron regeneration systems.

4.1.2 Improvements and alternative methods for measuring sMMO activity

Achieving synthetic methanotrophy has generally been a major challenge in a variety of host organisms. Active subunits of sMMO (MMOR and MMOB) have previously been expressed in *E. coli* but the hydroxylase (MMOH) component of sMMO has yet to be expressed. In addition, proper folding of the enzyme has been problematic (Murrell, McDonald, and Gilbert 2000; West et al. 1992). This is reflected in the complexity of the sMMO operon where proper folding and function is also dependent on the correct expression and processing of the genes involved. These proteins may also serve auxiliary functions which could cause unknown interactions, preventing formation of functional sMMO (Khider, Brautaset, and Irla 2021). Native methanotrophs and methylotrophs vary significantly in growth medium requirements. Due to some uncertainty related to the mechanisms associated with sMMO, it is unknown if certain nutrients or elements normally present in the environment of methanotrophs but lacking in other methylotrophic environments could play major roles in correct expression, folding, or function of sMMO. The influence of nitrogen- and sulfur sources especially could serve regulatory functions (Kalyuzhnaya, Puri, and Lidstrom 2015). These factors could also be applied to the chaperonins responsible for proper folding. Host organism chaperonins GroES/EL have previously been shown to increase conversion rate of sMMO in *E. coli*, suggesting some sequence overlap between species and serving a crucial role in functional expression (Clark 2019; Zill et al. 2022). If the adapted fluorescence-based coumarin assay or the assay using the oxidation of naphthalene had shown the presence of functional sMMO in *B. methanolicus*, additional chaperonins like for example GroEL2 from *M. capsulatus* (Bath) would have been applied to attempt to improve enzyme activity. As no functionally expressed sMMO was observed, the examination of other chaperonins was abandoned. With the knowledge gaps regarding aspects like sMMO gene expression, nutrient effects, or influence of metabolic pathway on sMMO, assessing and predicting appropriate targets for pathway engineering in production hosts is made exponentially more difficult.

Alternative methods for assessing the activity of functionally produced sMMO could be targeted at two areas: measuring an oxidized product from a specific substrate for sMMO, as intended with the coumarin- and naphthalene assays, or determining the presence of the protein itself. Several products from oxidized substrates of sMMO could be detected through chromatographic methods such as GC or HPLC. Oxidation of propylene to propylene oxide have previously been applied to determine the activity of sMMO in native

methanotrophs like *M. capsulatus* and *M. trichosporium* (Sirajuddin and Rosenzweig 2015), and could be accommodated for heterologously produced sMMO in *B. methanolicus* MGA3. Epoxidation of propene and the conversion of cyclohexanol to cyclohexanone could also be used to determine the presence and potential activity of sMMO (Park et al. 1992; Esmelindro et al. 2005). An alternative to the colorimetric assay using the interaction between o-dianisidine and 1-naphthol from oxidized naphthalene used in this study, is to determine the amount of 1-naphthol formed from potential sMMO by HPLC analysis. This would have provided a more accurate measure of formed 1-naphthol but would require further processing and the usage of HPLC equipment. As one of the aims of this study was to adapt and establish a simple and efficient proof-of-concept enzyme assay to screen for the activity of sMMO without the need for more complex equipment and sample preparation, the colorimetric naphthalene assay was chosen. Determining the presence of the protein itself could be done through several techniques. Sodium dodecyl sulfate-polyacrylamide denaturing gel electrophoresis (SDS-PAGE) would allow for size comparisons of proteins present in the strains and coupling this with an immunoblotting technique (Western blot), could examine the presence of sMMO (Burnette 1981; Blancher and Jones 2001). Other techniques include enzyme-linked immunosorbent assay (ELISA), mass spectrometry, and protein microarrays (Wang and Wilson 2013; Alhajj, Zubair, and Farhana 2023; Templin et al. 2002).

4.2 The effect of overproduction of homologous *hps* and *phi* on methanol tolerance and growth rate in *B. methanolicus*

As methanol is converted to formaldehyde by the action of MDH, the rate-limiting enzymes HPS and PHI assimilate formaldehyde by incorporating it into the RuMP cycle. These two enzymes play a major role in determining and regulating carbon flux into metabolic pathways. Increasing the assimilation of methanol through overexpression of *hps* and *phi* could therefore theoretically provide higher growth rates by increasing carbon flux towards its assimilation. This is further underlined by the upregulation of RuMP cycle genes when grown on methanol as carbon source (Delépine et al. 2020). In several studies, higher methanol tolerance was observed as the increased conversion of formaldehyde from methanol would be more rapidly assimilated (Price et al. 2016; Müller et al. 2014; Brautaset et al. 2007).

All the *B. methanolicus* strains homologously expressing *hps* and *phi* showed increased growth rates compared to the empty vector negative controls. The growth rates observed in this study showed that the *hps* and *phi* operon expressed with the *mdh* promoter in the high copy number pUB110Smp plasmid yielded the highest growth rate compared to the other strains. Previous experimental evidence has suggested that the native *hps* and *phi* promoter is stronger than the *mdh* promoter (Irla, Hakvåg, and Brautaset 2021), and the higher growth rate seen in the strain with the pUB110Smp plasmid in comparison to the strain with pTH1mp with the *mdh* promoter suggests that the high copy number potentially makes up for and supersedes the effect of the stronger native promoter. Supplementation of 400 mM methanol, showed that the strain with the pUB11Smp-hps-phi construct displayed a distinctly lower growth rate in comparison to the strains with the pTH-hps-phi constructs, suggesting that the native promoter more efficiently expresses *hps* and *phi* at higher methanol concentrations compared to the *mdh* promoter.

The reason for the reduced growth rate seen in the strain with the pUB110Smp plasmid using the *mdh* promoter can be a result of several factors. On such factor could be the metabolic burden brought on by the increased copy number in conjunction with the increased concentration of inducer. A high copy number and therefore an increased

transcription of the synthetic operon could lead to diminishing growth rates due to the metabolic requirements to produce the plasmid encoded proteins (Millan and MacLean 2017). The unsuccessful attempts at transforming *B. methanolicus* MGA3 with the high copy number pUB110Smp plasmid and the *hps* and *phi* operon controlled by the native promoter prevents an assessment of the native promoter together with a high copy number plasmid. Based on the results in this study and previous experimental evidence regarding the strength of the native promoter, this could have yielded a strain with average growth rates superseding that of the high copy number plasmid with the *mdh* promoter (Irla, Hakvåg, and Brautaset 2021). This further underlines the interest in assessing growth rates in strains using the high copy number plasmid in conjunction with the native promoter. Despite this, the results suggest that the overexpression of *hps* and *phi* could lead to more efficient methanol assimilation and methanol tolerance, with increased growth rates as a result.

4.3 Expanding the C1 substrate range for *B. methanolicus*

The two main targets for this study were the first two successive steps in one-carbon metabolism in methylotrophic bacteria. Although activity of sMMO in *B. methanolicus* MGA3 was not observed, the theoretical prospect of being able to utilize methane in synthetic methanotrophs warrant further investigation, especially in conjunction with the potential increased growth rates provided by homologously over-produced *hps* and *phi*.

Enabling the conversion of methane into methanol in synthetic methanotrophs, followed by assimilation in metabolic pathways with increased flux could lead to the creation of highly efficient microbial cell factories. These could be applied to the production of certain amino acids like L-glutamate, L-serine, and L-lysine, which *B. methanolicus* has shown to be efficient producers of (Brautaset et al. 2007). Other potential products include biodegradable polyesters, like PHAs, and block polymers like cadaverin and aminobutyric acid (GABA) (Schrader et al. 2009; Li, Yang, and Loh 2016; Irla et al. 2017; Müller et al. 2015). The usage of methane as carbon source provides both opportunities as well as certain problems. Methane is cheap, abundant, and mitigates climate change through its depletion from the atmosphere (Comer et al. 2017). On the other hand, methane is characterized by low solubility and mass transfer compared to liquid carbon sources, in addition to issues regarding the volatility of methane when combined with oxygen (In Yeub et al. 2014).

Homologous production of the rate-limiting HPS and PHI could subsequently shift the equilibrium towards the RuMP pathway, increasing carbon flux in synthetic pathways for value-added compounds (Price et al. 2016). As both heterologous expression of sMMO and homologous expression of *hps* and *phi* are plasmid-based, the increased metabolic burden of a co-expression strain containing constructs carrying sMMO, associated chaperonins, and *hps* and *phi* could lead to reduced growth rates (Millan and MacLean 2017). In addition, plasmid incompatibility must be considered to ensure variability in origin of replication, meaning three different plasmid backbones must be used (Abdelaal and Yazdani 2021). This could be rectified to some extent if host species chaperonins are shown to have enough similarity to donor chaperonins to yield functional sMMO, as demonstrated in *E. coli* (Clark 2019). This could also be alleviated through the addition of one or more of the genes directly into the genome using for example CRISP-Cas or integrative vectors (Arroyo-Olarte, Bravo Rodríguez, and Morales-Ríos 2021).

Large volumes of methane today are burned as natural gas at refinery sites as an unwanted biproduct of oil exploration or released into the environment. This results in large quantities

of methane being wasted or released as a potent GHG (Comer et al. 2017). The biotechnology sector benefits by having a cheap and abundant carbon source that does not compete as feedstocks with other sectors like the food industry. The petroleum industry benefits by gaining an additional market for a gas that normally would be unwanted, and the environment benefits by reduced release and increased capture of a potent GHG.

4.4 Future outlooks

The unsuccessful attempt to express heterologous sMMO represents the major obstacle towards synthetic methanotrophy in an industrial setting. Although native methanotrophic bacteria have certain applications, they are also characterized by difficult growth conditions and comparably low growth rates when compared to more common industrial production strains like *E. coli* and *S. cerevisiae*. As certain details surrounding the catalytic mechanisms of sMMO remain unknown, elucidating the functions and interactions of these mechanisms will enable more specific targets for pathway engineering. One such element is the mentioned "copper-switch". Although several proposed mechanisms exist, the full scope of the "copper-switch" remains unknown. Fully understanding the regulatory interactions of copper is a priority, seeing as this is one of the major regulatory mechanisms for sMMO production in native methanotrophs. The unknown elements also include several of the genes in the *smmo* operon, most notably the hypothetical protein (MCA1201) but also the genes *mmoD, mmoQ,* and *mmoS.* Utilizing gene knockouts and deletion strains of native methanotrophs could reveal some of the functions of these genes and their products. Metabolic pathway modeling using bioinformatics must also be considered, especially regarding some of the lesser understood pathways in native methanotrophs and their potential interactions with methane conversion. The aspect of electron regeneration for sMMO is also an area of interest, especially when using methylotrophic production hosts like *B. methanolicus*. Although *B. methanolicus* contains electron regeneration systems for enzymes like MDH, the additional need for reducing power in sMMO could be a factor limiting its heterologous production. In addition, attempting growth of the *B. methanolicus* strains heterologously expressing sMMO on methane should also be attempted.

The assimilation of methanol in *B. methanolicus* through homologous expression of *hps* and *phi* has shown promising results for biotechnological production. Growth experiments with the combination of native promoter with a high copy number plasmid should be conducted to assess its effect, as this study suggest this combination could potentially provide the most significant increase in growth rate, especially at higher methanol concentrations. Scalability is another aspect in need of additional research as the effects of homologous expression of *hps* and *phi* in larger bioreactors must be assessed before the strains can be applied in a biotechnological production setting. All in all, the usage of homologously expressed *hps* and *phi* could yield a stable and efficient *B. methanolicus* platform that could be used in the future for production of a range of chemicals and value-added compounds.

5 Conclusion

Utilizing methane through synthetic methanotrophy of the thermophilic methylotroph *B. methanolicus* MGA3 has been an area of seemingly great potential. Having a cheap and abundant carbon source available for production of value-added compounds using a strain with increased carbon assimilation could provide a new efficient production strain for the biotechnology industry. However, the practical application of functional expression of sMMO has proven difficult, whilst increasing the rate of methanol assimilation has had some interesting results.

This study aimed to target carbon metabolism in *B. methanolicus* by first creating strains capable of expressing functional sMMO alongside a suitable fluorescence-based enzyme assay for detecting and measuring the activity of said enzyme. Expression strains of *B. methanolicus* MGA3 carrying sMMO in conjunction with various chaperonins showed no presence of functional sMMO through several experiments each targeting specific parameters. Among these were substrate concentration, effect of shaking on enzyme stability, temperature, and the inhibitory effects of copper. The homologous expression of *hps* and *phi* responsible for assimilating formaldehyde into synthetic pathways showed some interesting results by suggesting increased growth rates when paired with a native promoter or high copy number plasmid. In addition, the native promoter indicated an increased methanol tolerance by displaying stabile growth rates in higher methanol concentrations compared to the plasmid constructs using the *mdh* promoter, which saw a decrease in average growth rate.

Although this study was unsuccessful in observing activity of sMMO in *B. methanolicus* MGA3, the various experiments conducted gave some insight into the different parameters of sMMO suitable for future research. Most of all, it highlighted the need for further elucidation of the mechanisms and systems associated with functional expression of sMMO in native methanotrophs, which includes the genes within the sMMO operon with unknown functions and roles. These include *mmoD, mmoQ, and mmoS*, and improving our understanding of how these genes and mechanisms interconnect will provide a better foundation for more specific elements within metabolic pathways to target using genetic engineering. The overexpression of *hps* and *phi* and the increased growth rates seen in this study demonstrated that modulating the amount of the rate-limiting enzymes of carbon assimilation in *B. methanolicus* MGA3 could prove an important tool in developing new production strains capable of a high output of value-added compounds. Future research would have to determine the effect on actual production of value-added compounds and the scalability of strains in a larger industrial setting.

Bibliography

Abdelaal, A. S., and S. S. Yazdani. 2021. 'A genetic toolkit for co-expression of multiple proteins of diverse physiological implication', *Biotechnol Rep (Amst)*, 32: e00692.

Alhajj, M., M. Zubair, and A. Farhana. 2023. 'Enzyme Linked Immunosorbent Assay.' in, *StatPearls* (StatPearls Publishing)

Antoniewicz, Maciek R. 2019. 'Synthetic methylotrophy: Strategies to assimilate methanol for growth and chemicals production', *Current Opinion in Biotechnology*, 59: 165-74.

Arroyo-Olarte, R. D., R. Bravo Rodríguez, and E. Morales-Ríos. 2021. 'Genome Editing in Bacteria: CRISPR-Cas and Beyond', *Microorganisms*, 9.

Bienick, M. S., K. W. Young, J. R. Klesmith, E. E. Detwiler, K. J. Tomek, and T. A. Whitehead. 2014. 'The interrelationship between promoter strength, gene expression, and growth rate', *PLOS ONE*, 9: e109105.

Blancher, C., and A. Jones. 2001. 'SDS -PAGE and Western Blotting Techniques', *Methods Mol Med*, 57: 145-62.

Brautaset, Trygve, Øyvind M. Jakobsen, Kjell D. Josefsen, Michael C. Flickinger, and Trond E. Ellingsen. 2007. 'Bacillus methanolicus: a candidate for industrial production of amino acids from methanol at 50°C', *Applied Microbiology and Biotechnology*, 74: 22-34.

Brusseau, Gregory A., Hsien-Chyang Tsien, Richard S. Hanson, and Lawrence P. Wackett. 1990. 'Optimization of trichloroethylene oxidation by methanotrophs and the use of a colorimetric assay to detect soluble methane monooxygenase activity', *Biodegradation*, 1: 19-29.

Burnette, W. Neal. 1981. '"Western Blotting": Electrophoretic transfer of proteins from sodium dodecyl sulfate-polyacrylamide gels to unmodified nitrocellulose and radiographic detection with antibody and radioiodinated protein A', *Analytical Biochemistry*, 112: 195-203.

Chistoserdova, Ludmila, Marina G. Kalyuzhnaya, and Mary E. Lidstrom. 2009. 'The Expanding World of Methylotrophic Metabolism', *Annual Review of Microbiology*, 63: 477-99.

Christendat, Dinesh, Adelinda Yee, Akil Dharamsi, Yuval Kluger, Mark Gerstein, Cheryl H. Arrowsmith, and Aled M. Edwards. 2000. 'Structural proteomics: prospects for high throughput sample preparation', *Progress in Biophysics and Molecular Biology*, 73: 339-45.

Cieśla, Łukasz M., Monika Waksmundzka-Hajnos, Karolina A. Wojtunik, and Mieczysław Hajnos. 2015. 'Thin-layer chromatography coupled with biological detection to screen natural mixtures for potential drug leads', *Phytochemistry Letters*, 11: 445-54.

Clark, Elizabeth Jane (San Francisco, CA, US), Zhu, Baolong (San Diego, CA, US), Greenfield, Derek Lorin (Kensington, CA, US), Jones, Stephanie Rhianon (Berkeley, CA, US), Helman, Noah Charles (El Cerrito, CA, US). 2019. "Functional Expression of Monooxygenases and Methods of Use." In. United States: Industrial Microbes, Inc. (Emeryville, CA, US).

Comer, A. D., M. R. Long, J. L. Reed, and B. F. Pfleger. 2017. 'Flux Balance Analysis Indicates that Methane Is the Lowest Cost Feedstock for Microbial Cell Factories', *Metab Eng Commun*, 5: 26-33.

Cotton, Charles A. R., Nico J. Claassens, Sara Benito-Vaquerizo, and Arren Bar-Even. 2020. 'Renewable methanol and formate as microbial feedstocks', *Current Opinion in Biotechnology*, 62: 168-80.

Curry, Charles L. 2007. 'Modeling the soil consumption of atmospheric methane at the global scale', *Global Biogeochemical Cycles*, 21.

Delépine, Baudoin, Marina Gil López, Marc Carnicer, Cláudia M. Vicente, Volker F. Wendisch, and Stéphanie Heux. 2020. 'Charting the Metabolic Landscape of the Facultative Methylotroph Bacillus methanolicus', *mSystems*, 5: e00745-20.

Drejer, Eivind B., Dennis Tin Chat Chan, Carsten Haupka, Volker F. Wendisch, Trygve Brautaset, and Marta Irla. 2020. 'Methanol-based acetoin production by genetically engineered Bacillus methanolicus', *Green Chemistry*, 22: 788-802.

Egan, Denise, Richard O'Kennedy, Elizabeth Moran, Dermot Cox, Ena Prosser, and R. Douglas Thornes. 1990. 'The Pharmacology, Metabolism, Analysis, and Applications of Coumarin and Coumarin-Related Compounds', *Drug Metabolism Reviews*, 22: 503-29.

Esmelindro, Maria Carolina, Enrique G. Oestreicher, Heiddy Márquez-Alvarez, Cláudio Dariva, Sílvia M. S. Egues, Christiane Fernandes, Adailton J. Bortoluzzi, Valderes Drago, and O. A. C. Antunes. 2005. 'Catalytic oxidation of cyclohexane by a binuclear Fe(III) complex biomimetic to methane monooxygenase', *Journal of Inorganic Biochemistry*, 99: 2054-61.

Foster, J. W., and R. H. Davis. 1966. 'A methane-dependent coccus, with notes on classification and nomenclature of obligate, methane-utilizing bacteria', *J Bacteriol*, 91: 1924-31.

Gibson, Daniel G., Lei Young, Ray-Yuan Chuang, J. Craig Venter, Clyde A. Hutchison, and Hamilton O. Smith. 2009. 'Enzymatic assembly of DNA molecules up to several hundred kilobases', *Nature Methods*, 6: 343-45.

Graham, D W, D G Korich, R P LeBlanc, N A Sinclair, and R G Arnold. 1992. 'Applications of a colorimetric plate assay for soluble methane monooxygenase activity', *Applied and Environmental Microbiology*, 58: 2231-36.

Green, Jeffrey, Stephen D. Prior, and Howard Dalton. 1985. 'Copper ions as inhibitors of protein C of soluble methane monooxygenase of Methylococcus capsulatus (Bath)', *European Journal of Biochemistry*, 153: 137-44.

Gregory, Gwendolyn J., R. Kyle Bennett, and Eleftherios T. Papoutsakis. 2022. 'Recent advances toward the bioconversion of methane and methanol in synthetic methylotrophs', *Metabolic Engineering*, 71: 99-116.

Hanson, R S, and T E Hanson. 1996. 'Methanotrophic bacteria', *Microbiological Reviews*, 60: 439-71.

Haynes, Chad A., and Ramon Gonzalez. 2014. 'Rethinking biological activation of methane and conversion to liquid fuels', *Nature Chemical Biology*, 10: 331-39.

Heggeset, Tonje M. B., Anne Krog, Simone Balzer, Alexander Wentzel, Trond E. Ellingsen, and Trygve Brautaset. 2012. 'Genome Sequence of Thermotolerant Bacillus methanolicus: Features and Regulation Related to Methylotrophy and Production of L-lysine and L-glutamate from Methanol', *Applied and Environmental Microbiology*, 78: 5170-81.

Heux, Stephanie, Trygve Brautaset, Julia A. Vorholt, Volker F. Wendisch, and Jean Charles Portais. 2018. 'Synthetic Methylotrophy: Past, Present, and Future.' in Marina G. Kalyuzhnaya and Xin-Hui Xing (eds.), *Methane Biocatalysis: Paving the Way to Sustainability* (Springer International Publishing: Cham).

Hou, C T, R Patel, A I Laskin, and N Barnabe. 1979. 'Microbial oxidation of gaseous hydrocarbons: epoxidation of C2 to C4 n-alkenes by methylotrophic bacteria', *Applied and Environmental Microbiology*, 38: 127-34.

Hwang, In Yeub, Anh Duc Nguyen, Thu Thi Nguyen, Linh Thanh Nguyen, Ok Kyung Lee, and Eun Yeol Lee. 2018. 'Biological conversion of methane to chemicals and fuels: technical challenges and issues', *Applied Microbiology and Biotechnology*, 102: 3071-80.

In Yeub, Hwang, Lee Seung Hwan, Choi Yoo Seong, Park Si Jae, Na Jeong Geol, Chang In Seop, Kim Choongik, Kim Hyun Cheol, Kim Yong Hwan, and Lee Jin Won. 2014. 'Biocatalytic Conversion of Methane to Methanol as a Key Step for Development of Methane-Based Biorefineries', *Journal of Microbiology and Biotechnology*, 24: 1597-605.

Irla, M., S. Hakvåg, and T. Brautaset. 2021. 'Developing a Riboswitch-Mediated Regulatory System for Metabolic Flux Control in Thermophilic Bacillus methanolicus', *Int J Mol Sci*, 22.

Irla, M., T. M. Heggeset, I. Nærdal, L. Paul, T. Haugen, S. B. Le, T. Brautaset, and V. F. Wendisch. 2016. 'Genome-Based Genetic Tool Development for Bacillus

methanolicus: Theta- and Rolling Circle-Replicating Plasmids for Inducible Gene Expression and Application to Methanol-Based Cadaverine Production', *Front Microbiol*, 7: 1481.
Irla, Marta, Eivind B. Drejer, Trygve Brautaset, and Sigrid Hakvåg. 2020. 'Establishment of a functional system for recombinant production of secreted proteins at 50 °C in the thermophilic Bacillus methanolicus', *Microbial Cell Factories*, 19: 151.
Irla, Marta, Ingemar Nærdal, Trygve Brautaset, and Volker F. Wendisch. 2017. 'Methanol-based γ-aminobutyric acid (GABA) production by genetically engineered Bacillus methanolicus strains', *Industrial Crops and Products*, 106: 12-20.
Izumi, Yoshikazu, Toyokazu Yoshida, Silvia Susana Miyazaki, Toshio Mitsunaga, Takashi Ohshiro, Masayuki Shimao, Atsuro Miyata, and Tadashi Tanabe. 1993. 'l-Serine production by a methylotroph and its related enzymes', *Applied Microbiology and Biotechnology*, 39: 427-32.
Jahng, D., and T. K. Wood. 1994. 'Trichloroethylene and chloroform degradation by a recombinant pseudomonad expressing soluble methane monooxygenase from Methylosinus trichosporium OB3b', *Appl Environ Microbiol*, 60: 2473-82.
Joergensen, Lars, and Hans Degn. 1987. 'Growth rate and methane affinity of a turbidostatic and oxystatic continuous culture ofMethylococcuscapsulatus (Bath)', *Biotechnology Letters*, 9: 71-76.
Kalyuzhnaya, Marina G., Aaron W. Puri, and Mary E. Lidstrom. 2015. 'Metabolic engineering in methanotrophic bacteria', *Metabolic Engineering*, 29: 142-52.
Khider, May L. K., Trygve Brautaset, and Marta Irla. 2021. 'Methane monooxygenases: central enzymes in methanotrophy with promising biotechnological applications', *World Journal of Microbiology and Biotechnology*, 37: 72.
Kim, Seon Won, Pil Kim, Hyun S. Lee, and Jung H. Kim. 1996. 'High production of Poly-β-hydroxybutyrate (PHB) from Methylobacterium organophilum under potassium limitation', *Biotechnology Letters*, 18: 25-30.
Kirschke, Stefanie, Philippe Bousquet, Philippe Ciais, Marielle Saunois, Josep G. Canadell, Edward J. Dlugokencky, Peter Bergamaschi, Daniel Bergmann, Donald R. Blake, Lori Bruhwiler, Philip Cameron-Smith, Simona Castaldi, Frédéric Chevallier, Liang Feng, Annemarie Fraser, Martin Heimann, Elke L. Hodson, Sander Houweling, Béatrice Josse, Paul J. Fraser, Paul B. Krummel, Jean-François Lamarque, Ray L. Langenfelds, Corinne Le Quéré, Vaishali Naik, Simon O'Doherty, Paul I. Palmer, Isabelle Pison, David Plummer, Benjamin Poulter, Ronald G. Prinn, Matt Rigby, Bruno Ringeval, Monia Santini, Martina Schmidt, Drew T. Shindell, Isobel J. Simpson, Renato Spahni, L. Paul Steele, Sarah A. Strode, Kengo Sudo, Sophie Szopa, Guido R. van der Werf, Apostolos Voulgarakis, Michiel van Weele, Ray F. Weiss, Jason E. Williams, and Guang Zeng. 2013. 'Three decades of global methane sources and sinks', *Nature Geoscience*, 6: 813-23.
Klein, Vivien Jessica, Luciana Fernandes Brito, Fernando Perez-Garcia, Trygve Brautaset, and Marta Irla. 2023. 'Metabolic engineering of thermophilic Bacillus methanolicus for riboflavin overproduction from methanol', *Microbial Biotechnology*, 16: 1011-26.
Knief, Claudia. 2015. 'Diversity and Habitat Preferences of Cultivated and Uncultivated Aerobic Methanotrophic Bacteria Evaluated Based on pmoA as Molecular Marker', *Frontiers in Microbiology*, 6.
Komives, Claire F, Louis Yip-Yan Cheung, Stefanie B Pluschkell, and Michael C Flickinger. 2005. 'Growth of Bacillus methanolicus in seawater-based media', *Journal of Industrial Microbiology and Biotechnology*, 32: 61-66.
Krog, Anne, Tonje M. B. Heggeset, Jonas E. N. Müller, Christiane E. Kupper, Olha Schneider, Julia A. Vorholt, Trond E. Ellingsen, and Trygve Brautaset. 2013. 'Methylotrophic Bacillus methanolicus Encodes Two Chromosomal and One Plasmid Born NAD+ Dependent Methanol Dehydrogenase Paralogs with Different Catalytic and Biochemical Properties', *PLOS ONE*, 8: e59188.
Lee, B. 1991. 'Isoenthalpic and isoentropic temperatures and the thermodynamics of protein denaturation', *Proceedings of the National Academy of Sciences*, 88: 5154-58.

Li, Zibiao, Jing Yang, and Xian Jun Loh. 2016. 'Polyhydroxyalkanoates: opening doors for a sustainable future', *NPG Asia Materials*, 8: e265-e65.
Mazimba, Ofentse. 2017. 'Umbelliferone: Sources, chemistry and bioactivities review', *Bulletin of Faculty of Pharmacy, Cairo University*, 55: 223-32.
Millan, Alvaro San, and R. Craig MacLean. 2017. 'Fitness Costs of Plasmids: a Limit to Plasmid Transmission', *Microbiology Spectrum*, 5: 5.5.02.
Miller, A., W. Keener, M. Watwood, and F. Roberto. 2002. 'A rapid fluorescence-based assay for detecting soluble methane monooxygenase', *Applied Microbiology and Biotechnology*, 58: 183-88.
Murrell, J. C., I. R. McDonald, and B. Gilbert. 2000. 'Regulation of expression of methane monooxygenases by copper ions', *Trends Microbiol*, 8: 221-5.
Murrell, J. C., and T. J. Smith. 2010. 'Biochemistry and Molecular Biology of Methane Monooxygenase.' in Kenneth N. Timmis (ed.), *Handbook of Hydrocarbon and Lipid Microbiology* (Springer Berlin Heidelberg: Berlin, Heidelberg).
Müller, Jonas E. N., Tonje M. B. Heggeset, Volker F. Wendisch, Julia A. Vorholt, and Trygve Brautaset. 2015. 'Methylotrophy in the thermophilic Bacillus methanolicus, basic insights and application for commodity production from methanol', *Applied Microbiology and Biotechnology*, 99: 535-51.
Müller, Jonas E. N., Boris Litsanov, Miriam Bortfeld-Miller, Christian Trachsel, Jonas Grossmann, Trygve Brautaset, and Julia A. Vorholt. 2014. 'Proteomic analysis of the thermophilic methylotroph Bacillus methanolicus MGA3', *PROTEOMICS*, 14: 725-37.
Parapouli, M., A. Vasileiadis, A. S. Afendra, and E. Hatziloukas. 2020. 'Saccharomyces cerevisiae and its industrial applications', *AIMS Microbiol*, 6: 1-31.
Park, S., N. N. Shah, R. T. Taylor, and M. W. Droege. 1992. 'Batch cultivation of Methylosinus trichosporium OB3b: II. Production of particulate methane monooxygenase', *Biotechnol Bioeng*, 40: 151-7.
Parsons, J. S., William Seaman, and J. T. Woods. 1955. 'Spectrophotometric Determination of 1-Naphthol in 2-Naphthol Utilizing Difference in Reaction Rates', *Analytical Chemistry*, 27: 21-24.
Pieja, A. J., M. C. Morse, and A. J. Cal. 2017. 'Methane to bioproducts: the future of the bioeconomy?', *Curr Opin Chem Biol*, 41: 123-31.
Price, J. Vincent, Long Chen, W. Brian Whitaker, Eleftherios Papoutsakis, and Wilfred Chen. 2016. 'Scaffoldless engineered enzyme assembly for enhanced methanol utilization', *Proceedings of the National Academy of Sciences*, 113: 12691-96.
Price, P. B., and T. Sowers. 2004. 'Temperature dependence of metabolic rates for microbial growth, maintenance, and survival', *Proc Natl Acad Sci U S A*, 101: 4631-6.
Rigby, Matthew, Stephen A. Montzka, Ronald G. Prinn, James W. C. White, Dickon Young, Simon O'Doherty, Mark F. Lunt, Anita L. Ganesan, Alistair J. Manning, Peter G. Simmonds, Peter K. Salameh, Christina M. Harth, Jens Mühle, Ray F. Weiss, Paul J. Fraser, L. Paul Steele, Paul B. Krummel, Archie McCulloch, and Sunyoung Park. 2017. 'Role of atmospheric oxidation in recent methane growth', *Proceedings of the National Academy of Sciences*, 114: 5373-77.
Sanchez, Sergio, Romina Rodríguez-Sanoja, Allison Ramos, and Arnold L. Demain. 2018. 'Our microbes not only produce antibiotics, they also overproduce amino acids', *The Journal of Antibiotics*, 71: 26-36.
Schrader, Jens, Martin Schilling, Dirk Holtmann, Dieter Sell, Murillo Villela Filho, Achim Marx, and Julia A. Vorholt. 2009. 'Methanol-based industrial biotechnology: current status and future perspectives of methylotrophic bacteria', *Trends in Biotechnology*, 27: 107-15.
Semrau, Jeremy D., Sheeja Jagadevan, Alan A. DiSpirito, Ashraf Khalifa, Julie Scanlan, Brandt H. Bergman, Brittani C. Freemeier, Bipin S. Baral, Nathan L. Bandow, Alexey Vorobev, Daniel H. Haft, Stéphane Vuilleumier, and J. Colin Murrell. 2013. 'Methanobactin and MmoD work in concert to act as the 'copper-switch' in methanotrophs', *Environmental Microbiology*, 15: 3077-86.

Sim, E. S., H. Dharmarajan, Dssk Boorgu, L. Goyal, M. Weinstock, R. Whelan, M. E. Freiser, T. E. Corcoran, N. Jabbour, E. Wang, and D. H. Chi. 2021. 'Novel Use of Vitamin B2 as a Fluorescent Tracer in Aerosol and Droplet Contamination Models in Otolaryngology', *Ann Otol Rhinol Laryngol*, 130: 280-85.

Sirajuddin, Sarah, and Amy C. Rosenzweig. 2015. 'Enzymatic Oxidation of Methane', *Biochemistry*, 54: 2283-94.

Sirirote, Pramote, Yamane Tsuneo, and Shimizu Shoichi. 1988. 'l-serine production from methanol and glycine with an immobilized methylotroph', *Journal of Fermentation Technology*, 66: 291-97.

Smith, T. J., and H. Dalton. 2004. 'Chapter 6 Biocatalysis by methane monooxygenase and its implications for the petroleum industry.' in Rafael Vazquez-Duhalt and Rodolfo Quintero-Ramirez (eds.), *Studies in Surface Science and Catalysis* (Elsevier).

Smith, Thomas J., and Tim Nichol. 2018. 'Engineering Soluble Methane Monooxygenase for Biocatalysis.' in Marina G. Kalyuzhnaya and Xin-Hui Xing (eds.), *Methane Biocatalysis: Paving the Way to Sustainability* (Springer International Publishing: Cham).

Stanley, S. H., S. D. Prior, D. J. Leak, and H. Dalton. 1983. 'Copper stress underlies the fundamental change in intracellular location of methane mono-oxygenase in methane-oxidizing organisms: Studies in batch and continuous cultures', *Biotechnology Letters*, 5: 487-92.

Stanley, S. H., and University of Warwick. 1977. 'A study of the physiology and gas limited growth of methylococcus capsulatus', University of Warwick.

Stolzenberger, Jessica, Steffen N. Lindner, and Volker F. Wendisch. 2013. 'The methylotrophic Bacillus methanolicus MGA3 possesses two distinct fructose 1,6-bisphosphate aldolases', *Microbiology*, 159: 1770-81.

Strong, P. J., S. Xie, and W. P. Clarke. 2015. 'Methane as a Resource: Can the Methanotrophs Add Value?', *Environmental Science & Technology*, 49: 4001-18.

Tan, Dan, Ying Wang, Yi Tong, and Guo-Qiang Chen. 2021. 'Grand Challenges for Industrializing Polyhydroxyalkanoates (PHAs)', *Trends in Biotechnology*, 39: 953-63.

Templin, Markus F., Dieter Stoll, Monika Schrenk, Petra C. Traub, Christian F. Vöhringer, and Thomas O. Joos. 2002. 'Protein microarray technology', *Drug Discovery Today*, 7: 815-22.

Theisen, Matthew, and James C. Liao. 2017. 'Industrial Biotechnology: Escherichia coli as a Host.' in, *Industrial Biotechnology*.

Wackett, Lawrence P., and David T. Gibson. 1983. 'Rapid Method for Detection and Quantitation of Hydroxylated Aromatic Intermediates Produced by Microorganisms', *Applied and Environmental Microbiology*, 45: 1144-47.

Wang, P., and S. R. Wilson. 2013. 'Mass spectrometry-based protein identification by integrating de novo sequencing with database searching', *BMC Bioinformatics*, 14 Suppl 2: S24.

Wang, Vincent C. C., Suman Maji, Peter P. Y. Chen, Hung Kay Lee, Steve S. F. Yu, and Sunney I. Chan. 2017. 'Alkane Oxidation: Methane Monooxygenases, Related Enzymes, and Their Biomimetics', *Chemical Reviews*, 117: 8574-621.

Wang, X., X. Wang, X. Lu, C. Ma, K. Chen, and P. Ouyang. 2019. 'Methanol fermentation increases the production of NAD(P)H-dependent chemicals in synthetic methylotrophic Escherichia coli', *Biotechnol Biofuels*, 12: 17.

Wendisch, Volker F. 2020. 'Metabolic engineering advances and prospects for amino acid production', *Metabolic Engineering*, 58: 17-34.

Wernicke, Hans-Jürgen, Ludolf Plass, and Friedrich Schmidt. 2014. 'Methanol Generation.' in Martin Bertau, Heribert Offermanns, Ludolf Plass, Friedrich Schmidt and Hans-Jürgen Wernicke (eds.), *Methanol: The Basic Chemical and Energy Feedstock of the Future: Asinger's Vision Today* (Springer Berlin Heidelberg: Berlin, Heidelberg).

West, Charlotte A., George P. C. Salmond, Howard Dalton, and J. Colin Murrell. 1992. 'Functional expression in Escherichia coli of proteins B and C from soluble methane monooxygenase of Methylococcus capsulatus (Bath)', *Microbiology*, 138: 1301-07.

Wilfinger, W. W., K. Mackey, and P. Chomczynski. 1997. 'Effect of pH and ionic strength on the spectrophotometric assessment of nucleic acid purity', *Biotechniques*, 22: 474-6, 78-81.

Xin, J. Y., L. R. Sun, H. Y. Lin, S. Zhang, and C. G. Xia. 2019. 'Hybridization of Particulate Methane Monooxygenase by Methanobactin-Modified AuNPs', *Molecules*, 24.

Yang, Hui, Xue Xiao, Xue Song Zhao, Lan Hu, Xian Feng Xue, and Jie Song Ye. 2016. 'Study on Fluorescence Spectra of Thiamine and Riboflavin', *MATEC Web Conf.*, 63: 03013.

Yasin, Muhammad, Yeseul Jeong, Shinyoung Park, Jiyeong Jeong, Eun Yeol Lee, Robert W. Lovitt, Byung Hong Kim, Jinwon Lee, and In Seop Chang. 2015. 'Microbial synthesis gas utilization and ways to resolve kinetic and mass-transfer limitations', *Bioresource Technology*, 177: 361-74.

Ye, Changqing, Jinsuo Ma, Pengju Han, Shuoran Chen, Ping Ding, Bin Sun, and Xiaomei Wang. 2019. 'Preparation and application of solid-state upconversion materials based on sodium polyacrylate', *RSC Advances*, 9: 17691-97.

Zhou, Qingxiang, Man Lei, Jing Li, Kuifu Zhao, and Yongli Liu. 2016. 'Determination of 1-naphthol and 2-naphthol from environmental waters by magnetic solid phase extraction with Fe@MgAl-layered double hydroxides nanoparticles as the adsorbents prior to high performance liquid chromatography', *Journal of Chromatography A*, 1441: 1-7.

Zill, D., E. Lettau, C. Lorent, F. Seifert, P. K. Singh, and L. Lauterbach. 2022. 'Crucial Role of the Chaperonin GroES/EL for Heterologous Production of the Soluble Methane Monooxygenase from Methylomonas methanica MC09', *ChemBioChem*, 23: e202200195.

Øverland, Margareth, Anne-Helene Tauson, Karl Shearer, and Anders Skrede. 2010. 'Evaluation of methane-utilising bacteria products as feed ingredients for monogastric animals', *Archives of Animal Nutrition*, 64: 171-89.

Appendix A: Growth media, buffers, and solutions

Below are all media, buffers, and solutions used in this study for synthetic methanotrophy and homologous expression of *hps* and *phi.* In the cases where agar plates were made, the medium was supplemented with 15 g of bacteriological agar (Oxoid™, Cat. no. LP0011B) per 1000 mL. This was the case for SOB, LB, and NMS media. All media, buffers, and solutions were autoclaved at 121°C for 20 minutes, unless stated otherwise.

SOB medium

Component	Mass (g/L)	Volume (mL/L)
Hanahan's Broth SOB Medium (Cat. no. H8032)	28.0	
Ion free water		Up to 1000 mL

LB medium

Component	Mass (g/L)	Volume (mL/L)
Tryptone	10.0	
Yeast extract	5.0	
NaCl	5.0	
Ion free water		Up to 1000 mL

MVcM High Salt Buffer 10X

Component	Concentration (M)	Mass (g/L)	Volume (mL/L)
K_2HPO_4	0.235	40.93	
Yeast extract	0.108	14.9	
NaCl	0.16	21.14	
Ion free water			Up to 1000 mL

MVcM/MVcMY

The components for the two media are identical with the exception of the added yeast extract in the MVcMY medium.

Component	Mass (g/L)	Volume (mL/L)
MVcM High Salt Buffer 10X		100
Yeast extract (MVcMY)	0.25	
Ion free water		Up to 1000

The pH was adjusted to 7.2 using NaOH before autoclaving.

yB

Component	Mass (g/500 mL)	Volume (mL/500 mL)
Tryptone	10.0	
Yeast extract	2.5	
KCl	0.38	
$MgSO_4$ (1 M)		17
Ion free water		483

The pH was adjusted to 7.6 using KOH before autoclaving. The 1 M $MgSO_4$ was filter sterilized and added after autoclaving.

TfBI

Component	Mass (g/500 mL)	Volume (mL/500 mL)
CH_3CO_2K	1.47	
$MnCl_2$	4.95	
RbCl	6.05	
$CaCl_2$	0.74	
Glycerol		75
Ion free water		Up to 500 mL

The pH was adjusted to 5.8 using 0.2 M acetic acid, before being filter sterilized.

TfBII

Component	Mass (g/500 mL)	Volume (mL/500 mL)
MOPS (pH 7, 100 mM)		10
$CaCl_2$	1.10	
RbCl	0.12	
Glycerol		15
Ion free water		Up to 500 mL

The solution was stored at 4°C in the dark after autoclaving.

Nitrate Mineral Salts (ATCC medium 1306: NMS)

The official ATCC medium stated the amounts of certain hydration levels of some of the compounds. In the cases where these were not available, the amount of an alternative hydration level is stated next to it. The calculations for amounts with different hydration levels are added in appendix E. The official medium recipe also states to use purified agar (e.g., Oxoid L28) when making agar plates. This was not available, so the bacteriological agar listed in the first section in appendix A was used.

Component	Mass (g/L)	Volume (mL/L)
$MgSO_4 \cdot 7H_2O$	1.0	
$CaCl_2 \cdot 6H_2O$/ $CaCl_2 \cdot 2H_2O$	0.20/0.075	
Chelated iron solution (see below)		2.0
KNO_3	1.0	
Trace element solution (*M. capsulatus,* see below)		0.5
KH_2PO_4	0.272	
$Na_2HPO_4 \cdot 12H_2O$/ $Na_2HPO_4 \cdot 2H_2O$	0.717/0.215	
Distilled deionized water		Up to 1000 mL

The pH was adjusted to 6.8 before autoclaving.

Chelated Iron Solution

Component	Mass (g/L)	Volume (mL/L)
Ferric (III) ammonium citrate	0.1	
EDTA, sodium salt	0.2	
HCl (concentrated)		0.3
Distilled deionized water		100

The solution was not autoclaved, or filter sterilized.

Trace Element Solution (*M. capsulatus* (Bath))

Component	Mass (mg/L)	Volume (mL/L)
EDTA	500.0	
$FeSO_4 \cdot 7H_2O$	200.0	
$ZnSO_4 \cdot 7H_2O$	10.0	
$MnCl_2 \cdot 4H_2O$	3.0	
H_3BO_3	30.0	
$CoCl_2 \cdot 6H_2O$	20.0	
$CaCl_2 \cdot 2H_2O$	1.0	
$NiCl_2 \cdot 6H_2O$	2.0	
$Na_2MoO4 \cdot 2H_2O$	3.0	
Ion free water		Up to 1000 mL

Trace Element Solution (*B. methanolicus* MGA3)

The copper-deficient trace element solution used in the third and fourth experiment of the fluorescence-based coumarin assay is identical to the listed solution with the copper omitted.

Component	Concentration (M)	Mass (g/L)	Volume (mL/L)
$FeSO_4 \cdot 7H_2O$	0.020	5.56	
$CuCl_2 \cdot 2H_2O$	0.00016	0.027	
$CaCl_2 \cdot 2H_2O$	0.050	7.35	
$CoCl_2 \cdot 6H_2O$	0.00017	0.040	
$MnCl_2 \cdot 4H_2O$	0.050	9.90	
$ZnSO_4 \cdot 7H_2O$	0.0010	0.288	
$Na_2MoO_4 \cdot 2H_2O$	0.0002	0.048	
H_3BO_3	0.0005	0.031	
HCl (concentrated)	1.99		80
Distilled deionized water			Up to 1000 mL

Electroporation buffer (EPB)

Component	Concentration (M)	Mass (g/L)	Volume (mL/L)
HEPES	0.001	0.06	
PEG_{8000}		62.5	
Ion free water			Up to 500 mL

The solution was filter sterilized.

MOPS (20 mM/100 mM, pH 7)

Two concentrations of MOPS were utilized in this study: 20 mM for use in TfBII, and 100 mM for use in the fluorescence-based coumarin assay in the experiments using crude extract. Calculations for the two concentrations are added in appendix E, and all solutions that required specific concentrations followed the same calculations.

Component	Mass (g/500 mL)	Volume (mL/L)
Alfa Aesar MOPS, 98.5+% (CAS. 1132-61-2)	2.093 (20 mM) 10.463 (100 mM)	
Ion free water		Up to 500 mL

pH was adjusted to 7 using NaOH and filter sterilzed.

Coumarin (100 mM)

Component	Mass (g/50 mL)	Volume (mL/L)
Coumarin	0.7307	
Ethanol (96%)		50

7-hydroxycoumarin (100 mM)

Component	Mass (g/50 mL)	Volume (mL/L)
7-hydroxycoumarin	0.8107	
Ethanol (96%)		50

Sodium Formate (200 mM)

Component	Mass (g/50 mL)	Volume (mL/L)
Sodium formate	0.6802	
Distilled deionized water		50

TRIS-HCl (50 mM, pH 7.5)

Component	Mass (g/L)	Volume (mL/L)
Tris	6.057	
Ion free water		Up to 1000 mL

The pH was adjusted to 7.5 using HCl, followed by sterile filtration.

$MgSO_4$ (1 M)

Component	Mass (g/L)	Volume (mL/L)
$MgSO_4 \cdot 7H_2O$	123.74	
Ion free water		Up to 1000 mL

Xylose (50%)

Component	Mass (g/L)	Volume (mL/L)
D-(+)-xylose	50	
Ion free water		150

The solution was not autoclaved, or filter sterilized.

O-dianisidine (5 mg/mL)

Component	Mass (mg/L)	Volume (mL/L)
o-dianisidine	25.0	
Methanol		5.0

The solution was not autoclaved, or filter sterilized.

Appendix B: Primers

All primers used in this study are presented below. Forward and reverse have been abbreviated "Fwd" and "Rev", respectively.

Table B.1: Primers used in this study.

Primer name	Sequence	Description
VPJF	TCTAATCCTTCTAAAAAATATAATTTAGAAAACTAAG	Colony PCR primer Fwd
VPJR	GGTGCGGGCCTCTTCGCTATTACG	Colony PCR primer Rev
hps-phi 1	TAAATAGGAGGTAGTACTGATGGAACTTCAATTAGCTCTAGA	*hps-phi* Fwd for pTH1mp and pUB110Smp
hps-phi 2	TGGCGGGTACCATATGGATCCTACTCAAGATTAGCATGTCTTC	*hps-phi* Rev for pTH1mp and pUB110Smp
hps-phi 3	TTACGCCAAGCTTGGCTGCATTCGCCGTCATTTTTATTTCT	*hps-phi* Fwd for both pTH1mp and pUB110Smp without *mdh* promoter
hps-phi 4	GAAATAAAAATGACGGCGAATGCAGCCAAGCTTGGCGTAA	pTH1mp and pUB110Smp Rev without *mdh* promoter
hps-phi 5	GAATTCAAGCTTTAAACATGACTCAAGATTAGCATGTCTTCC	*hps-phi* Rev for pTH1mp without *mdh* promoter
hps-phi 6	AAGACATGCTAATCTTGAGTCATGTTTAAAGCTTGAATTCCCGG	pTH1mp Fwd without *mdh* promoter
hps-phi 7	GGAATTCAAGCTTTAAACATACTCAAGATTAGCATGTCTTCC	*hps-phi* Rev for pUB110Smp without *mdh* promoter
hps-phi 8	AAGACATGCTAATCTTGAGTATGTTTAAAGCTTGAATTCCCGGG	pUB110Smp Fwd without *mdh* promoter

Appendix C: DNA ladder

The ladder used in this study was the Thermo Fischer Scientific GeneRuler 1 kb Plus (Cat. nr. SM1331). The ladder contained 15 DNA fragments ranging from 75 to 20 000 bp.

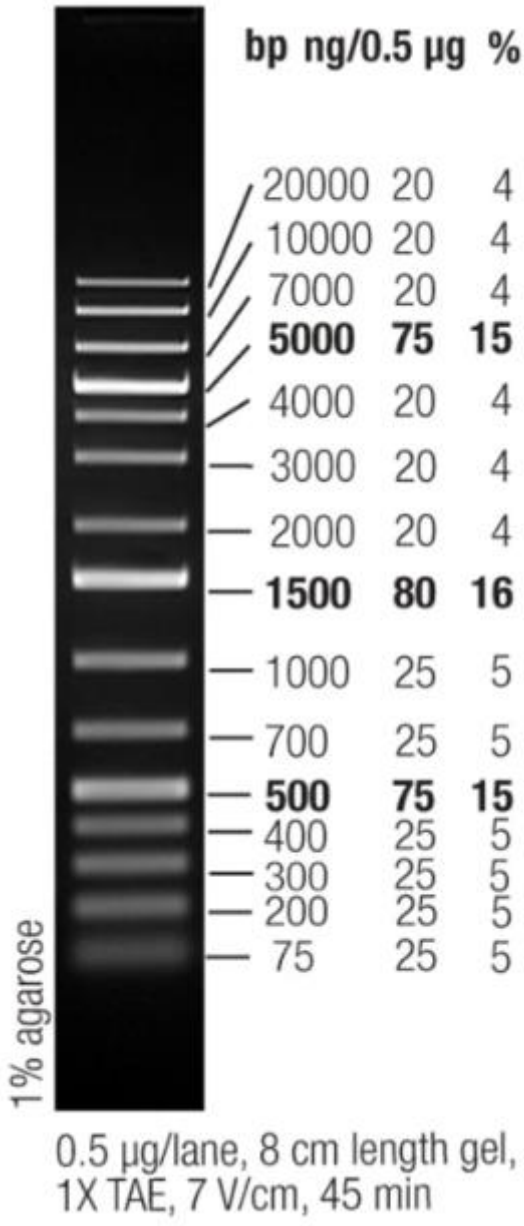

Figure C.1: Thermo Fischer Scientific GeneRuler 1 kb Plus DNA ladder used as a reference to determine size of DNA fragments on agarose gel (0.8%).

Appendix D: Plasmid maps

All plasmid backbones and constructs are presented below. The specific backbone is presented first, followed by all constructs using the backbone with their respective inserts. The plasmid backbones and constructs were cloned *in silico* as stated in section 2.9. Section 2.2, table 2.2 describes each plasmid backbone and construct with their respective inserts and antibiotic resistance.

---

pBV2xp backbone:

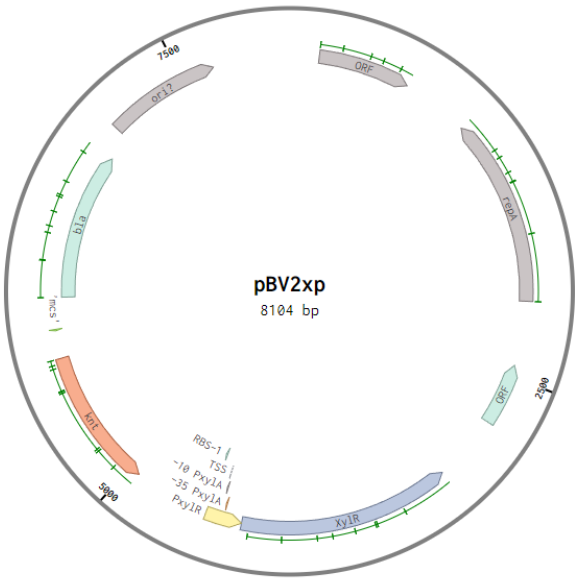

(A): pBV2xp backbone

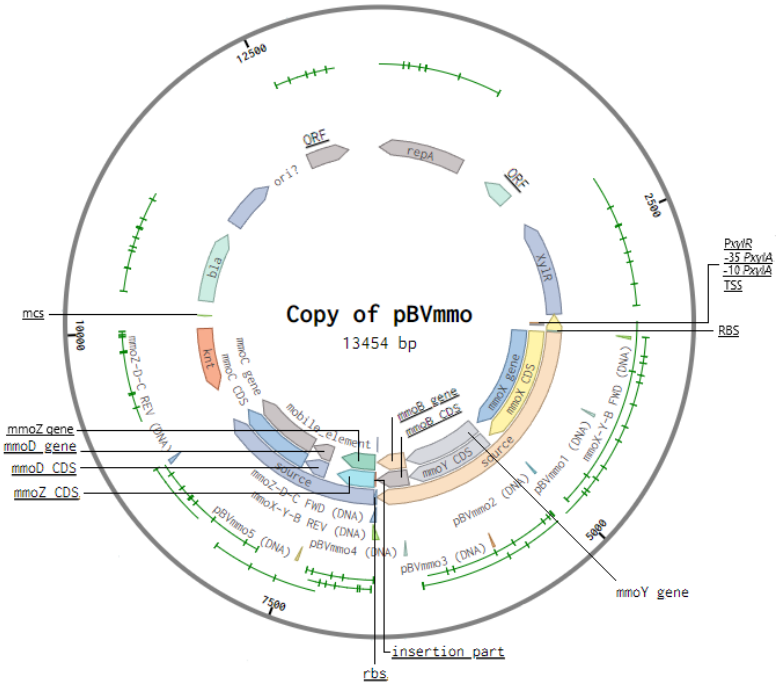

(B): pBV2xp-mmo

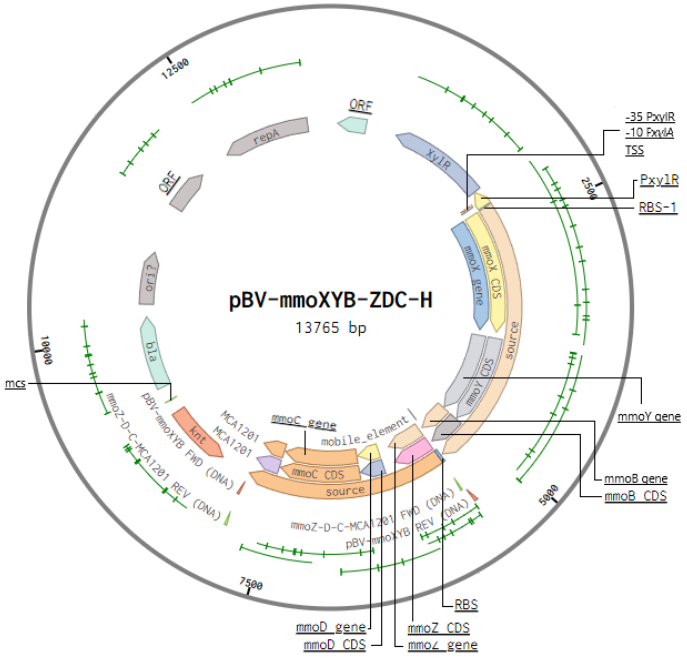

(C): pBV2xp-mmoH

pTH1mp backbone:

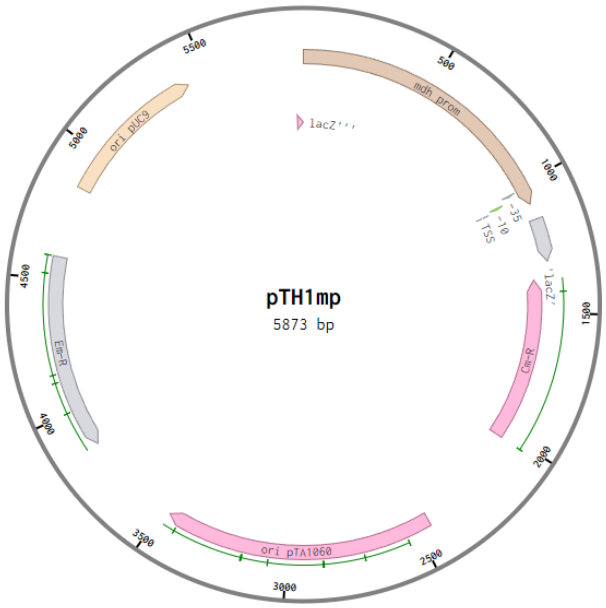

(A): pTH1mp backbone

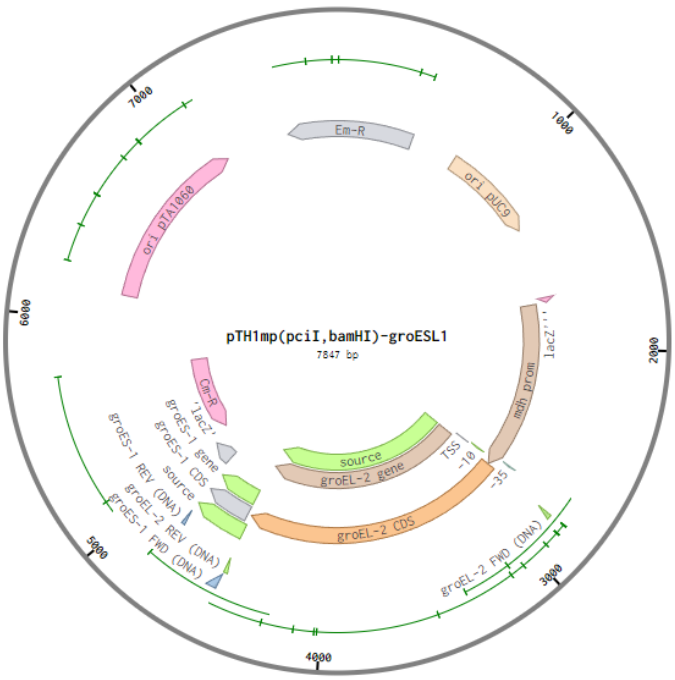

(B): pTH1mp-groESL1

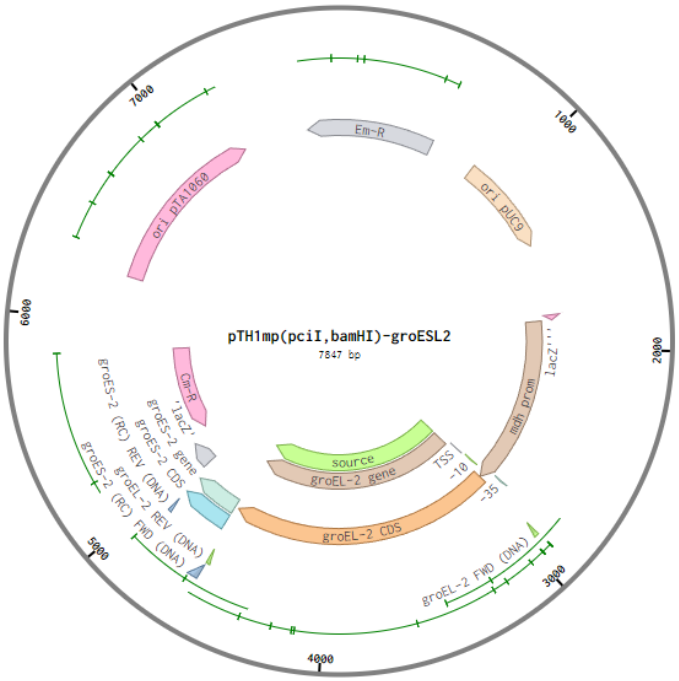

(C): pTH1mp-groESL_BM

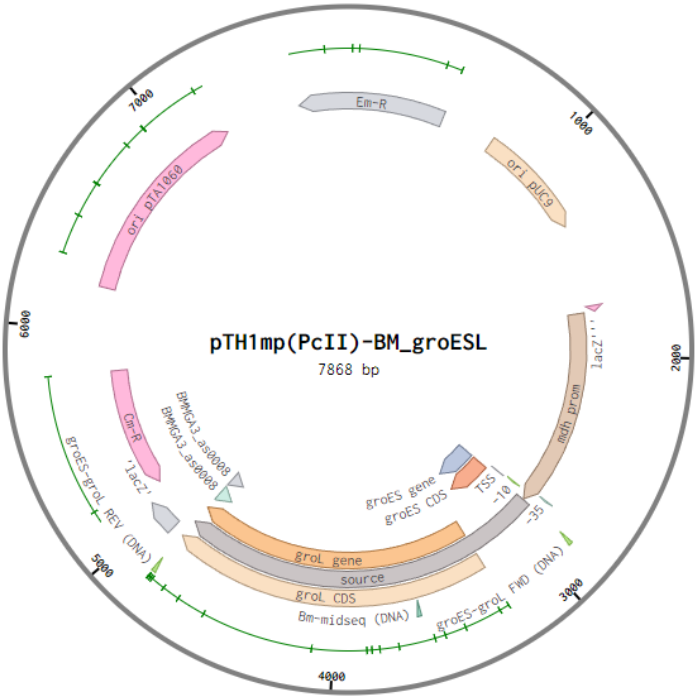

(D): pTH1mp-groESL_BM

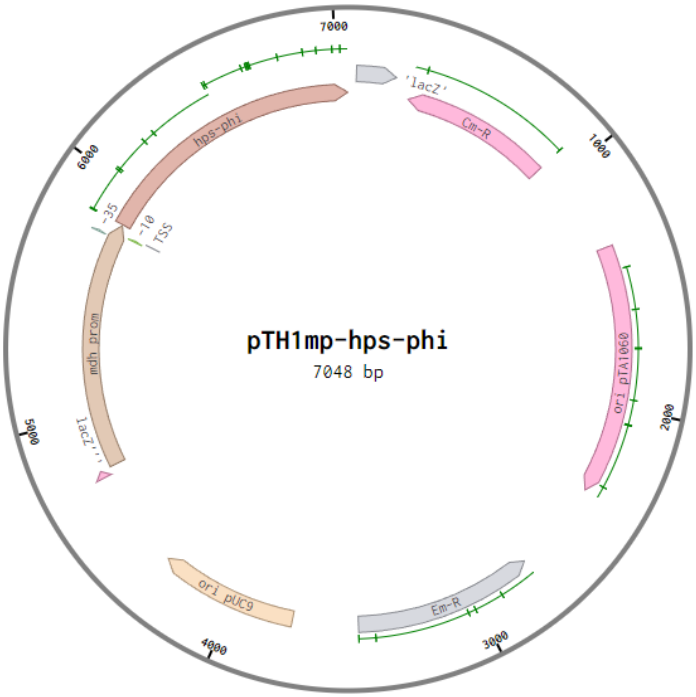

(E): pTH1mp-hps-phi

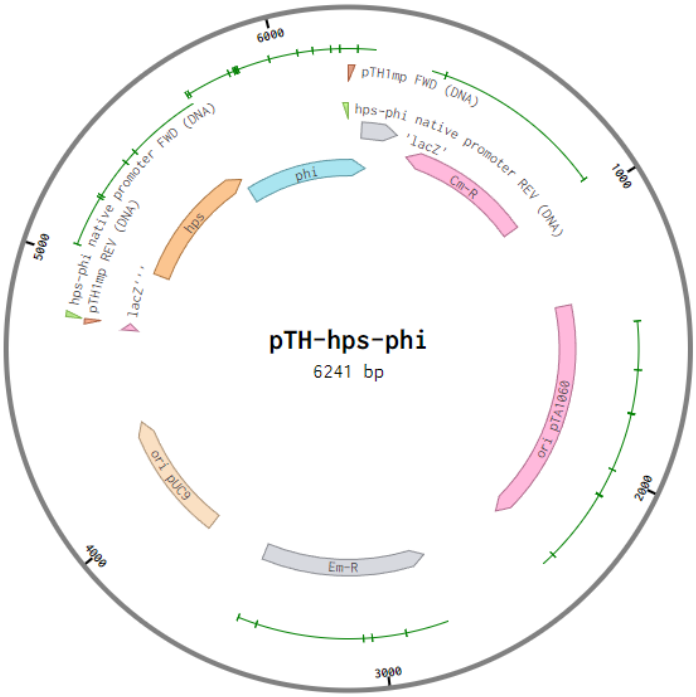

(F): pTH-hps-phi

pUB110Smp backbone:

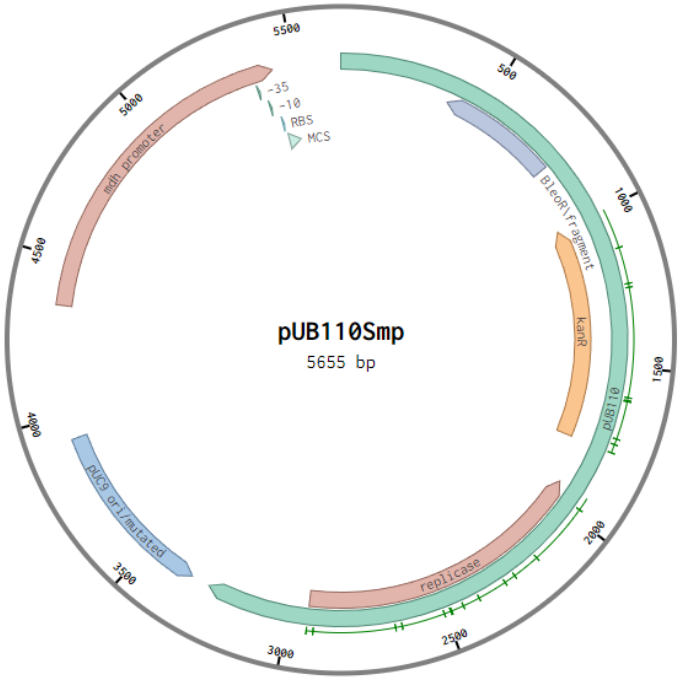

(A): pUB110Smp backbone

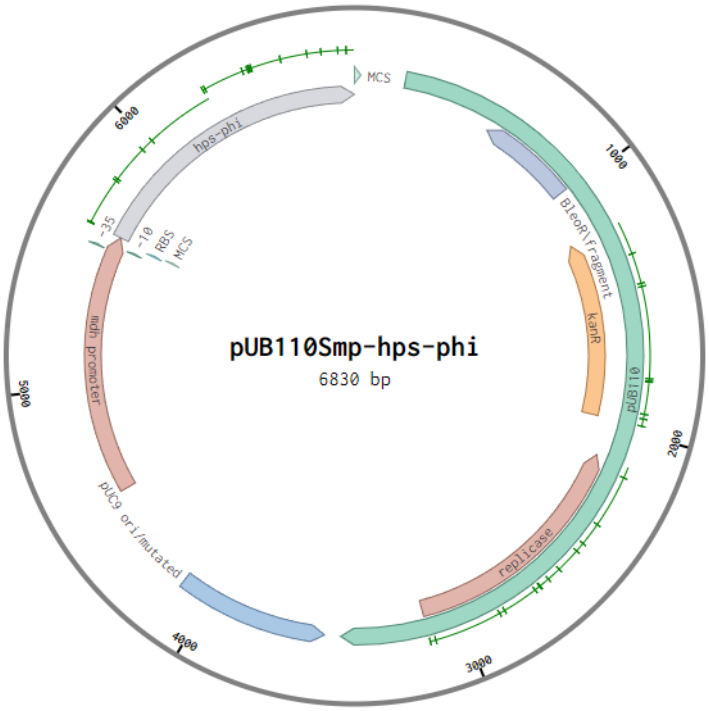

(B): pUB110Smp-hps-phi

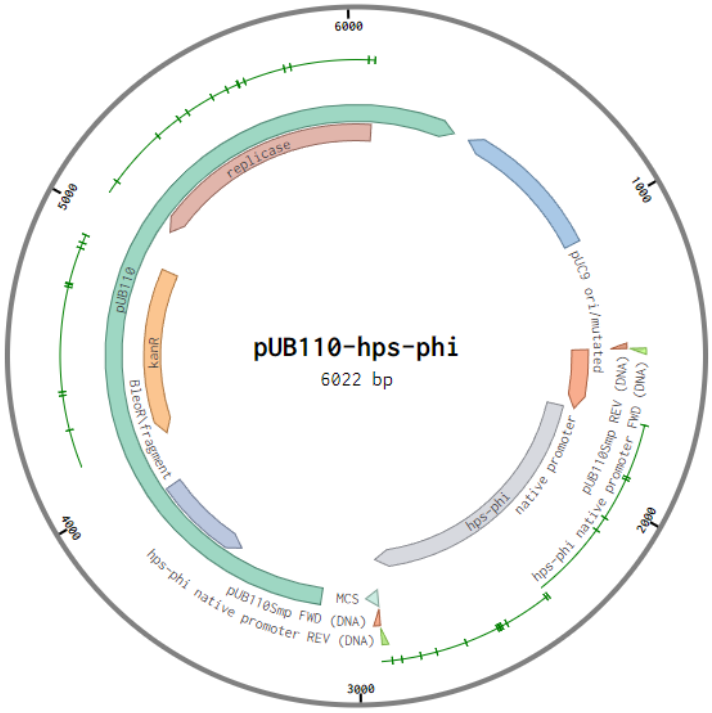

(C): pUB110-hps-phi

Appendix E: Calculations

Inoculation volume

Inoculation volume is calculated as the amount of liquid from a pre-culture needed to achieve a specific OD_{600} value of a main culture when inoculated. The volume is calculated from equation (1) and rearranged as equation (2). Equation (3) displays equation (2) with terms related to inoculation.

$$\boldsymbol{C_1V_1 = C_2V_2} \quad (1)$$

$$\boldsymbol{V_1 = \frac{C_2}{C_1} \times V_2} \quad (2)$$

$$\boldsymbol{V_{inocul} = \frac{OD_{600\,MC}}{OD_{600\,PC}} \times V_{MC}} \quad (3)$$

V_{inocul} = inoculation volume/volume of pre-culture to use for inoculation

$OD_{600\,MC}$ = Measured OD_{600} of main culture

$OD_{600\,PC}$ = Measured OD_{600} of pre-culture

V_{MC} = volume of main culture

Example:

The required inoculation volume for a 40 mL main culture to an initial OD_{600} of 0.2 with a measured OD_{600} in the pre-culture of 1.5. Each main culture requires inoculation with 5.33 mL of the pre-culture for an initial OD_{600} of 0.2 (equation (4)). In the cases where calculated V_{inoc} was more than 2 mL: 5 x V_{inoc} was centrifuged and resuspended in 5 mL of the chosen medium, before 1 mL was used to inoculate each main culture to achieve an initial OD_{600} of 0.2 (equation (5)).

$$\boldsymbol{V_{inocul} = \frac{0.2}{1.5} \times 40\ mL\ = 5.33\ mL} \quad (4)$$

$$\boldsymbol{5.33 \times 5 = 26.7\ mL\ centrifuged} \quad (5)$$

Standard deviation

The standard deviation was calculated between each triplicate for each condition in every sample in the growth experiment described in sections 2.12 and 3.4.2. The triplicates represented samples under the same conditions, and the standard deviation gave a measure of how spread the datapoints were from the mean value of the sample. The standard deviations were calculated in Microsoft Office 365 Excel (2023) using the function "STDEV". Equation (6) shows the formula for calculating standard deviation as the square root of the sample variance, s^2.

$$\boldsymbol{s^2} = \sqrt{\frac{\sum_{i=1}^{n}(x_i - \bar{x})^2}{(n-1)}} \tag{6}$$

n = number of values

x_i = sample value

$\bar{x}$ = mean sample value

Difference in hydration levels of chemicals

The official recipe of the NMS medium (ATCC medium 1306) listed certain chemicals with a set level of hydration. Two of these were not available in the required hydration, so chemicals with different levels were used. First the molar masses of both chemicals were determined, followed by calculating the percentage of the compound corresponding to the pure chemical without the added hydrate (equation (7)). The percentage difference between the two compounds was determined and applied to the available chemical.

Example:

The NMS medium listed $CaCl_2 \cdot 6H_2O$, whereas the available chemical at the time was $CaCl_2 \cdot 2H_2O$. Molar masses of the two: $CaCl_2 \cdot 6H_2O$ = 219.09 g/mol, and $CaCl_2 \cdot 2H_2O$ = 147.01 g/mol. Pure $CaCl_2$ = 110.98 g/mol. Percentage of pure compound in hydrates:

$$\boldsymbol{CaCl2 \cdot 6H2O} = \frac{\mathbf{100\%}}{\mathbf{219.09\ g/mol}} \times \mathbf{110.98}\frac{\boldsymbol{g}}{\boldsymbol{mol}} = \mathbf{50.65\%} \tag{7}$$

The same was done for $CaCl_2 \cdot 2H_2O$, yielding 75.49% which gave a 24.84% difference of pure $CaCl_2$ in $CaCl_2 \cdot 6H_2O$ compared to $CaCl_2 \cdot 2H_2O$. The resulting calculations showed that the medium required 75.16% $CaCl_2 \cdot 2H_2O$ of the listed amount of $CaCl_2 \cdot 6H_2O$. The recipe stated 0.20 g of $CaCl_2 \cdot 6H_2O$, resulting in 0.1503 g of $CaCl_2 \cdot 2H_2O$.

Average growth rates of *B. methanolicus* MGA3 strains

The average growth rates of each strain were calculated using the following method: Logarithmic plots were made for each replicate per strain for all timepoints. The resulting growth rate was obtained from the graph trendline equation. The average growth rate was then calculated based on the three replicates and standard deviation was obtained as explained above.

Example:

Example calculations for the strain THEV at 200 mM methanol concentration.

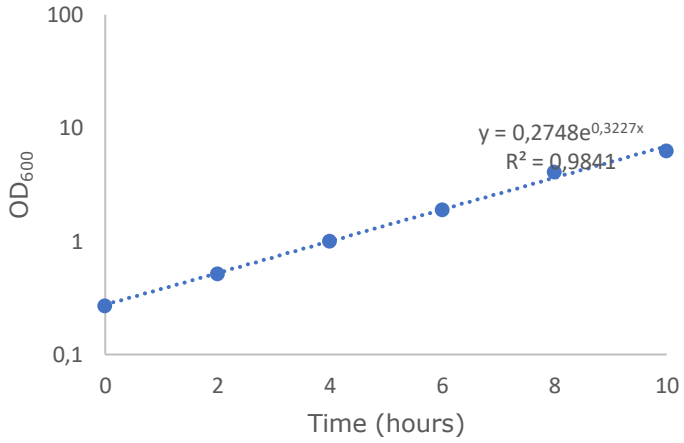

Figure E.1: Logarithmic plot of the first replicate of THEV strain at 200 mM methanol using linear regression. The resulting equation yielded a growth rate of 0.3227 h^{-1}.

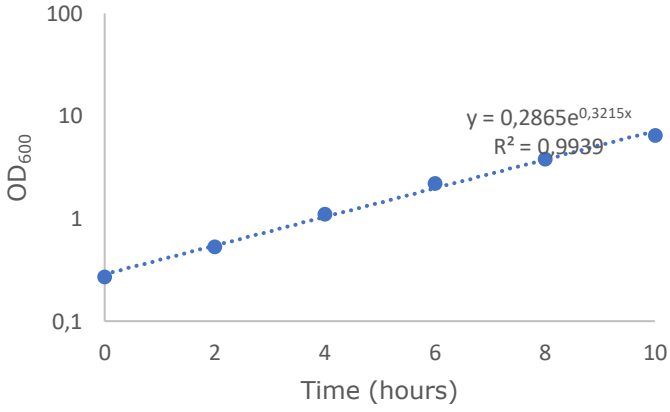

Figure E.2: Logarithmic plot of the second replicate of THEV at 200 mM methanol using linear regression. The resulting equation yielded a growth rate of 0.3215 h^{-1}.

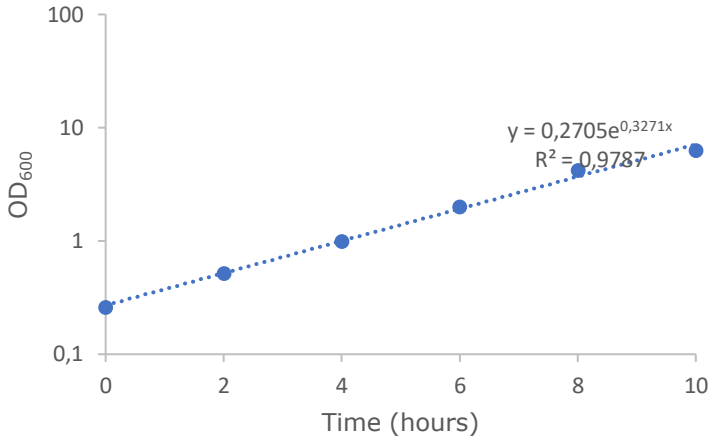

Figure E.3: Logarithmic plot of the third replicate of THEV strain at 200 mM methanol using linear regression. The resulting equation yielded a growth rate of 0.3271 h^{-1}.

Table E.1: Growth rate per replicate and the resulting average growth rate of the strain under the specified condition.

Growth rate per replicate (h^{-1})	Average growth rate (h^{-1})
0.3227	0.3238
0.3215	
0.3271	

Appendix F: Emission- and excitation scans of 7-hydroxycoumarin

Standards of 7-hydroxycoumarin were scanned to determine the optimum wavelengths for excitation and emission measurements as stated in section 2.10.1. Figures F.1 and F.2 show the emission scans, and figures F.3 and F.4 show the excitation scans.

Emission:

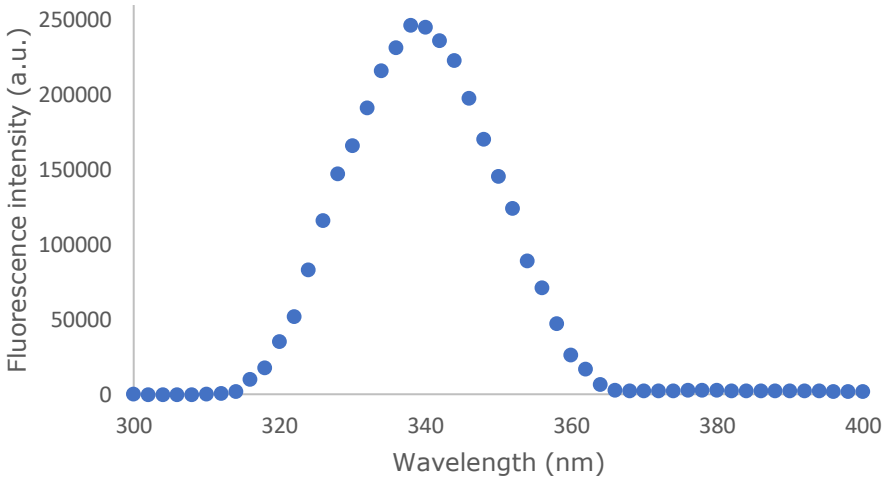

Figure F.1: Emission scan of 7-hydroxycoumarin displaying a slight secondary peak at ca. 370-390 nm. The emission scan had a start- and end wavelength of 300 nm and 600 nm respectively, with excitation wavelength set to 338 nm, based on Miller et al. 2001. The Graph only displays wavelengths from 300 nm to 400 nm as the fluorescence intensity above 400 nm showed a steady decrease.

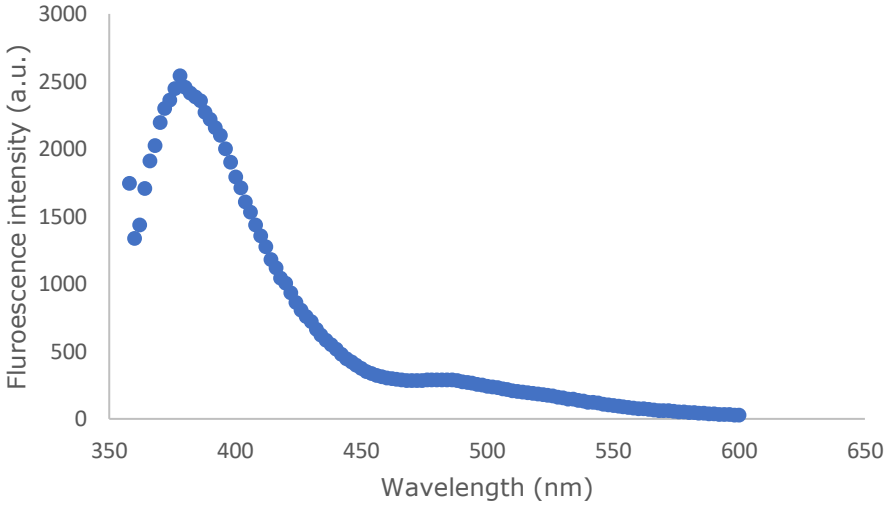

Figure F.2: Emission scan of 7-hydroxycoumarin. The figure displays the perceived peak at ca. 370-390 nm, with a maximum fluorescence intensity at 378 nm.

Excitation:

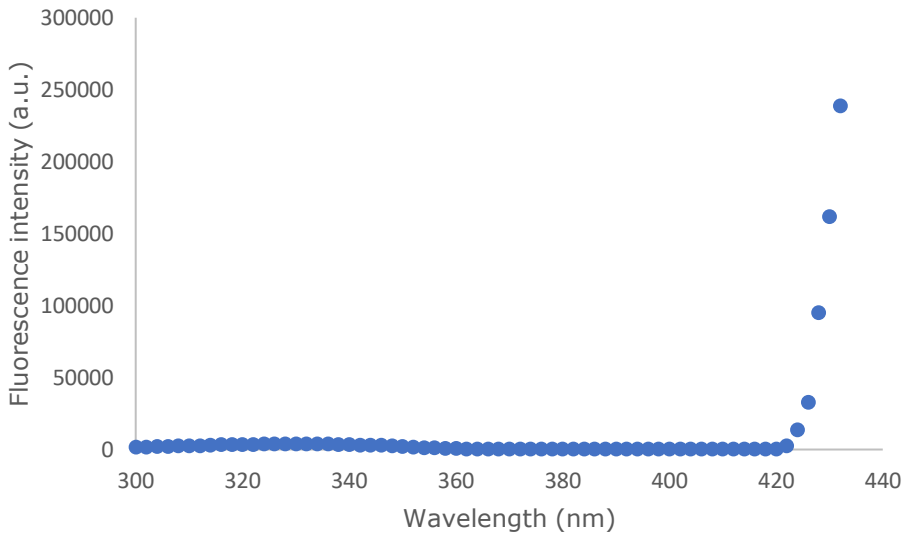

Figure F.3: Excitation scan of 7-hydroxycoumarin displaying a slight secondary peak at ca. 320-340 nm. The excitation scan had a start- and end wavelength of 300 nm and 600 nm, respectively, with emission wavelength set to 450 nm, based on Miller et al. 2001. The Graph only displays wavelengths from 300 nm to 440 nm as detector saturation occurred above that, yielding no fluorescence intensity.

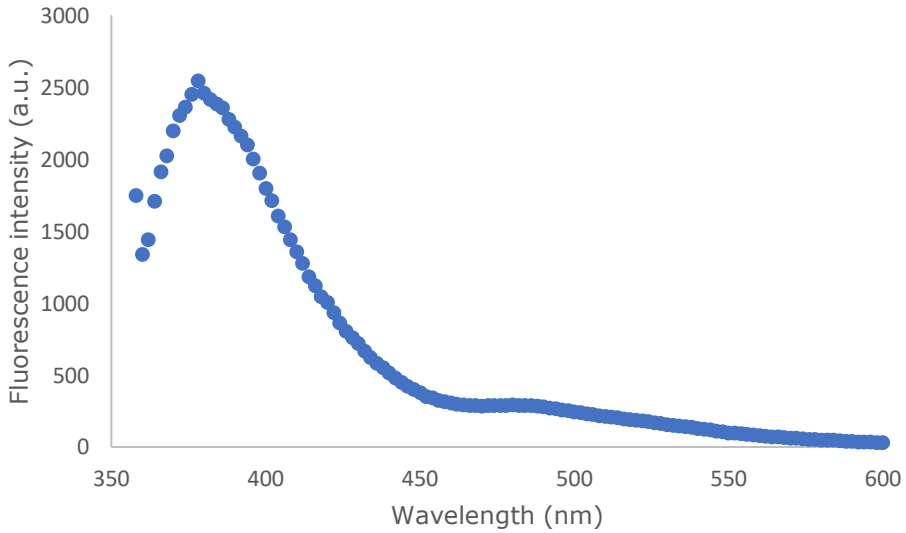

Figure F.4: Excitation scan of 7-hydroxycoumarin. The figure displays the perceived peak at ca. 320-340 nm, with a maximum fluorescence intensity at 330 nm.

Appendix G: Fluorescence measurements

This appendix contains the fluorescence intensity measurements raw data of all tested strains in all five individual experiments of the fluorescence-based coumarin enzyme assay for heterologously expressed sMMO. In addition, negative control samples, blank samples, and standard concentrations of 7-hydroxycoumarin are presented. Graphs depicting standard concentrations are derived from the average fluorescence intensity of each triplicate of 7-hydroxycoumarin. All samples of standard 7-hydroxycoumarin concentrations were taken from the same pre-prepared stock solutions for each time point.

Whole cell culture:

Figure G.1 shows the microplate setup for fluorescence intensity measurements. The setup corresponds to figures G.1-G.4 and tables G.1-G.3.

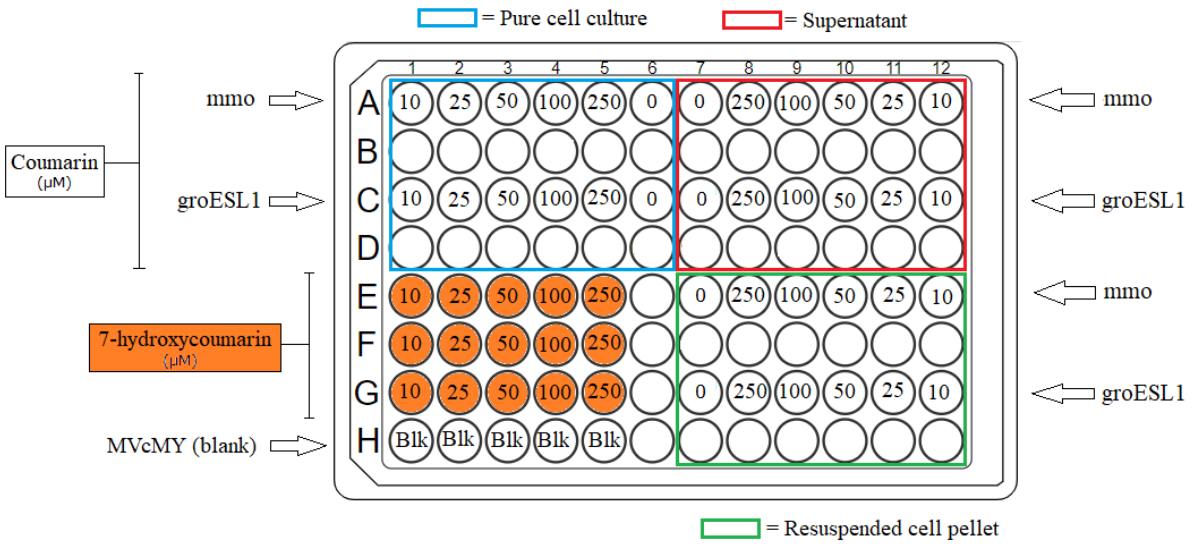

Figure G.1: Plate setup in the Thermo Fischer Scientific Nunc™ MicroWell™ 96-Well, flat-bottom black microplate for the first experiment using whole cell culture. All coumarin and 7-hydroxycoumarin concentrations were in µM.

Table G.1: Fluorescence intensity (a.u.) measurements in the mmo and groESL1 strains two hours after added coumarin in the experiment using whole cell culture. Blanks, standard concentrations of 7-hydroxycoumarin, and negative control samples are also displayed.

<>	1	2	3	4	5	6	7	8	9	10	11	12
A	8	7	5	5	6	6	5	5	3	1	3	4
C	11	10	12	10	9	11	10	8	11	10	9	8
E	85	243	749	1335	1945		-5	-5	-5	-5	-4	-5
F	86	254	838	1355	2018							
G	73	236	797	1312	1915		-1	-4	-3	0	0	-1
H	-4	-3	-4	-5	-3							

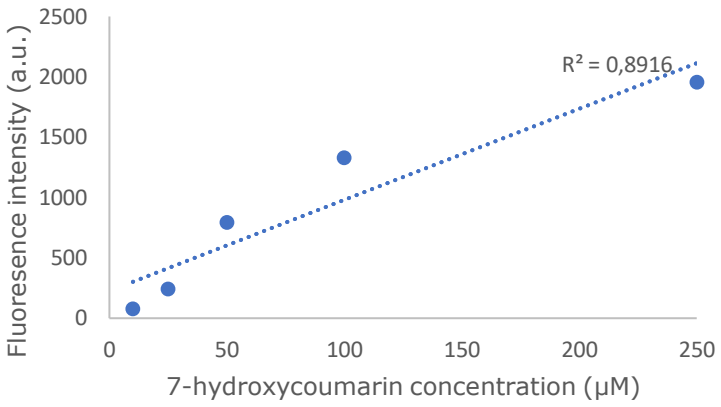

Figure G.2: Fluorescence intensity of standard 7-hydroxycoumarin samples at the listed concentrations in the two-hour sample.

Table G.2: Fluorescence intensity (a.u.) measurements in the mmo and groESL1 strains four hours after added coumarin in the experiment using whole cell culture. Blanks, standard concentrations of 7-hydroxycoumarin, and negative control samples are also displayed.

<>	1	2	3	4	5	6	7	8	9	10	11	12
A	10	6	7	6	6	4	5	6	3	5	4	5
C	14	14	13	12	9	14	12	10	11	12	13	12
E	54	298	735	1452	1785		-5	-4	-5	-5	-5	-2
F	82	331	771	1536	1920							
G	73	299	731	1420	1817		2	-5	1	3	1	2
H	-6	-4	-5	-4	-4							

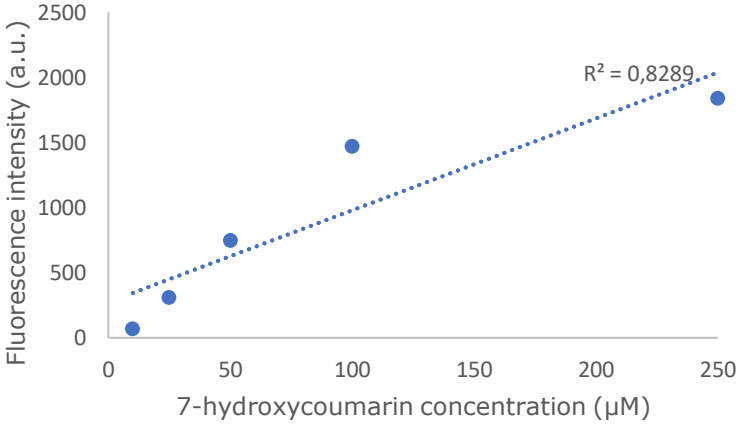

Figure G.3: Fluorescence intensity of standard 7-hydroxycoumarin samples at the listed concentrations in the four-hour sample.

Table G.3: Fluorescence intensity (a.u.) measurements in the mmo and groESL1 strains twenty-four hours after added coumarin in the experiment using whole cell culture. Blanks, standard concentrations of 7-hydroxycoumarin, and negative control samples are also displayed.

<>	1	2	3	4	5	6	7	8	9	10	11	12
A	27	27	28	19	24	27	28	23	18	27	22	28
C	33	33	32	31	30	33	30	28	29	30	30	32
E	78	240	677	1197	1539		10	9	9	9	9	8
F	73	262	662	1224	1625							
G	75	191	617	1108	1468		15	13	13	13	13	11
H	5	4	5	5	4							

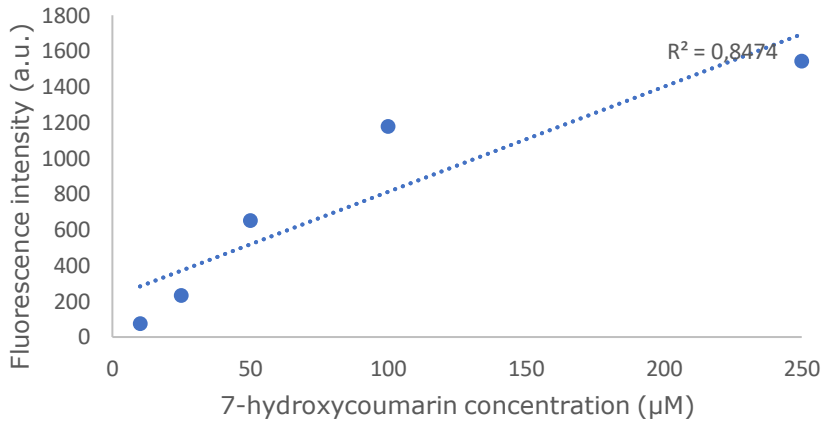

Figure G.4: Fluorescence intensity of standard 7-hydroxycoumarin samples at the listed concentrations in the twenty-four-hour sample.

Crude extract:

Negative fluorescence intensities were considered to be zero and are displayed as such in figure G.6 due to only positive measurable fluorescence being indicative of potential coumarin oxidation to 7-hydroxycoumarin by sMMO.

1st experiment:

Figure G.5 shows the microplate setup for fluorescence intensity measurements. The setup corresponds to figures G.6-G.10 and tables G.4-G.6.

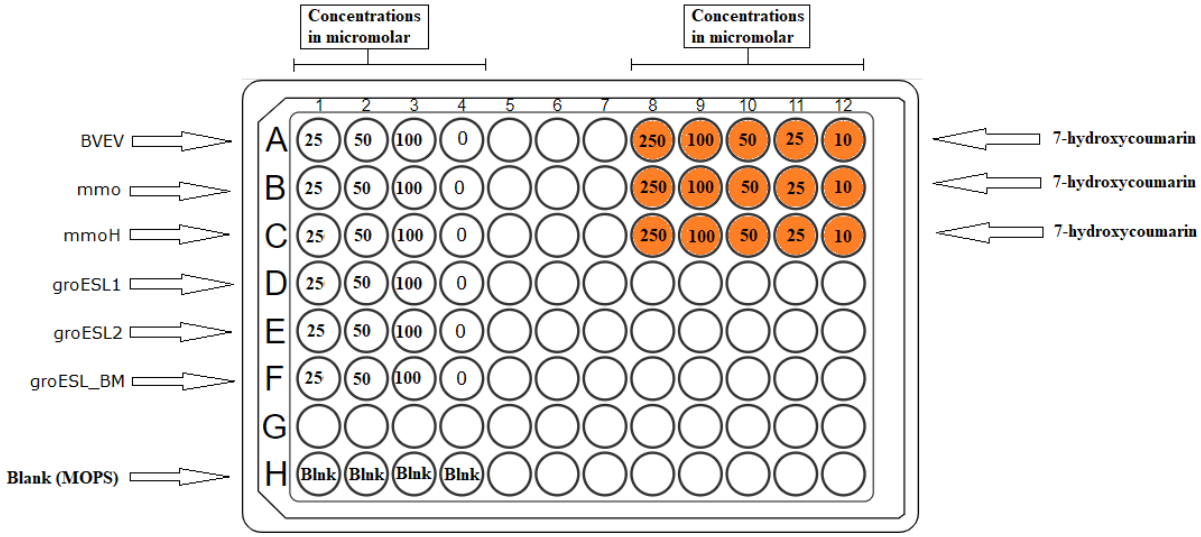

Figure G.5: Plate setup in the Thermo Fischer Scientific Nunc™ MicroWell™ 96-Well, flat-bottom black microplate for the 1st experiment using crude extract from sonicated cells. All coumarin and 7-hydroxycoumarin concentrations were in µM.

Table G.4: Fluorescence intensity (a.u.) measurements in the BVEV, mmo, mmoH, groESL1, groESL2, and groESL_BM strains four hours after added coumarin in the 1st experiment using crude extract from sonicated cells. Blanks, standard concentrations of 7-hydroxycoumarin, and negative control samples are also displayed.

<>	1	2	3	4	8	9	10	11	12
A	-1	2	0	1	2134	1603	819	318	97
B	-3	-2	-2	-2	2045	1531	881	342	70
C	2	1	1	0	2137	1565	872	345	66
D	-1	-3	0	-1					
E	-2	-3	0	-3					
F	-3	-4	-2	-2					
H	-7	-6	-7	-7					

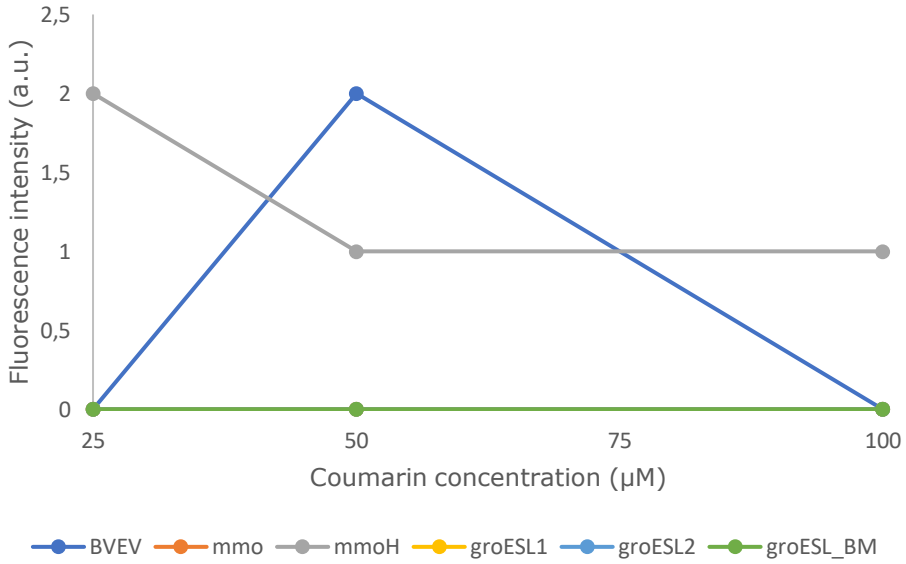

Figure G.6: Fluorescence intensity (a.u.) of the tested strains four hours after added coumarin in the 1st experiment using crude extract from sonicated cells. Strains with all negative fluorescence is shown as zero.

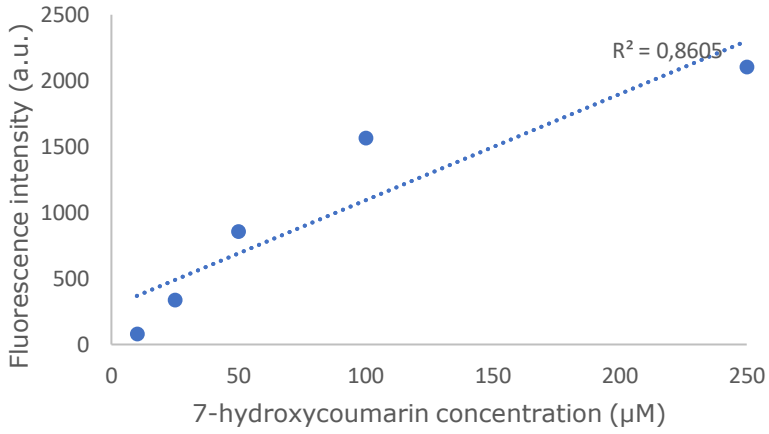

Figure G.7: Fluorescence intensity of standard 7-hydroxycoumarin samples at the listed concentrations in the four-hour sample.

Table G.5: Fluorescence intensity (a.u.) measurements in the BVEV, mmo, mmoH, groESL1, groESL2, and groESL_BM strains eight hours after added coumarin in the 1st experiment using crude extract from sonicated cells. Blanks, standard concentrations of 7-hydroxycoumarin, and negative control samples are also displayed.

<>	1	2	3	4	5	9	10	11	12
A	1	4	-1	-1	1972	1372	642	222	65
C	3	2	4	-3	2004	1341	638	168	58
D	4	4	5	1	2000	1272	606	215	88
E	2	4	3	-1					
F	3	5	3	-3					
G	3	2	2	-3					
H	-1	-2	-2	-3					

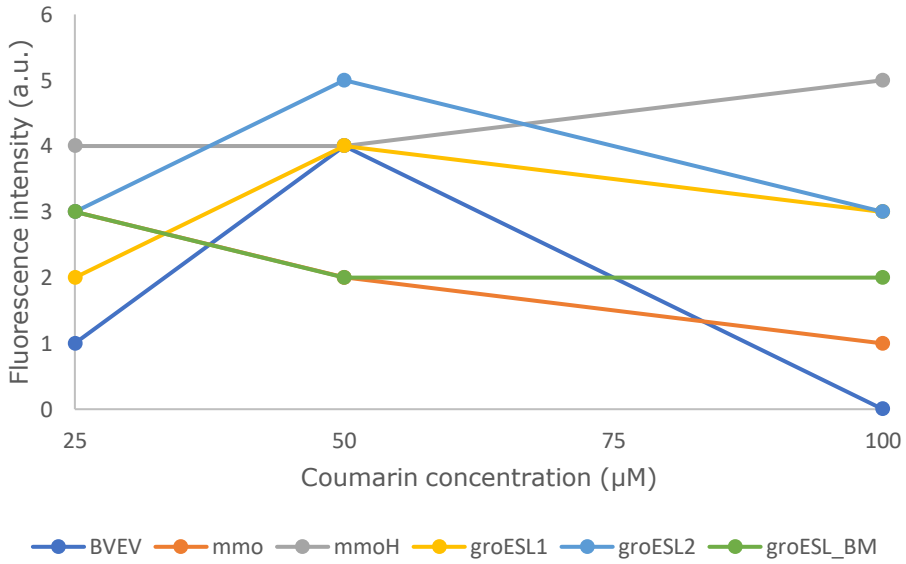

Figure G.8: Fluorescence intensity (a.u.) of the tested strains eight hours after added coumarin in the 1st experiment of the experiment using crude extract from sonicated cells.

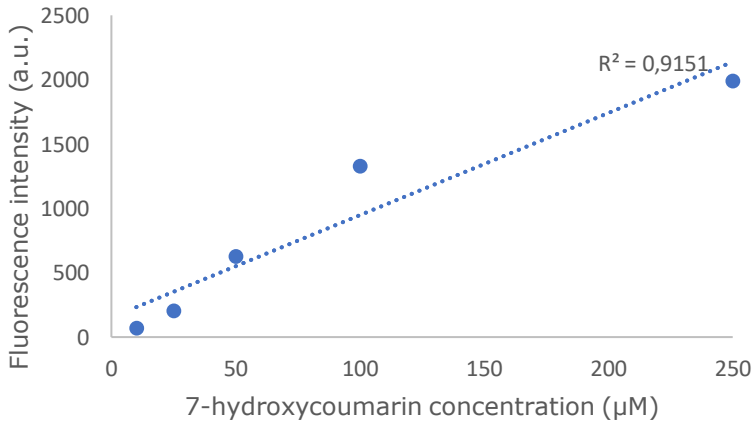

Figure G.9: Fluorescence intensity of standard 7-hydroxycoumarin samples at the listed concentrations in the eight-hour sample.

Table G.6: Fluorescence intensity (a.u.) measurements in the BVEV, mmo, mmoH, groESL1, groESL2, and groESL_BM strains twenty-four hours after added coumarin in the 1st experiment using crude extract from sonicated cells. Blanks, standard concentrations of 7-hydroxycoumarin, and negative control samples are also displayed.

<>	1	2	3	4	8	9	10	11	12
A	6	4	6	1	2053	1335	615	323	82
B	2	2	3	-2	2003	1367	642	233	96
C	4	4	4	2	2043	1394	620	242	95
D	3	2	2	-3					
E	3	1	2	-3					
F	2	1	2	-5					
H	-8	-9	-7	-8					

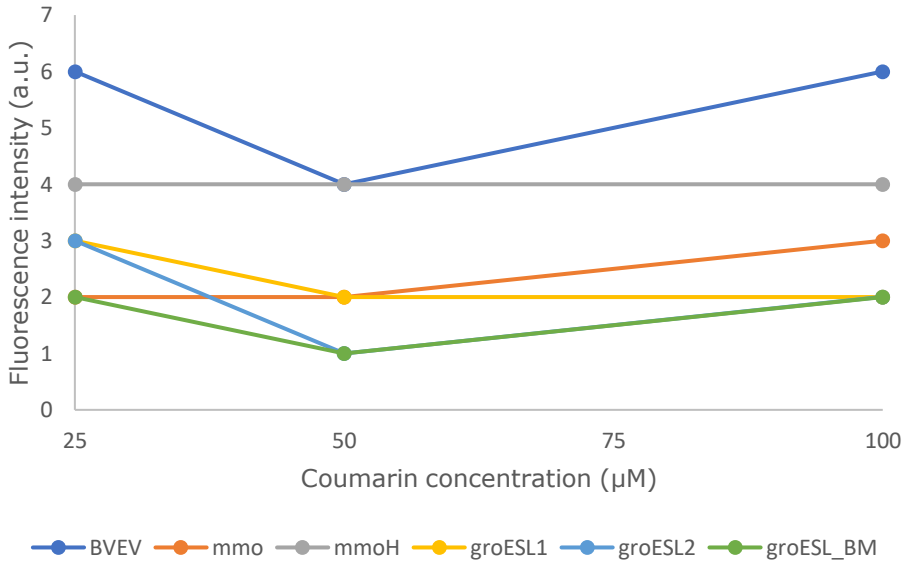

Figure G.10: Fluorescence intensity (a.u.) of the tested strains twenty-four hours after added coumarin in the 1st experiment using crude extract from sonicated cells.

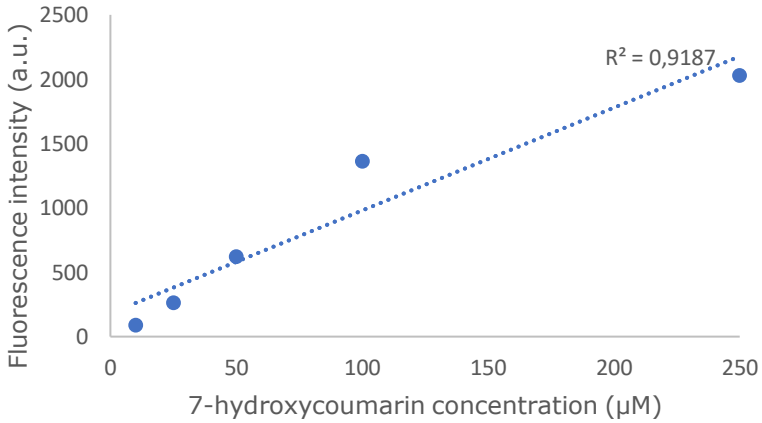

Figure G.10: Fluorescence intensity of standard 7-hydroxycoumarin samples at the listed concentrations in the twenty-four-hour sample.

2nd experiment:

Figure G.11 shows the microplate setup for fluorescence intensity measurements. The setup corresponds to figures G.12-G.19 and tables G.7-G.10.

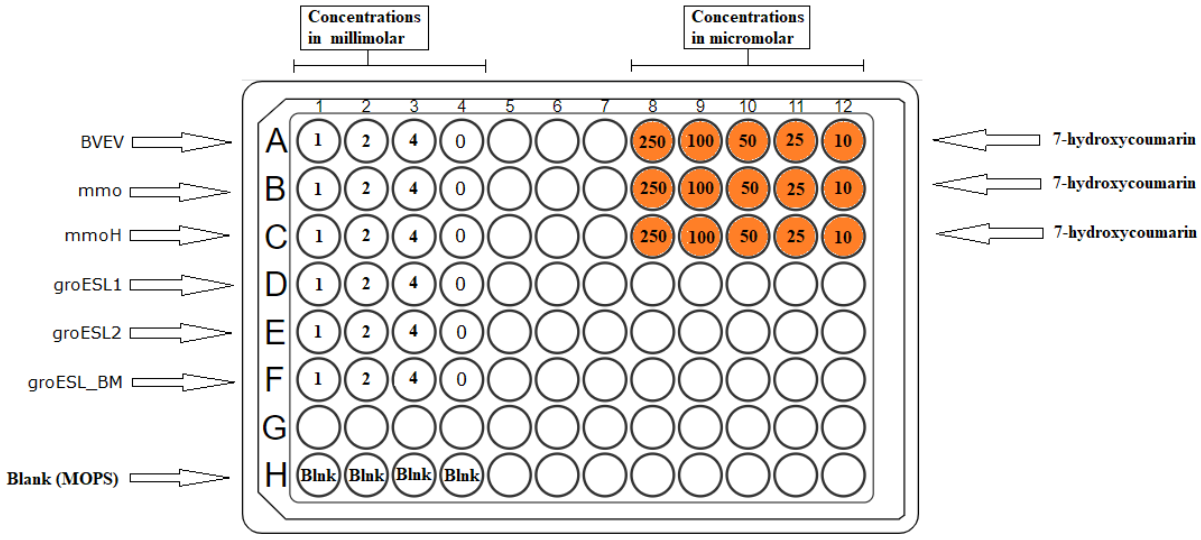

Figure G.11: Plate setup in the Thermo Fischer Scientific Nunc™ MicroWell™ 96-Well, flat-bottom black microplate for the 2nd experiment using crude extract from sonicated cells. Coumarin concentrations in the tested strains were in mM, and 7-hydroxycoumarin concentrations were in µM.

Table G.7: Fluorescence intensity (a.u.) measurements in the BVEV, mmo, mmoH, groESL1, groESL2, and groESL_BM strains two hours after added coumarin in the 2nd experiment using crude extract from sonicated cells. Blanks, standard concentrations of 7-hydroxycoumarin, and negative control samples are also displayed.

<>	1	2	3	4	8	9	10	11	12
A	5	5	5	0	2011	1508	802	314	92
B	2	3	4	-3	2110	1636	878	337	95
C	4	5	4	-4	2103	1637	872	324	98
D	2	3	1	-3					
E	2	2	4	-5					
F	-1	2	4	-3					
H	-8	-6	-7	-6					

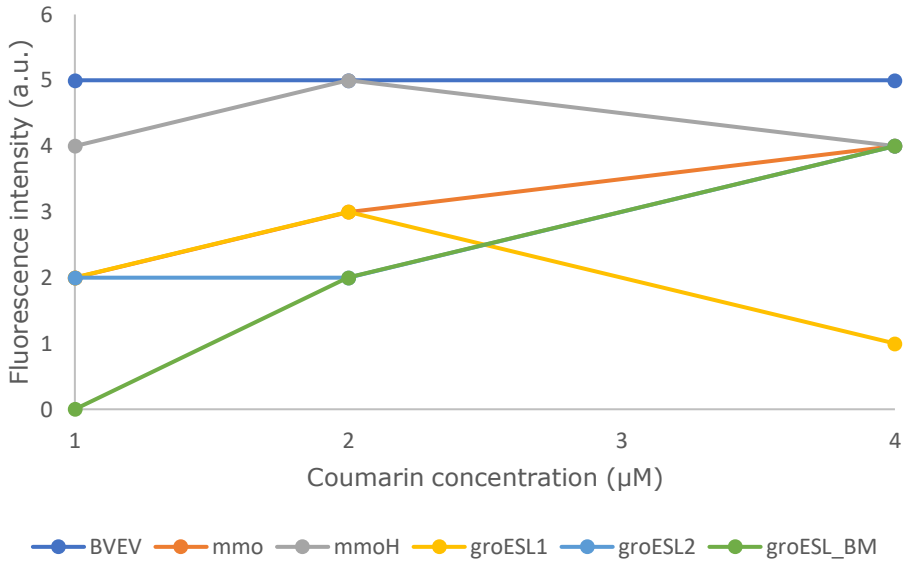

Figure G.12: Fluorescence intensity (a.u.) of the tested strains two hours after added coumarin in the 2nd of the experiment using crude extract from sonicated cells.

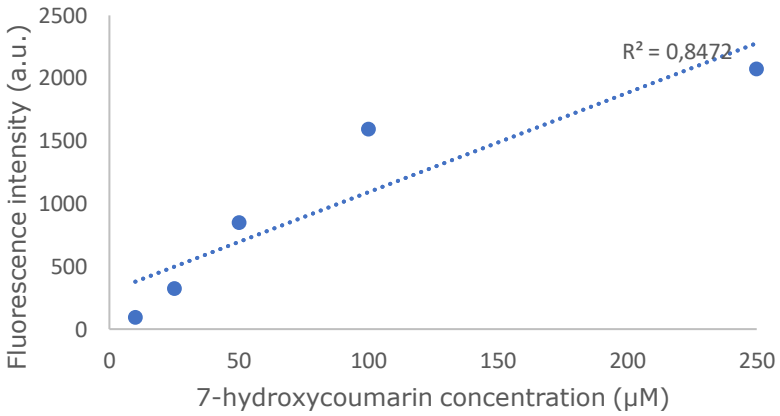

Figure G.13: Fluorescence intensity of standard 7-hydroxycoumarin samples at the listed concentrations in the two-hour sample.

Table G.8: Fluorescence intensity (a.u.) measurements in the BVEV, mmo, mmoH, groESL1, groESL2, and groESL_BM strains four hours after added coumarin in the 2nd experiment using crude extract from sonicated cells. Blanks, standard concentrations of 7-hydroxycoumarin, and negative control samples are also displayed.

<>	1	2	3	4	8	9	10	11	12
A	4	3	3	0	1982	1379	637	262	79
B	1	1	1	-2	1956	1395	689	274	81
C	3	2	3	-4	1953	1376	688	263	75
D	2	2	3	-5					
E	0	0	0	-4					
F	-1	-1	2	-3					
H	-8	-8	-8	-7					

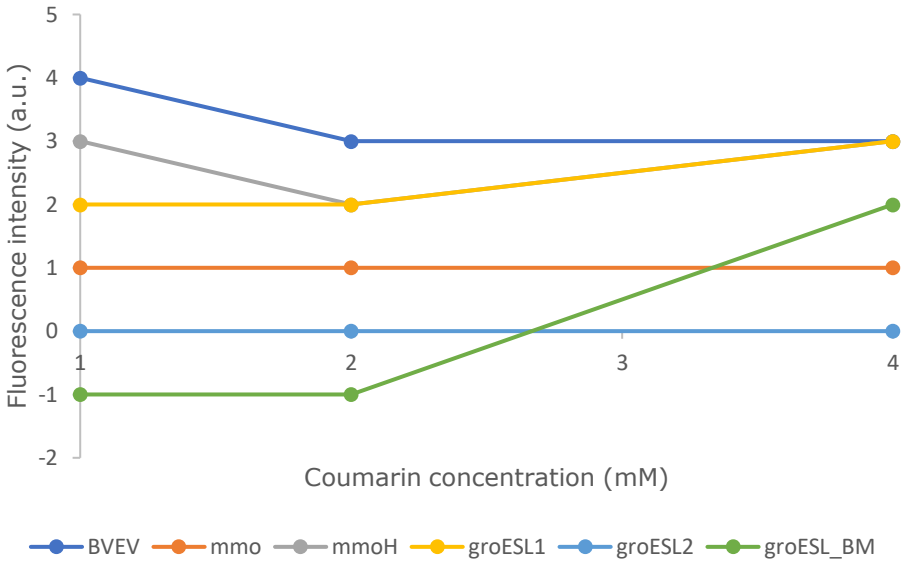

Figure G.14: Fluorescence intensity (a.u.) of the tested strains four hours after added coumarin in the 2nd of the experiment using crude extract from sonicated cells.

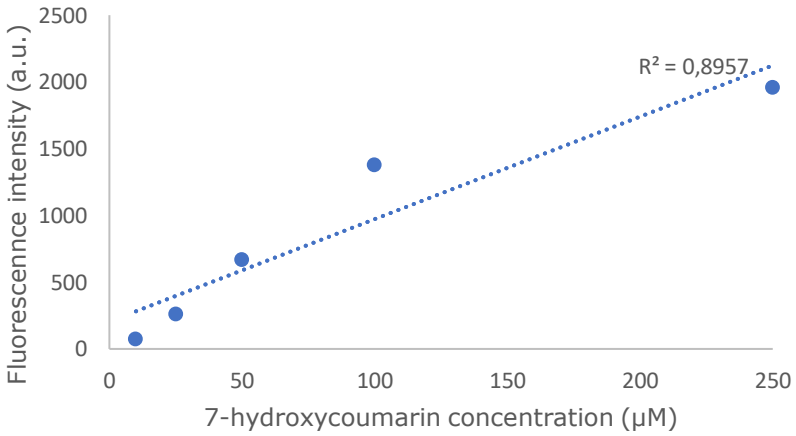

Figure G.15: Fluorescence intensity of standard 7-hydroxycoumarin samples at the listed concentrations in the four-hour sample.

Table G.9: Fluorescence intensity (a.u.) measurements in the BVEV, mmo, mmoH, groESL1, groESL2, and groESL_BM strains eight hours after added coumarin in the 2nd experiment using crude extract from sonicated cells. Blanks, standard concentrations of 7-hydroxycoumarin, and negative control samples are also displayed.

<>	1	2	3	4	8	9	10	11	12
A	5	5	6	2	2017	1383	671	267	78
B	4	4	4	0	2029	1355	656	256	82
C	6	4	2	-3	2020	1324	639	242	71
D	2	3	4	-2					
E	2	3	4	-2					
F	2	2	4	-3					
H	-5	-7	-8	-8					

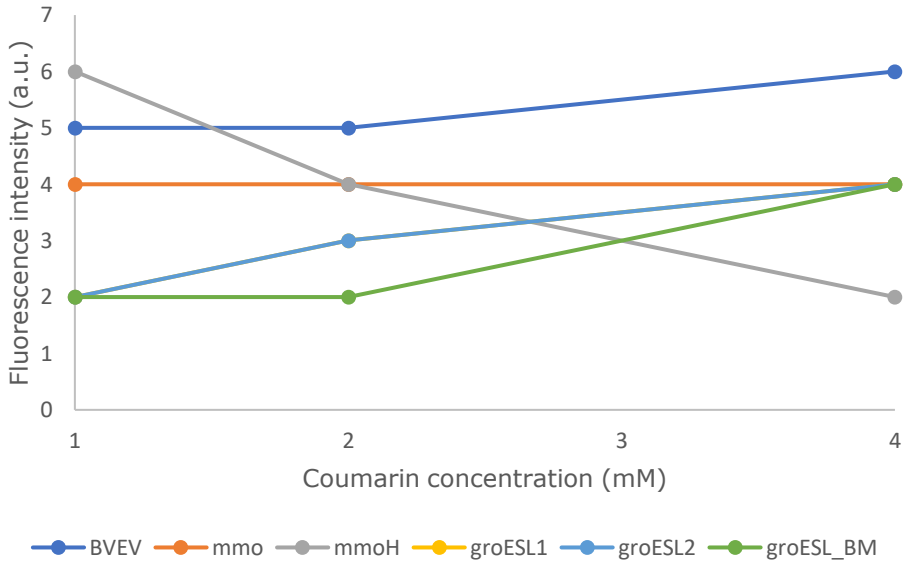

Figure G.16: Fluorescence intensity (a.u.) of the tested strains eight hours after added coumarin in the 2nd experiment using crude extract from sonicated cells.

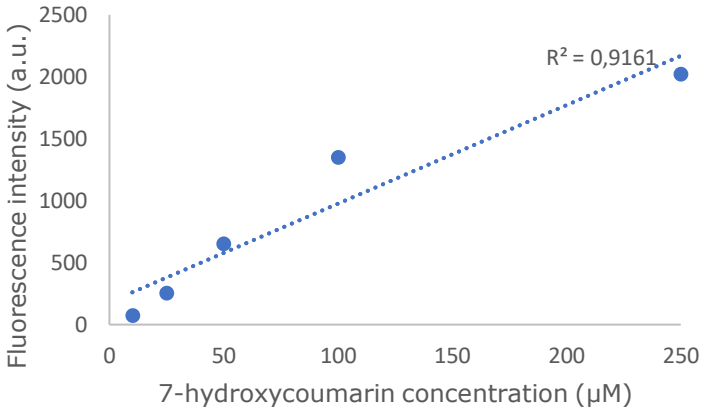

Figure G.17: Fluorescence intensity of standard 7-hydroxycoumarin samples at the listed concentrations in the eight-hour sample.

Table G.10: Fluorescence intensity (a.u.) measurements in the BVEV, mmo, mmoH, groESL1, groESL2, and groESL_BM strains twenty-four hours after added coumarin in the 2nd experiment using crude extract from sonicated cells. Blanks, standard concentrations of 7-hydroxycoumarin, and negative control samples are also displayed.

<>	1	2	3	4	8	9	10	11	12
A	5	6	8	1	2180	1465	671	245	75
B	4	4	2	-1	2165	1455	608	277	42
C	4	4	4	-3	2170	1492	704	246	77
D	4	3	5	-1					
E	1	3	4	-2					
F	1	2	2	-4					
H	-8	-9	-9	-9					

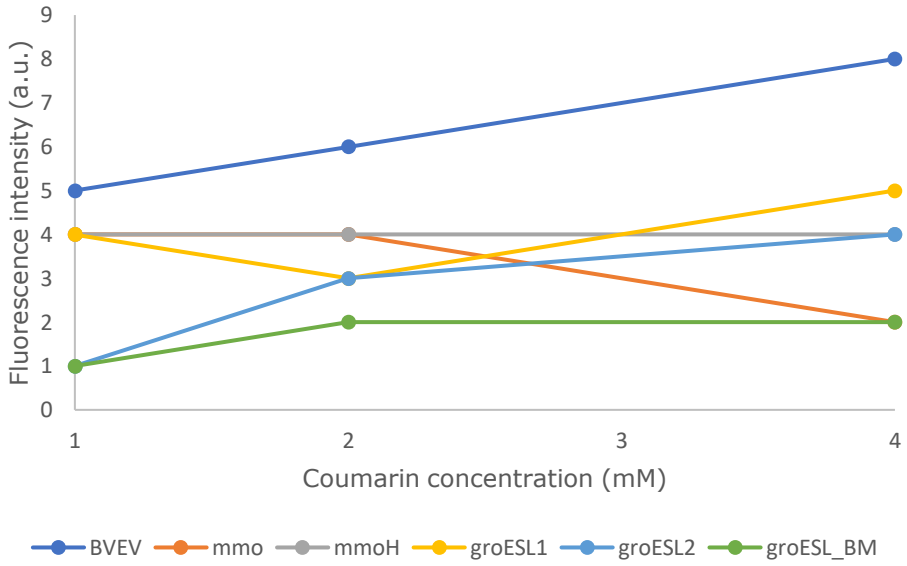

Figure G.18: Fluorescence intensity (a.u.) of the tested strains twenty-four hours after added coumarin in the 2nd experiment using crude extract from sonicated cells.

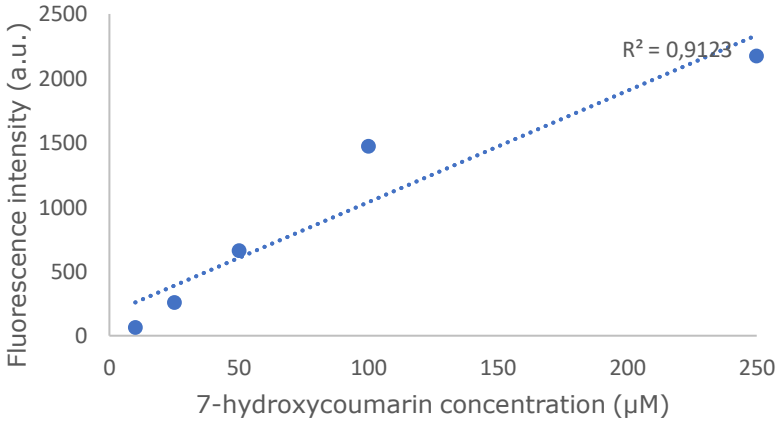

Figure G.19: Fluorescence intensity of standard 7-hydroxycoumarin samples at the listed concentrations in the twenty-four-hour sample.

3rd experiment:

Figure G.20 shows the microplate setup for fluorescence intensity measurements. The setup corresponds to figures G.21-G.26 and tables G.11-G.13.

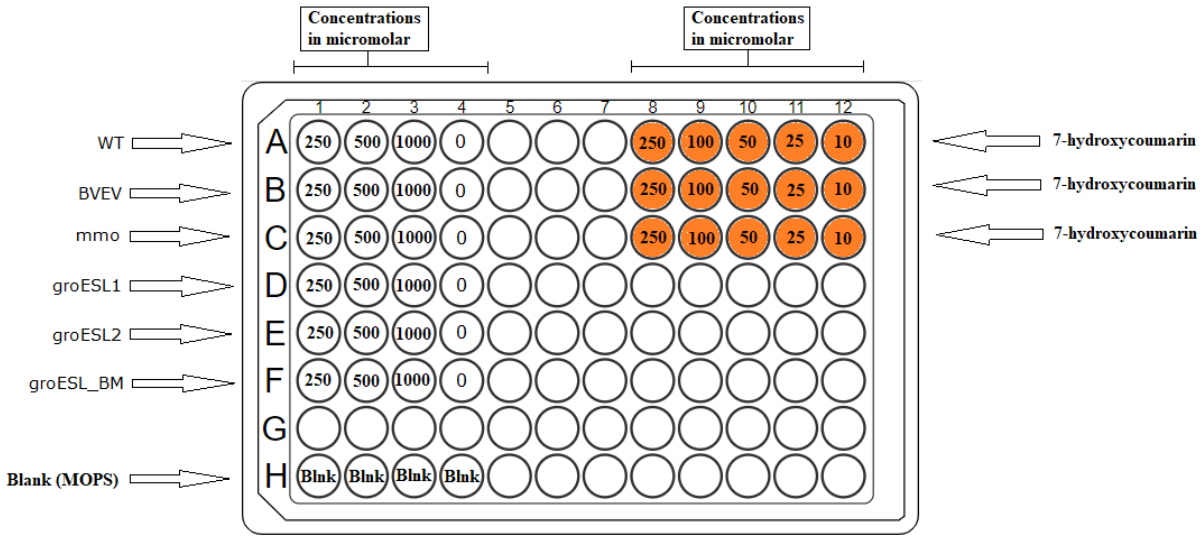

Figure G.20: Plate setup in the Thermo Fischer Scientific Nunc™ MicroWell™ 96-Well, flat-bottom black microplate for the 3rd experiment using crude extract from sonicated cells. All coumarin and 7-hydroxycoumarin concentrations were in µM.

Table G.11: Fluorescence intensity (a.u.) measurements in the WT, BVEV, mmo, groESL1, groESL2, and groESL_BM strains four hours after added coumarin in the 3rd experiment using crude extract from sonicated cells. Blanks, standard concentrations of 7-hydroxycoumarin, and negative control samples are also displayed.

<>	1	2	3	4	8	9	10	11	12
A	31	27	28	30	2105	1544	786	314	99
B	17	19	14	16	2097	1533	790	332	100
C	16	15	13	15	2011	1529	786	309	94
D	18	16	15	16					
E	17	15	13	17					
F	17	20	17	18					
H	1	2	1	0					

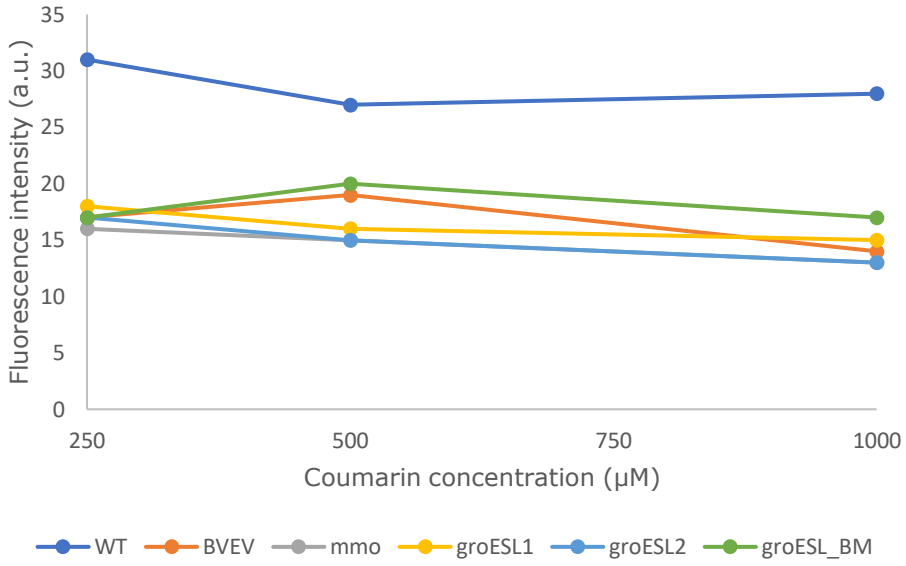

Figure G.21: Fluorescence intensity (a.u.) of the tested strains four hours after added coumarin in the 3rd experiment using crude extract from sonicated cells.

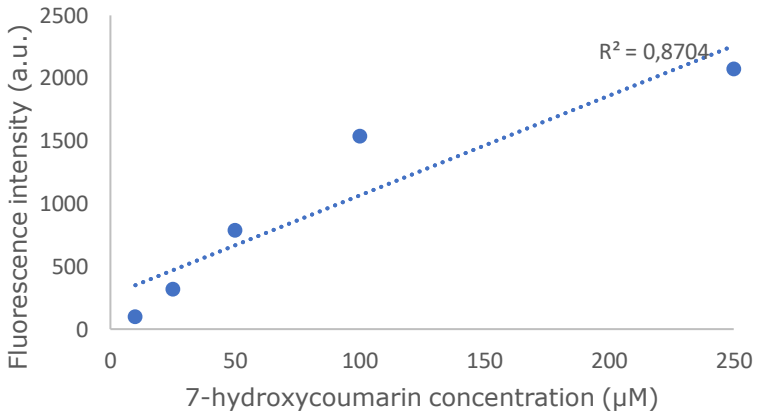

Figure G.22: Fluorescence intensity of standard 7-hydroxycoumarin samples at the listed concentrations in the four-hour sample.

Table G.12: Fluorescence intensity (a.u.) measurements in the WT, BVEV, mmo, groESL1, groESL2, and groESL_BM strains eight hours after added coumarin in the 3rd experiment using crude extract from sonicated cells. Blanks, standard concentrations of 7-hydroxycoumarin, and negative control samples are also displayed.

<>	1	2	3	4	8	9	10	11	12
A	26	24	24	22	2110	1482	754	297	89
B	9	9	9	12	2121	1520	771	298	85
C	10	8	8	9	2113	1486	738	285	88
D	8	9	8	8					
E	8	7	8	8					
F	9	12	8	9					
H	-6	-9	-6	-9					

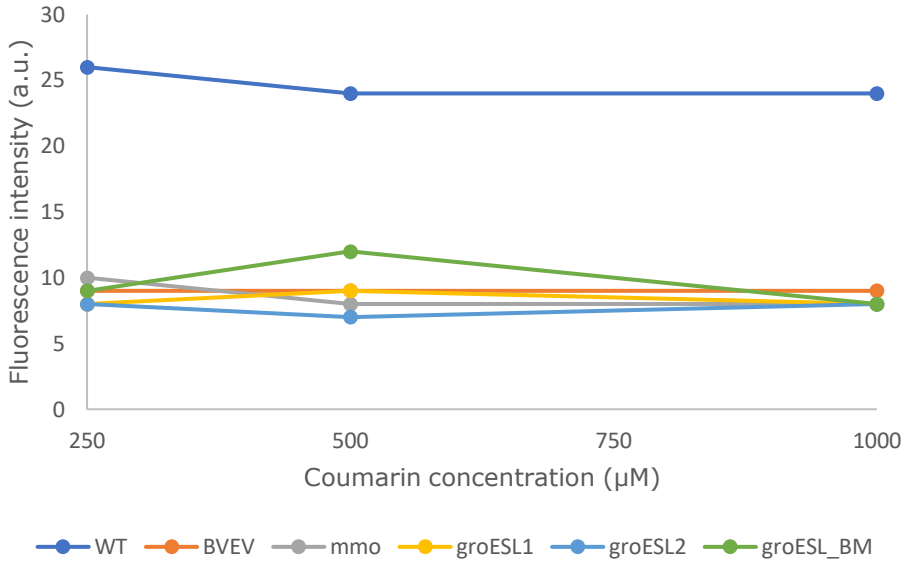

Figure G.23: Fluorescence intensity (a.u.) of the tested strains eight hours after added coumarin in the 3rd experiment using crude extract from sonicated cells.

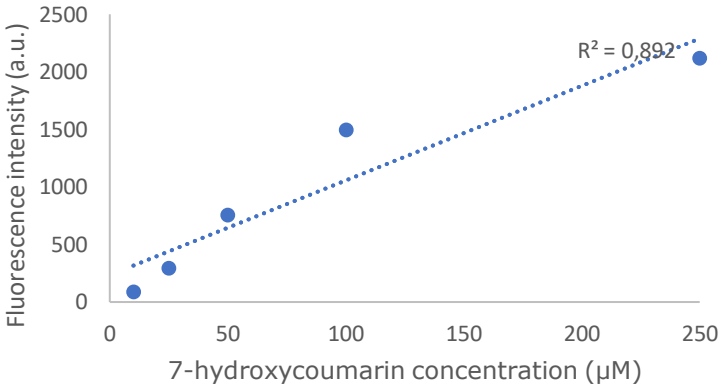

Figure G.24: Fluorescence intensity of standard 7-hydroxycoumarin samples at the listed concentrations in the eight-hour sample.

Table G.13: Fluorescence intensity (a.u.) measurements in the WT, BVEV, mmo, groESL1, groESL2, and groESL_BM strains twenty-four hours after added coumarin in the 3rd experiment using crude extract from sonicated cells. Blanks, standard concentrations of 7-hydroxycoumarin, and negative control samples are also displayed.

<>	1	2	3	4	8	9	10	11	12
A	27	23	26	23	2081	1327	613	241	72
B	10	10	8	12	2068	1373	626	241	71
C	12	10	8	11	2056	1323	629	246	74
D	9	7	9	13					
E	9	8	7	11					
F	9	10	8	11					
H	-9	-9	-7	-7					

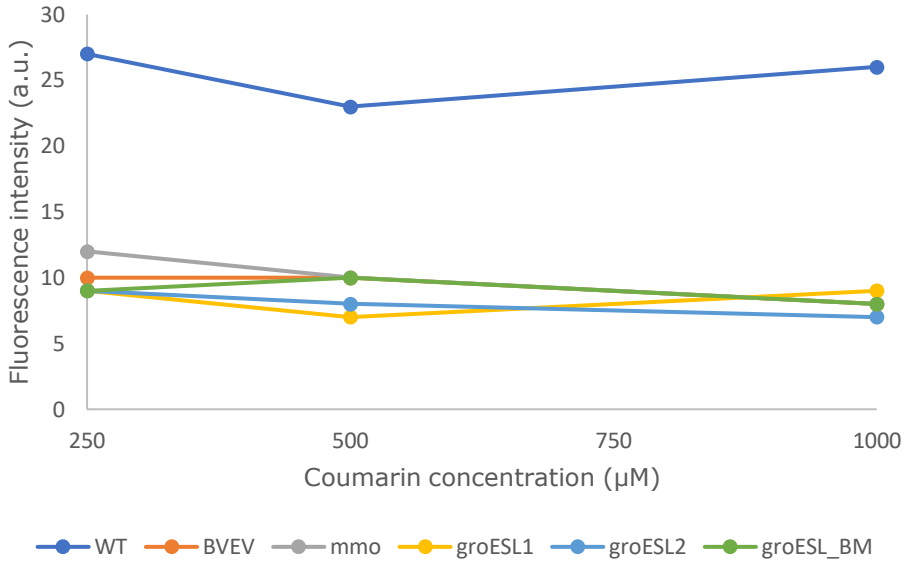

Figure G.25: Fluorescence intensity (a.u.) of the tested strains twenty-four hours after added coumarin in the 3rd experiment using crude extract from sonicated cells.

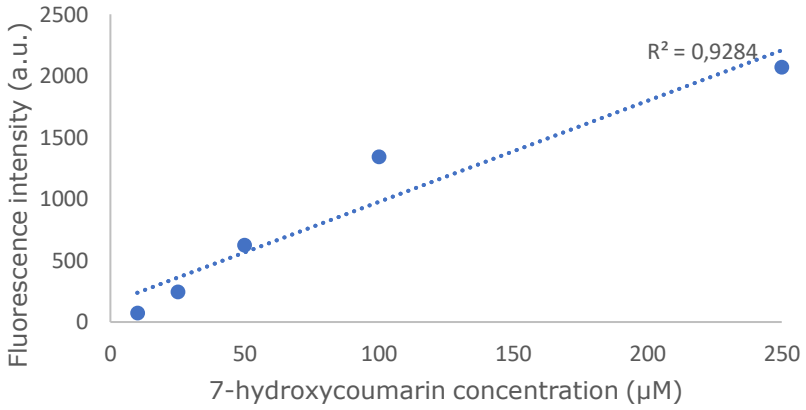

Figure G.26: Fluorescence intensity of standard 7-hydroxycoumarin samples at the listed concentrations in the twenty-four-hour sample.

4th experiment:

Figure G.27 shows the microplate setup for fluorescence intensity measurements. The setup corresponds to figures G.28-G.2 and tables G.14-G.1.

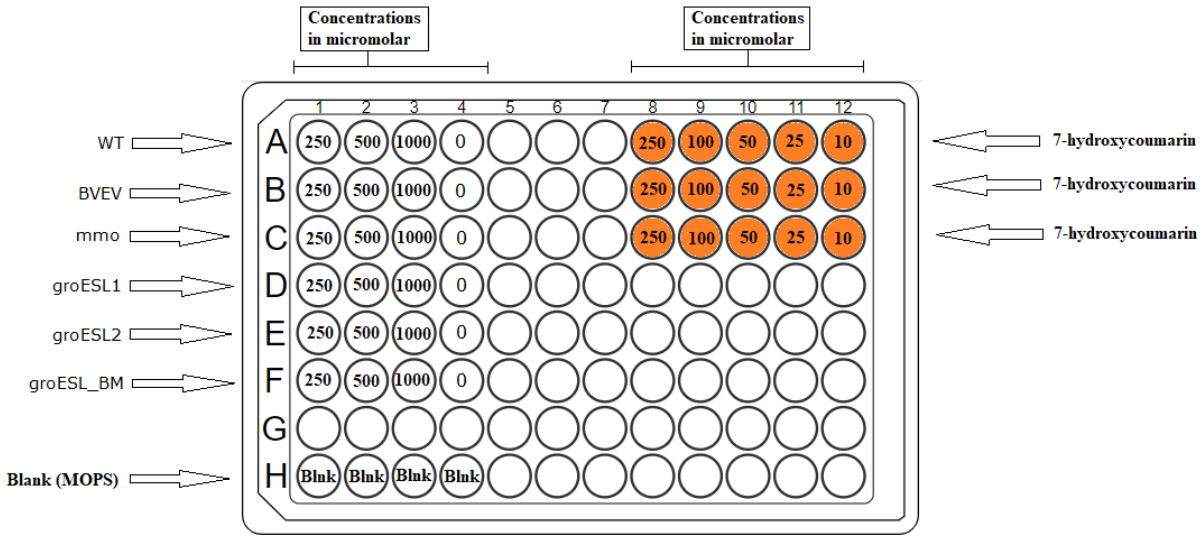

Figure G.27: Plate setup in the Thermo Fischer Scientific Nunc™ MicroWell™ 96-Well, flat-bottom black microplate for the 4th experiment using crude extract from sonicated cells. All coumarin and 7-hydroxycoumarin concentrations were in µM.

Table G.14: Fluorescence intensity (a.u.) measurements in the WT, BVEV, mmo, groESL1, groESL2, and groESL_BM strains two hours after added coumarin in the 4th experiment using crude extract from sonicated cells. Blanks, standard concentrations of 7-hydroxycoumarin, and negative control samples are also displayed.

<>	1	2	3	4	8	9	10	11	12
A	23	20	14	33	2074	1381	642	242	76
B	21	21	17	9	2098	1423	686	258	80
C	27	23	17	11	2094	1404	667	268	77
D	17	16	13	7					
E	22	18	18	23					
F	37	6	8	37					
H	-6	-6	-7	-7					

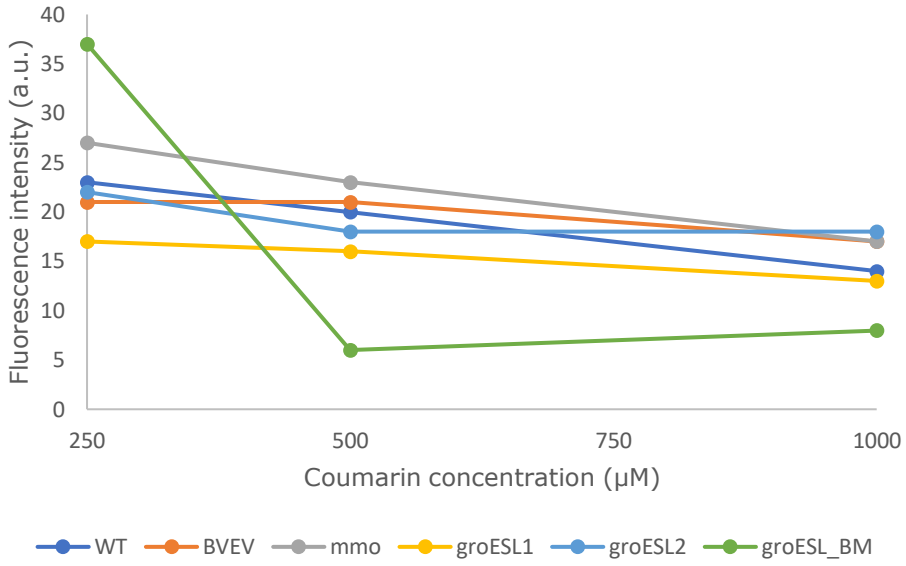

Figure G.28: Fluorescence intensity (a.u.) of the tested strains two hours after added coumarin in the 4th experiment using crude extract from sonicated cells.

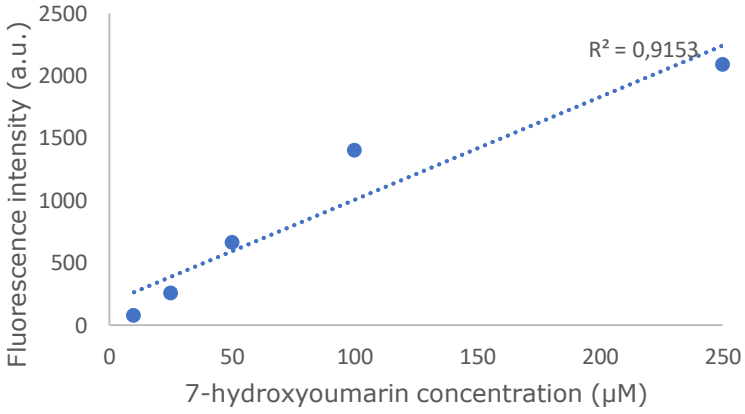

Figure G.29: Fluorescence intensity of standard 7-hydroxycoumarin samples at the listed concentrations in the two-hour sample.

Table G.15: Fluorescence intensity (a.u.) measurements in the WT, BVEV, mmo, groESL1, groESL2, and groESL_BM strains four hours after added coumarin in the 4th experiment using crude extract from sonicated cells. Blanks, standard concentrations of 7-hydroxycoumarin, and negative control samples are also displayed.

<>	1	2	3	4	8	9	10	11	12
A	29	25	19	34	1943	1311	584	231	70
B	26	26	23	16	1804	1353	607	248	74
C	30	24	23	19	2016	1156	623	237	50
D	24	21	19	16					
E	29	26	21	31					
F	30	13	14	41					
H	2	1	1	1					

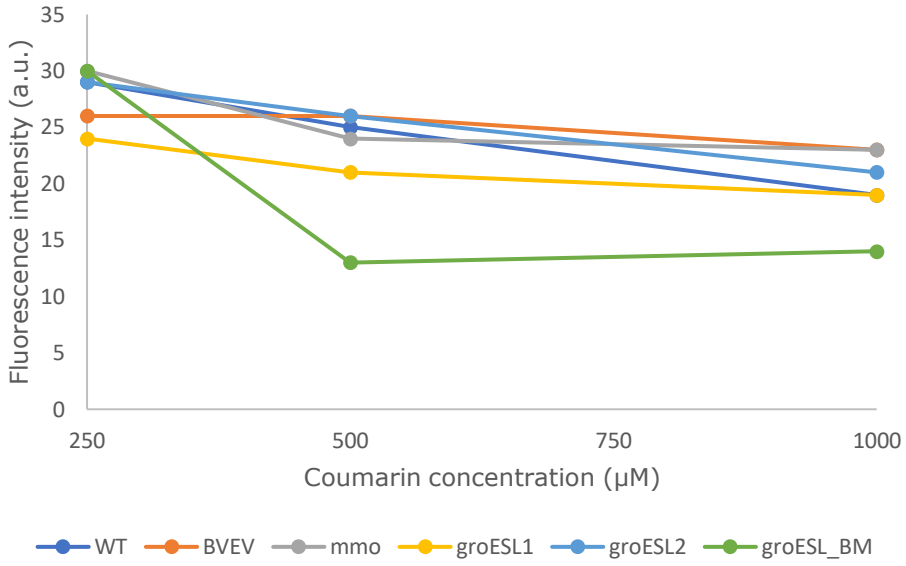

Figure G.30: Fluorescence intensity (a.u.) of the tested strains four hours after added coumarin in the 4th experiment using crude extract from sonicated cells.

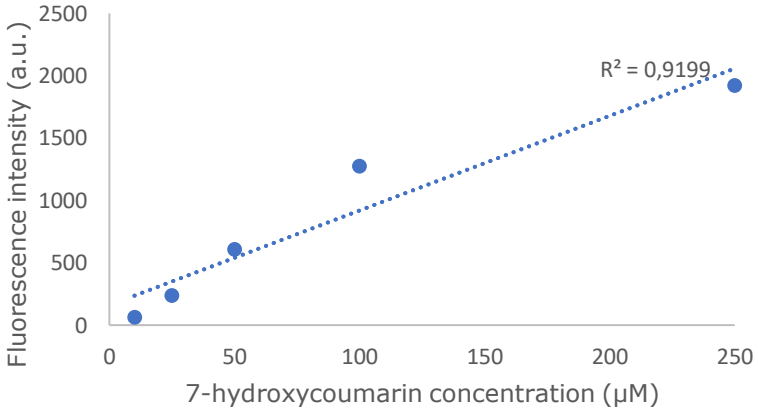

Figure G.31: Fluorescence intensity of standard 7-hydroxycoumarin samples at the listed concentrations in the four-hour sample.

Table G.15: Fluorescence intensity (a.u.) measurements in the WT, BVEV, mmo, groESL1, groESL2, and groESL_BM strains eight hours after added coumarin in the 4th experiment using crude extract from sonicated cells. Blanks, standard concentrations of 7-hydroxycoumarin, and negative control samples are also displayed.

<>	1	2	3	4	8	9	10	11	12
A	23	17	12	22	1970	1224	615	218	63
B	16	15	12	10	1975	1353	661	241	69
C	20	16	15	8	2042	1288	687	259	66
D	8	13	9	7					
E	22	17	14	10					
F	19	4	4	28					
H	-6	-7	-6	-8					

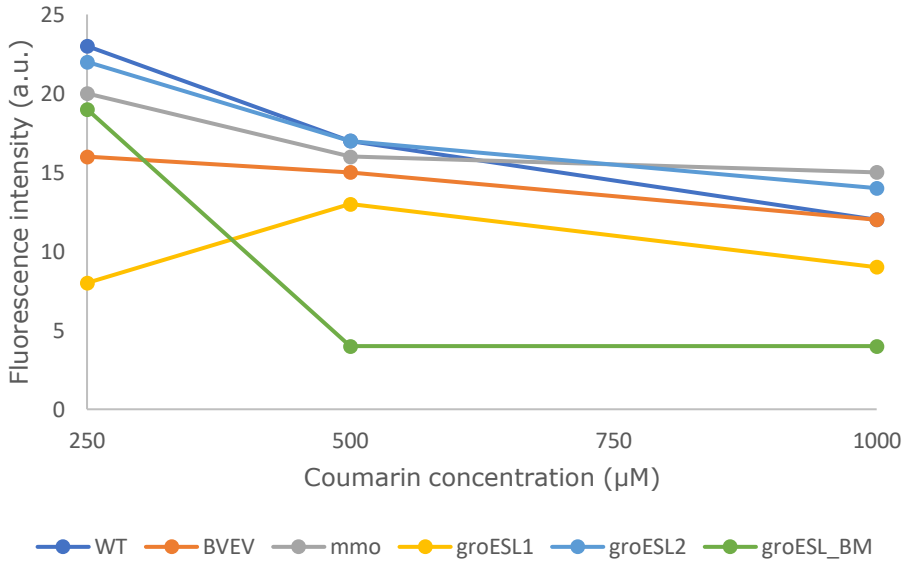

Figure G.32: Fluorescence intensity (a.u.) of the tested strains eight hours after added coumarin in the 4th experiment using crude extract from sonicated cells.

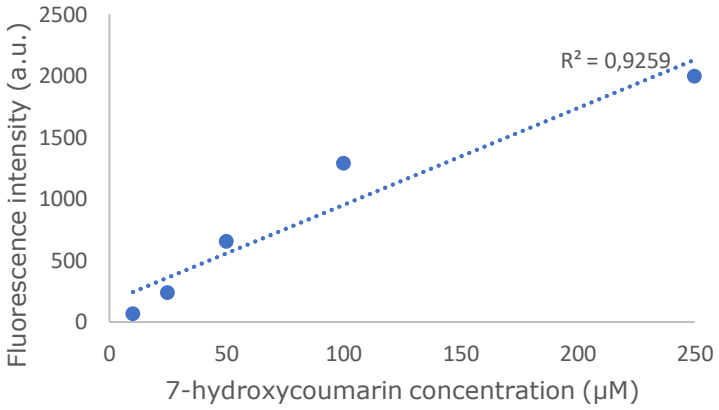

Figure G.33: Fluorescence intensity of standard 7-hydroxycoumarin samples at the listed concentrations in the eight-hour sample.

Table G.16: Fluorescence intensity (a.u.) measurements in the WT, BVEV, mmo, groESL1, groESL2, and groESL_BM strains twenty-four hours after added coumarin in the 4th experiment using crude extract from sonicated cells. Blanks, standard concentrations of 7-hydroxycoumarin, and negative control samples are also displayed.

<>	1	2	3	4	8	9	10	11	12
A	14	11	10	15	1979	1268	547	209	57
B	8	8	9	9	2019	1321	582	213	59
C	13	12	9	11	2025	1357	596	220	52
D	8	6	4	8					
E	10	12	9	12					
F	11	5	4	19					
H	-7	-6	-8	-7					

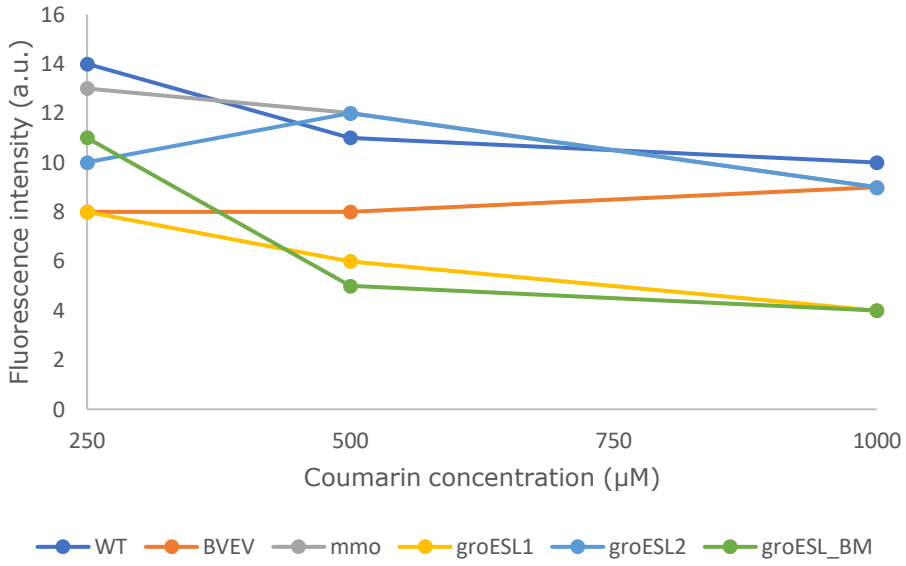

Figure G.34: Fluorescence intensity (a.u.) of the tested strains twenty-four hours after added coumarin in the 4th experiment using crude extract from sonicated cells.

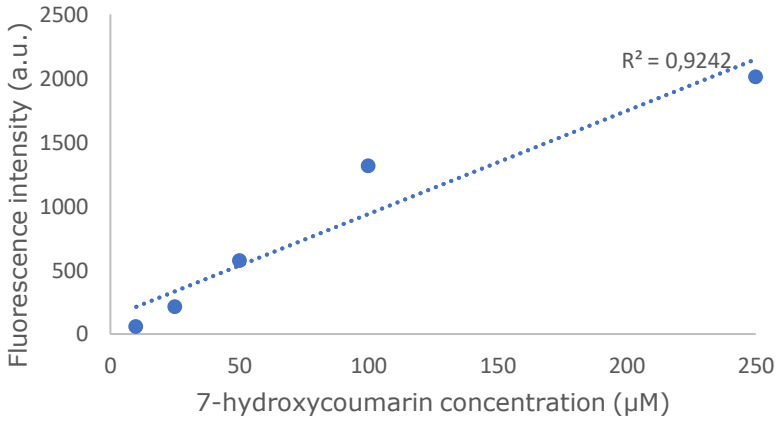

Figure G.33: Fluorescence intensity of standard 7-hydroxycoumarin samples at the listed concentrations in the twenty-four-hour sample.

Appendix H: OD_{600} measurements for the 1st experiment of the fluorescence-based coumarin enzyme assay using whole cell cultures

The initial experiment using whole cell cultures relied on overnight-cultures with sufficient growth. Due to several of these not achieving sufficient growth, only the strains BVEV, mmo, mmoH, and groESL1 had main cultures inoculated. The main cultures of BVEV and mmoH were discarded after 3.5 hours due to not achieving sufficient growth, meaning that only the mmo and groESL1 strains had the substrate (coumarin) added.

Table H.1: Initial OD_{600} values of main cultures of the strains with sufficient growth in overnight pre-culture immediately after inoculation.

	Coumarin concentration (µM)					
Strain	**10**	**25**	**50**	**100**	**250**	**Control**
BVEV	0.09	0.07	0.08	0.10	0.09	0.08
mmo	0.08	0.09	0.10	0.10	0.08	0.07
mmoH	0.08	0.10	0.07	0.07	0.08	0.08
groESL1	0.18	0.16	0.16	0.18	0.17	0.18

Table H.2: OD_{600} values of main cultures two hours after inoculation.

	Coumarin concentration (µM)					
Strain	**10**	**25**	**50**	**100**	**250**	**Control**
BVEV	0.04	0.03	0.03	0.04	0.05	0.03
mmo	0.10	0.12	0.11	0.12	0.10	0.08
mmoH	0.04	0.04	0.03	0.04	0.04	0.04
groESL1	0.58	0.57	0.65	0.61	0.57	0.59

Table H.3: OD_{600} values of main cultures three and a half hours after inoculation. The B.m-groESL1 strain was not measured due to having sufficient OD_{600} from the previous measurement.

	Coumarin concentration (µM)					
Strain	**10**	**25**	**50**	**100**	**250**	**Control**
BVEV	0.06	0.05	0.05	0.06	0.07	0.05
mmo	0.18	0.23	0.24	0.24	0.22	0.20
mmoH	0.06	0.07	0.06	0.06	0.07	0.06

Table H.4: OD_{600} values of main cultures two hours after added coumarin and five and a half hours after inoculation.

	Coumarin concentration (µM)					
Strain	**10**	**25**	**50**	**100**	**250**	**Control**
mmo	0.68	0.54	0.64	0.57	0.58	0.64
groESL1	2.80	2.90	3.20	2.80	2.60	3.00

Table H.5: OD_{600} values of main cultures four hours after added coumarin and seven and a half hours after inoculation.

	Coumarin concentration (µM)					
Strain	**10**	**25**	**50**	**100**	**250**	**Control**
mmo	0.74	0.68	0.73	0.65	0.69	0.71
groESL1	4.40	3.00	3.60	4.00	4.20	3.10

Table H.6: OD_{600} values of main cultures six hours after added coumarin and nine hours after inoculation.

	Coumarin concentration (µM)					
Strain	**10**	**25**	**50**	**100**	**250**	**Control**
mmo	1.40	0.70	1.00	0.70	0.80	0.80
groESL1	4.40	3.00	3.60	4.00	4.20	3.10

Table H.6: OD_{600} values of main cultures twenty-four hours after added coumarin and twenty-seven and a half hours after inoculation.

	Coumarin concentration (µM)					
Strain	**10**	**25**	**50**	**100**	**250**	**Control**
mmo	3.40	4.20	3.80	3.20	3.60	3.70
groESL1	3.70	3.00	3.50	3.80	3.65	2.72

Appendix I: Agar plates used in the naphthalene oxidation assay for sMMO

Images of agar plates with the tested *B. methanolicus* MGA3 strains as stated in section 2.11. Images A-G display the tested strains of *B.* methanolicus MGA3.

(A): WT

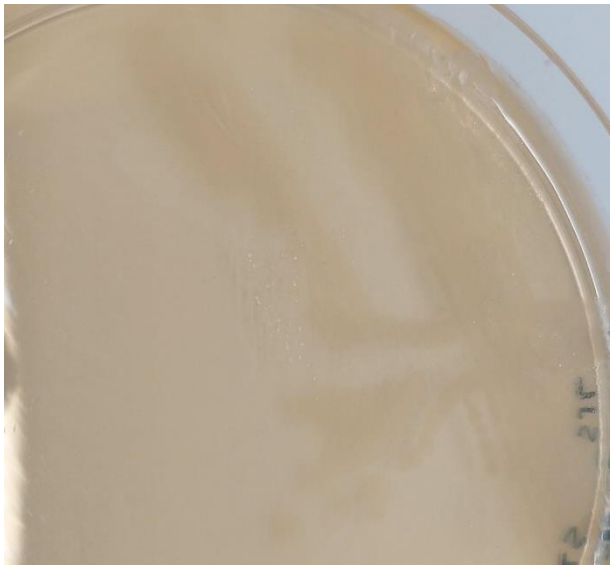

(B): mmo

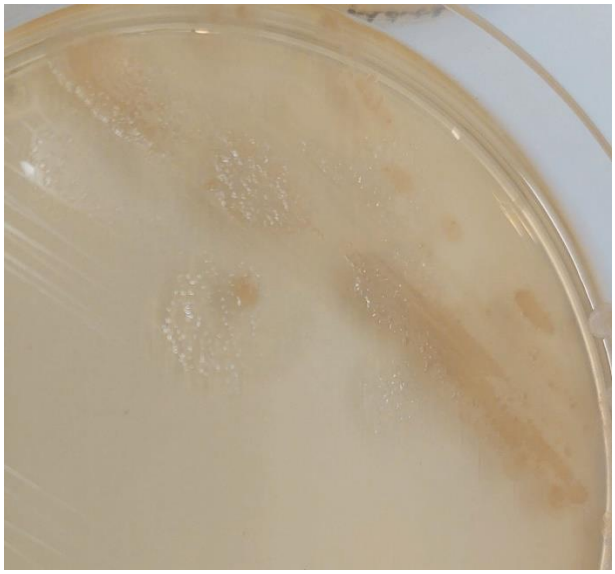

(C): mmoH

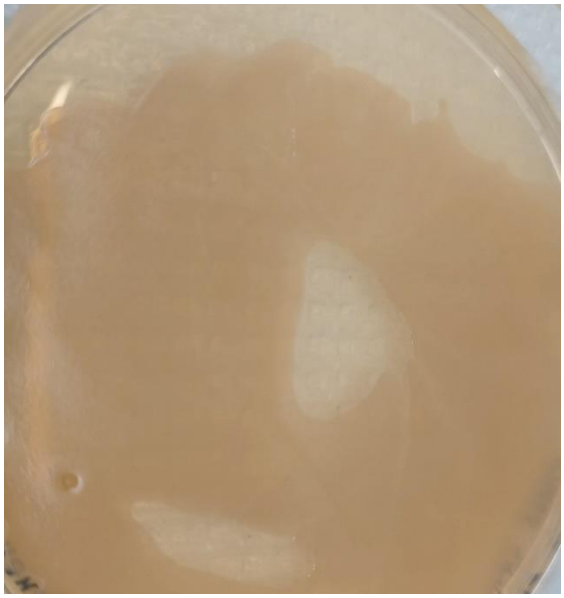

(D): groESL1

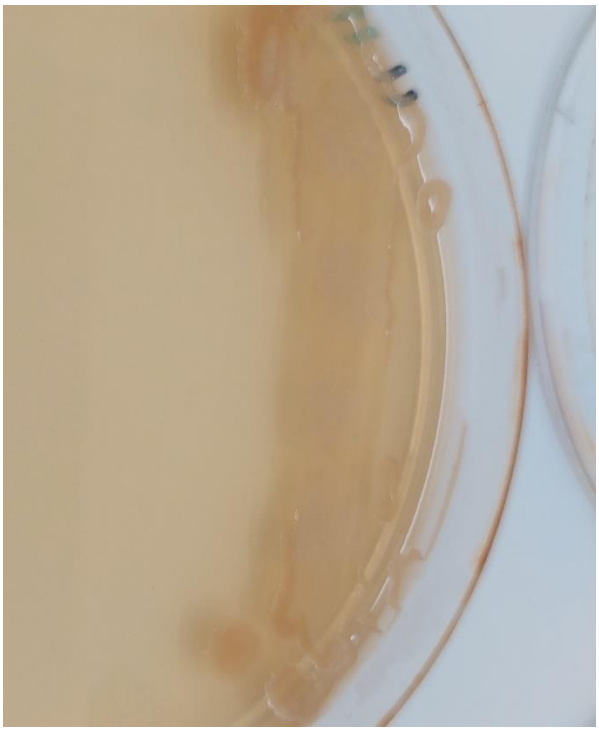

(E): groESL2

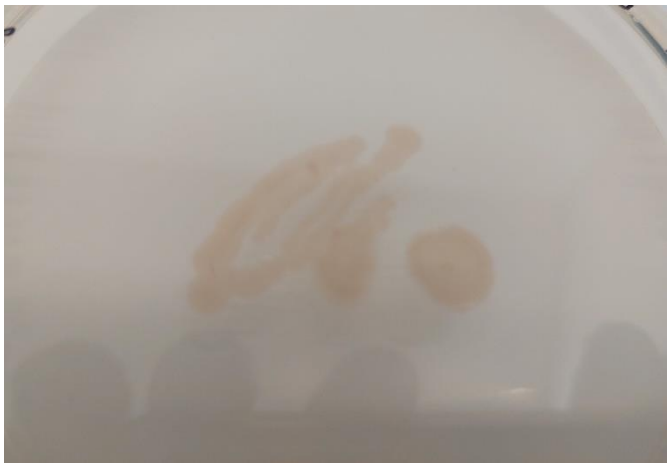

(F): groESL_BM

Appendix J: Sequence alignment of constructs with *hps* and *phi*

The sequence alignment data from the plasmid constructs used in the growth experiment with *B. methanolicus* strains homologously expressing *hps* and *phi* with native- and *mdh* promoter. The sequence alignments were assessed using the Benchling online cloud-based bioinformatics platform (Benchling, 2023, retrieved 17 april from www.benchling.com). Mismatching bases to the construct are shown in red.

---

pTH1mp-hps-phi:

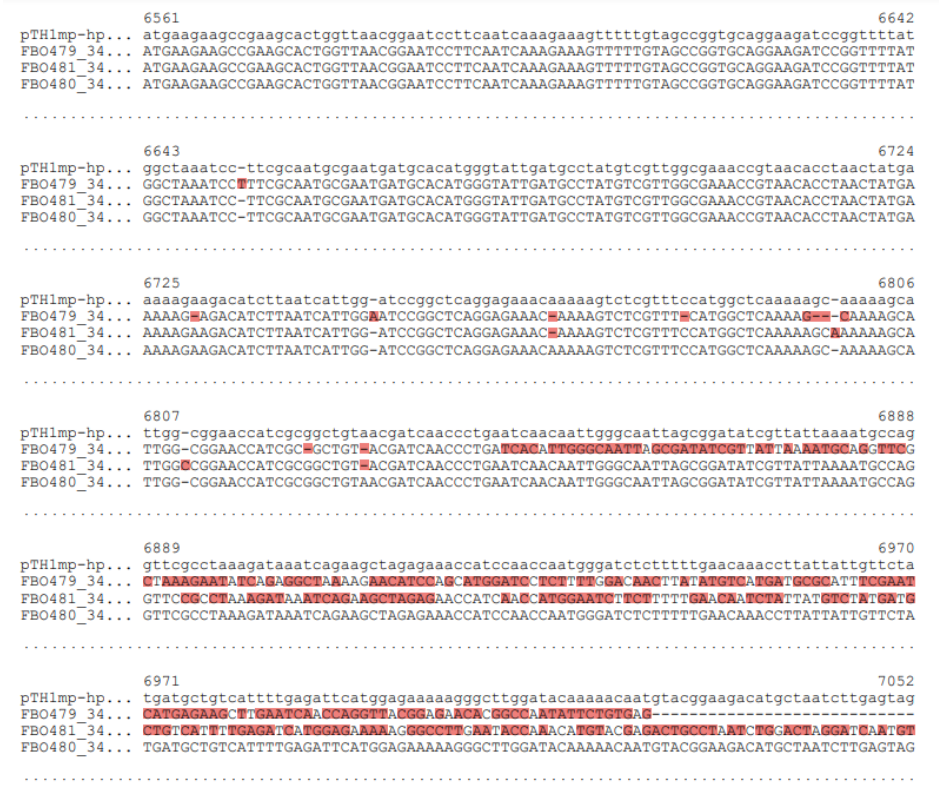

pTH-hps-phi:

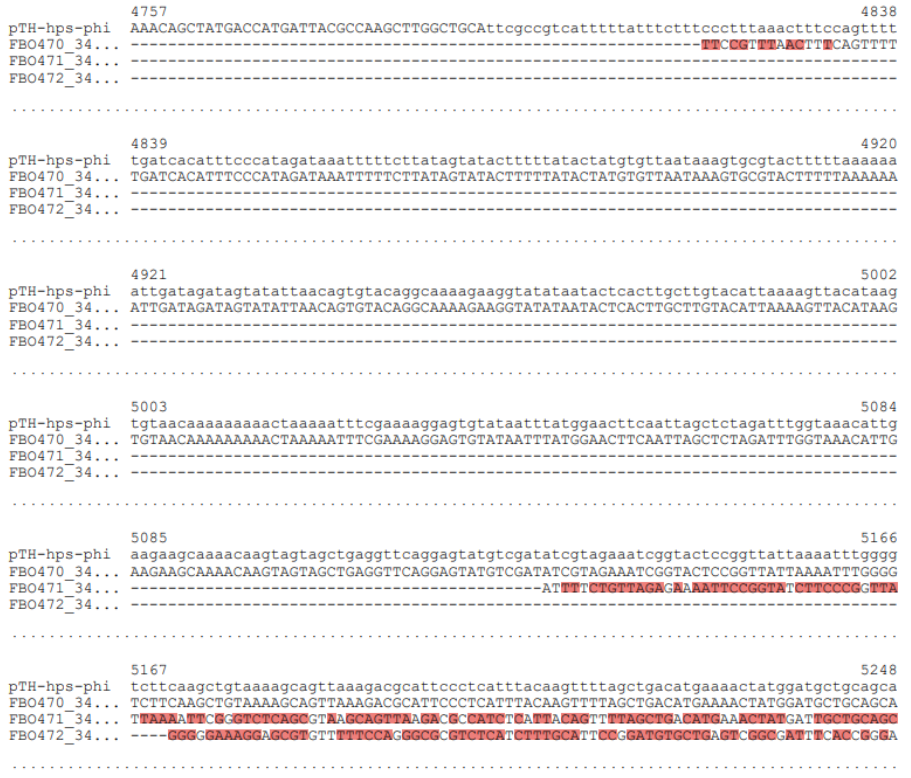

pUB110Smp-hps-phi:

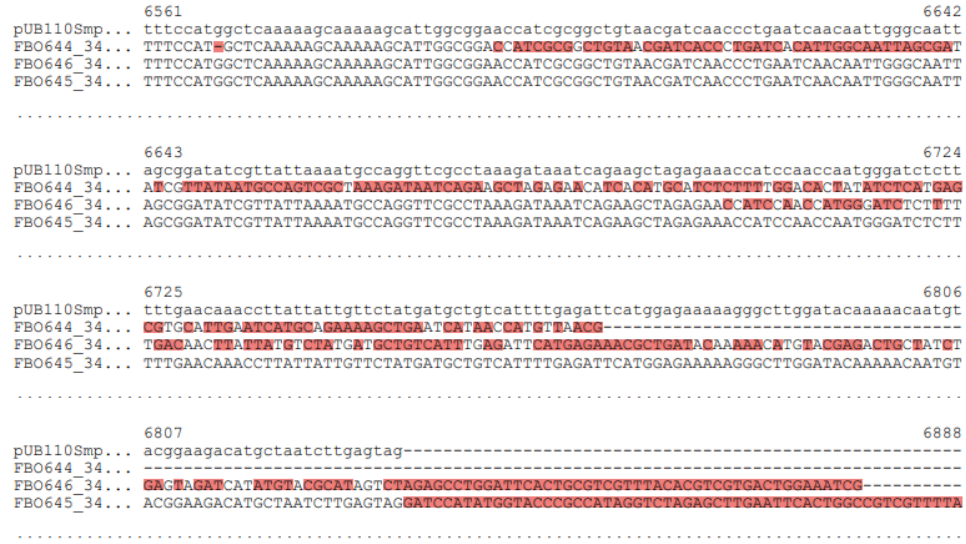

pUB110-hps-phi:

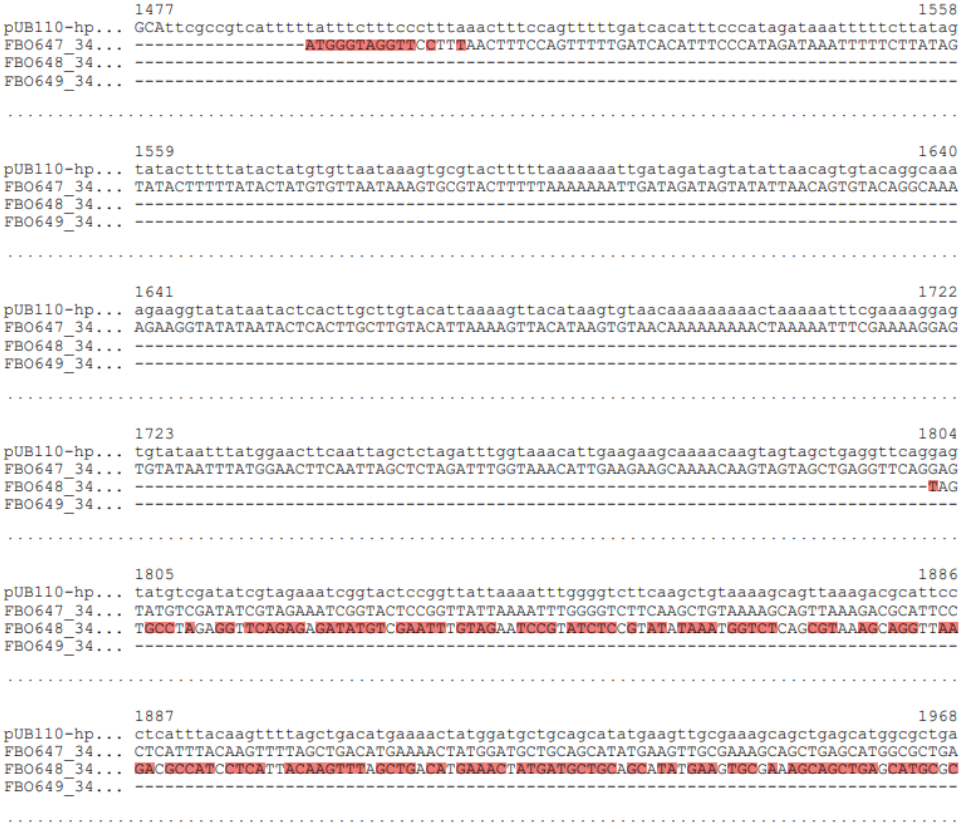

Appendix K: OD_{600} measurements of *hps-phi* growth experiment

The OD_{600} measurements for each strain of *B. methanolicus* MGA3 used in the growth experiment is presented in table K.1. Samples were taken every two hours until stable or decreasing OD_{600} values were observed.

Table K.1: OD_{600} measurements of all tested strains at 200 mM and 400 mM methanol.

Strain	Inoc OD	2 hours	4 hours	6 hours	8 hours	10 hours	12 hours
THEV (200 mM)	0.27	0.52	1.00	1.90	4.10	6.30	4.50
THEV (200 mM)	0.27	0.53	1.10	2.20	3.80	6.50	5.50
THEV (200 mM)	0.26	0.52	1.00	2.00	4.20	6.30	5.00
THEV (400 mM)	0.27	0.49	1.10	1.90	4.60	6.20	3.80
THEV (400 mM)	0.27	0.48	0.90	1.80	4.10	5.60	3.90
THEV (400 mM)	0.24	0.47	0.90	1.90	4.80	5.00	3.60
THMet.P (200 mM)	0.21	0.46	0.87	1.70	3.70	5.90	4.10
THMet.P (200 mM)	0.25	0.44	0.85	1.60	3.80	6.20	5.10
THMet.P (200 mM)	0.25	0.45	0.87	1.70	3.80	6.20	4.30
THMet.P (400 mM)	0.22	0.39	0.73	1.50	3.50	5.50	3.70
THMet.P (400 mM)	0.22	0.40	0.75	1.40	3.40	5.20	3.80
THMet.P (400 mM)	0.23	0.38	0.73	1.30	3.30	5.60	3.80
THNat.P (200 mM)	0.29	0.46	0.80	1.80	4.40	6.30	4.50
THNat.P (200 mM)	0.25	0.45	0.80	1.80	3.90	6.60	4.90
THNat.P (200 mM)	0.25	0.42	0.90	1.90	4.20	7.00	5.30
THNat.P (400 mM)	0.23	0.39	0.80	1.50	3.10	6.10	5.20
THNat.P (400 mM)	0.25	0.43	0.90	1.70	3.30	6.60	4.60
THNat.P (400 mM)	0.25	0.40	0.70	1.70	3.30	6.70	4.60
UBEV (200 mM)	0.23	0.44	0.92	1.90	4.30	6.10	4.80
UBEV (200 mM)	0.26	0.43	0.83	1.60	3.10	4.10	5.60
UBEV (200 mM)	0.23	0.42	0.84	1.70	4.00	6.40	4.40
UBEV (400 mM)	0.26	0.42	0.78	1.70	3.70	5.60	3.90
UBEV (400 mM)	0.23	0.42	0.80	1.70	3.50	5.70	3.80
UBEV (400 mM)	0.21	0.45	0.84	1.90	4.00	5.40	3.80
UBMet.P (200 mM)	0.24	0.43	0.82	1.60	4.00	6.70	5.50
UBMet.P (200 mM)	0.21	0.42	0.76	1.70	3.60	6.70	6.00
UBMet.P (200 mM)	0.20	0.41	0.74	1.60	3.60	6.20	5.30
UBMet.P (400 mM)	0.25	0.45	0.85	1.70	3.40	6.50	4.70
UBMet.P (400 mM)	0.26	0.44	0.80	1.50	3.40	6.30	4.70
UBMet.P (400 mM)	0.24	0.44	0.84	1.60	2.90	4.30	5.70

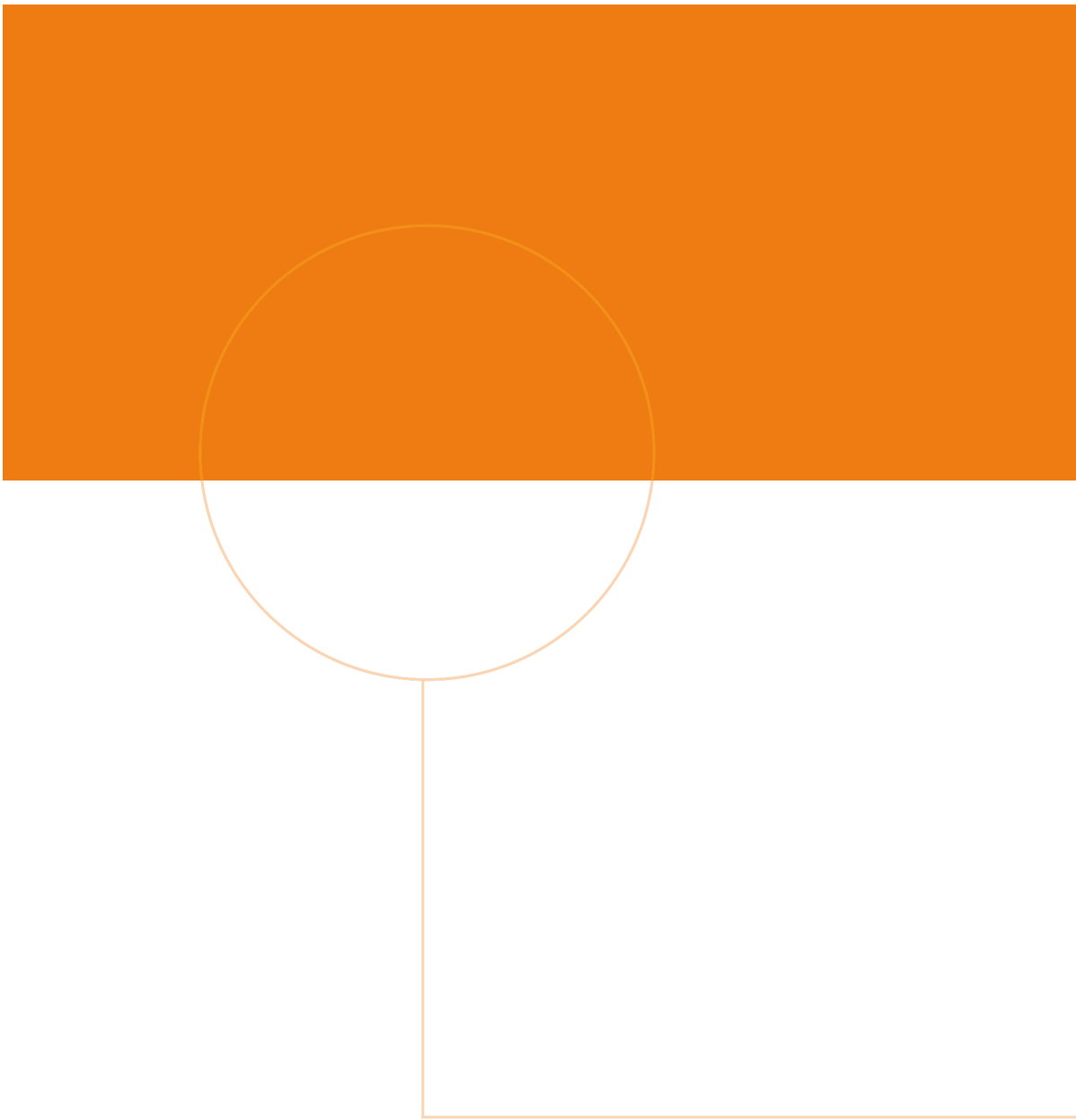

NTNU

Norwegian University of
Science and Technology